To the Graduate Council:

I am submitting herewith a thesis written by James Thomas Gambill entitled "Oxygen Transfer Rates in a Single Concentric Tube Airlift Reactor". I have examined the final copy of this thesis for form and content and recommend that it be accepted in partial fulfillment of the requirements for the degree of Master of Science, with a major in Chemical Engineering.

George C. Frazier

George C. Frazier, Major Professor

We have read this thesis
and recommend its acceptance:

Tse Wei Wang

Donald Dougall

Accepted for the Council:

C W Minkel

Vice Provost
and Dean of the Graduate School

STATEMENT OF PERMISSION TO USE

In presenting this thesis in partial fulfillment of the requirements for a Master's degree at the University of Tennessee, Knoxville, I agree that the library shall make it available to borrowers under the rules of the Library. Brief quotations from this thesis are allowable without special permission, provided that accurate acknowledgement is made.

Permission for extensive quotation from or reproduction of this thesis may be granted by my major professor, or in his absence, by the Head of Interlibrary Services when, in the opinion of either, the proposed use of the material is for scholarly purposes. Any copying or use of this material for financial gain shall not be allowed without my written permission.

James Thomas Gambill

James Thomas Gambill

Date: 7/13/89

OXYGEN TRANSFER RATES IN A SINGLE CONCENTRIC TUBE AIRLIFT REACTOR

A Thesis
Presented for the
Master of Science
Degree
The University of Tennessee, Knoxville

James T. Gambill
August 1989

ACKNOWLEDGEMENTS

The author is indebted to Dr. G. C. Frazier for his wisdom and advice in guiding this project to completion. For their counsel, the author wishes to express his appreciation to his other committee members: Dr. D. K. Dougall at the Botany Department and Dr. T. W. Wang at the Chemical Engineering Department.

Additional thanks go to Dr. D. K. Dougall for generously supplying the components and facilities needed for producing the cell growth media used in the experimental portion of this work.

The author wishes to express his appreciation to chemical engineering professor Dr. C. E. Moore and his process control graduate students who permitted extensive use of their computers and patiently tolerated crippling onslaughts of malicious software.

The present investigation would not have been possible without the help of the faculty and staff of the Chemical Engineering Department to whom the author owes his gratitude.

Most importantly, the author would like to express his appreciation to his family and friends for the love and moral support he received, for which he will always be grateful.

ABSTRACT

The study of oxygen absorption in airlift reactors has encompassed various reactor types and design configurations as well as a wide range of operational parameters and fluid compositions. Recent investigations have concentrated on airlift reactor types with liquid recycle. Many workers report the volumetric mass transfer coefficient, $k_l a$ for oxygen in terms of superficial gas velocity. Although the works are for absorption in reactors of similar design, reports from independent sources are seemingly inconsistent. In an attempt to unify in one correlation mass transfer from different systems, one report in particular relates $k_l a$ to operational parameters and gassing rates on dimensionless coordinates for two reactor types.

Three gassing rates each for three liquid compositions -- distilled water, five weight percent sucrose, and wild carrot media (pH = 4.5) -- were studied to determine the volumetric mass transfer coefficient as well as the specific interfacial area for oxygen in absorption and desorption operations of a single concentric tube airlift reactor (internal diameter = 14 cm) with sparging in the central draft tube (internal diameter = 6.3 cm). Preliminary experiments in a bubble column were performed to determine how bubble diameter related to orifice size, liquid composition and gassing rate. Air or nitrogen was sparged at relatively constant bubble size through one of three perforated plate spargers into 2300 milliliters of liquid at volumetric gas flow rates ranging up to 26.6 mls/sec.

The average liquid-phase mass transfer coefficient, $k_l a$, the specific interfacial area, a, and the liquid phase mass transfer coefficient, k_l were analysed relative to gassing rate and operational parameters. The results are compared to data and correlations produced by reporters working with reactors of similar design. The data correlated to the gassing rate alone produced results similar to other reports, but indicate that more operational parameters should be incorporated into the correlations. The data from the present work were also compared to those reported on dimensionless coordinates. The present work produced smaller dimensionless mass transfer data than the reported values such that a correlation on the data extrapolated below but parallel to the reported correlation. The disparities among data

produced in the present work and data to which they were compared have been attributed to the differences in sparging configuration and bubble size and to the lower gas phase turbulence generated in the present work.

TABLE OF CONTENTS

LIST OF TABLES

LIST OF FIGURES

FIGURE PAGE

NOMENCLATURE

$a =$	specific interfacial area	$cm^2\ cm^{-3}$
$A =$	the major semiaxis of an oblate spheroid	cm
$A_d =$	downcomer cross sectional area	cm^2
$A_i =$	area of surface i	cm^2
$A_r =$	riser cross sectional area	cm^2
$a_0 =$	coefficient defined in equation 2.7	---
$a_1 =$	coefficient defined in equation 2.7	sec cm
$a_2 =$	coefficient defined in equation 2.7	$sec^2\ cm^{-2}$
$a_3 =$	coefficient defined in equation 2.7	$sec^3\ cm^{-3}$
$B =$	the minor semiaxis of an oblate spheroid	cm
$Bo =$	Bond number	---
$c_g =$	concentration in the gas phase	$mol\ cm^{-3}$
$c_{gi} =$	concentration in the gas phase at the interface	$mol\ cm^{-3}$
$c_g^* =$	concentration in the gas phase in equilibrium with the liquid phase concentration	$mol\ cm^{-3}$
$c_l' =$	c_l observed by a dissolved oxygen probe	$mol\ cm^{-3}$
$c_l =$	concentration in the liquid phase	$mol\ cm^{-3}$
$c_{li} =$	concentration in the liquid phase at the interface	$mol\ cm^{-3}$
$c_l^0 =$	concentration in the liquid phase when absorption begins	$mol\ cm^{-3}$
$c_l^* =$	concentration in the liquid phase in equilibrium with the gas phase concentration	$mol\ cm^{-3}$
$C_1 =$	coefficient defined in equation 2.5	---
$C_2 =$	coefficient defined in equation 2.5	---
$C_3 =$	coefficient defined in equation 2.5	---
$D =$	bubble column diameter	cm
$D_b =$	mean bubble diameter	cm
$D_j =$	diameter of single bubble j	cm
$D_l =$	liquid phase diffusivity	$cm^2\ sec^{-1}$
$D_o =$	diameter of the sparging orifice	cm
$D_r =$	riser diameter	cm
$D_{sm} =$	Sauter mean bubble diameter	cm
$dv_x/dy =$	liquid flow velocity change in the y-direction	$cm\ sec^{-1}$

e	eccentricity of an oblate spheroid	---
f =	bubble formation rate	bub. min^{-1}
f_s =	stroboscopic flash rate ("stop frequency")	min^{-1}
g =	acceleration of gravity	cm sec^{-2}
G=	free energy of a system	g cm sec^{-2}
g_c =	gravitational constant	N s^2 kg^{-1} m^{-1}
Ga =	Galileo number	---
G_h =	excess free energy of a homogeneous system	g cm sec^{-2}
h =	liquid column height in equation 4.45	cm
H=	height of the ungassed liquid in the reactor	cm
H_d =	height of dispersion (gas-liquid mix)	cm
k =	proportionality constant defined by eq'n. 4.1	cm sec^{-1}
k_g =	gas phase mass transfer coefficient for oxygen	cm sec^{-1}
k_l =	liquid phase mass transfer coeff. for oxygen	cm sec^{-1}
K_l =	overall mass transfer coefficient for oxygen	cm sec^{-1}
k_la =	volumetric mass transfer coefficient for oxygen	cm sec^{-1}
m_j =	number of bubbles having diameter Dj	cm
m =	Henry's constant	---
N_a =	flux of material a	mol$cm^{-2}sec^{-1}$
N_b =	average number of dispersed gas bubbles	---
N_o =	number of orifices in the orifice plate	---
N_{O_2} =	flux of oxygen	mol$cm^{-2}sec^{-1}$
P/V =	pneumatic gassing power	N cm^{-3}
P_1 =	pressure at the top of the dispersion	N cm^{-2}
q =	gas flow rate through an orifice	cm^3 sec^{-1}
Q=	volumetric liquid flow rate	cm^3 sec^{-1}
Q_o=	gas flow rate through an orifice	cm^3 sec^{-1}
R =	radius of the "very long" tube in eq'n 4.43	cm
r =	capillary tube radius in equation 4.45	cm
Re =	Reynolds' number	---
Re_o =	gas Reynolds' number at the orifice	---
s_b =	mean bubble surface area	cm^3
Sc =	Schmidt number	---
Sh =	Sherwood number	---
St =	Stanton number	---
t =	time	sec

$T=$	characteristic response time of an electrode	sec
$u_g =$	gas superficial velocity (vol. flow/area)	cm sec^{-1}
$u_l =$	liquid superficial velocity (vol. flow/area)	cm sec^{-1}
$v =$	volume of a spherical bubble	cm^3
$v_a =$	absolute liquid velocity in the annulus	cm sec^{-1}
$v_b =$	mean bubble volume	cm^3
$V_g =$	gas volume dispersed in the liquid phase	cm^3
$V_l =$	total liquid volume	cm^3
$v_r =$	absolute liquid velocity in the riser	cm sec^{-1}
$v_{sb} =$	rise velocity of a single bubble	cm sec^{-1}
vvm =	volumetric gas flow rate on a minute basis per unit liquid volume	min^{-1}
$z=$	the distance between two successive gas bubbles rising in the liquid phase at terminal velocity	cm
$z_a =$	the apparent distance between two successive gas bubbles at stroboscopic stop frequency f_s	cm

Greek Symbols

$\alpha =$	A_d/A_r	---
$\Delta\rho =$	$\rho_l - \rho_g$	g cm^{-3}
$\Delta c =$	concentration gradient	mol cm^{-3}
$\Delta p =$	pressure gradient driving liquid flow	g cm^{-1} sec^{-2}
$\varepsilon=$	gas holdup	---
$\gamma =$	liquid surface tension	g sec^{-2}
$\mu =$	liquid viscosity	g cm^{-1} sec^{-1}
$\pi =$	3.1415927	---
$\rho_g =$	gas density	g cm^3
$\rho_l =$	liquid density	g cm^3
$\tau_{yx} =$	liquid shear force per unit area	g cm^{-1} sec^{-2}

Chemical Symbols

$e^- =$	electron

H^+ = proton

H_2O = water molecule

O_2 = oxygen molecule

SO_3^{2-} = sulfite ion

SO_4^{2-} = sulfate ion

1 INTRODUCTION

"Airlift" generally refers to the principle on which two- or three-phase bioreactors or fermentors of this type are constructed. Gas dispersed in the liquid phase rises and tends to lift and suspend the biomass that is maintained in the liquid phase. The airlift principle has received a lot of attention ever since its first application in the Scholler-IG vat more than 50 years ago (Onken, Weiland, 1983). A large number of fermentation processes of interest are aerobic; that is, the reactor must supply oxygen to the suspended biomass to maintain it. The problem is that it is difficult to fulfill the oxygen demand in a production size fermentor due to the low solubility of oxygen in the medium (Goldberg, 1985). As the biomass accumulates, the demand for oxygen usually increases until the oxygen availability becomes growth limiting (Aiba, Humphrey, Millis; 1973). Thus, it becomes increasingly important to supply oxygen to all parts of the airlift reactor.

The conventional method for oxygenating an airlift reactor is with a continuous flow stirred tank bioreactor (CSTR). The CSTR design has dominated the fermentation industry since its successful application to submerged culture systems during the antibiotic era (Margaritis, Wallace 1984). The CSTR uses a mechanical agitator to force liquid convection throughout the reactor vessel. Also, the agitator (e. g. an impeller) contributes to the redistribution of the dispersed gas bubbles.

The CSTR is not without its disadvantages. The controlled cultivation of biomass requires aseptic fermentation. In order to maintain these conditions in a CSTR, special seals are required around the rotating shaft (Margaritis, Sheppard, 1981). It has been argued that the CSTR is not cost effective; power required to run a CSTR is consumed by the mechanical agitator. More importantly, plant cells which are many times larger than bacterial cells are much more sensitive to the shearing rates produced by mechanical agitation (Townsley, Webster, 1983).

The recent development of several new cell growth technologies has led to the increased demand for a design of airlift reactors that do not utilize mechanical agitation. For example, the explosive growth of recombinant DNA technologies (Margaritis and Wallace, 1984) and the development of new

methods for producing single-cell protein from unconventional carbon sources (Onken and Weiland, 1983) have led to further investigations of bubble columns and other airlift reactor designs. Some airlift reactor designs do not have mechanical agitation and use only the power input from the dispersed gas to mix the system. Reactors of this type are more cost efficient than the CSTR because the only power input is the pneumatic power. There are also no special design considerations for a rotating shaft.

The bubble column is a common design of nonmechanically agitated airlift reactors, but the high gassing rates required for aerobic fermentation can produce plug flow of the liquid phase. However, it has been shown that the addition of baffles to the bubble column will stabilize and control the flow of liquid in the airlift reactor (De Nevers, 1968). The production of stable flow patterns in the airlift reactor reduces the oxygen mass transfer rate for a given gassing rate (Bello, Robinson and Moo-Young, 1985), but allows gassing rates to exceed those at which plug flow would occur in a bubble column (Sheppard, 1978). The result is greater mass transfer potential in airlift reactors with liquid recycle. Thus, with liquid recycle produced by the addition of baffles to bubble columns, greater mass transfer rates can be achieved.

Several designs of liquid-recycle airlift reactors have been developed, the external loop reactor, the concentric-tube reactor and the split-cylinder airlift reactor, to name a few. The production of single-cell protein and the biological treatment of wastewater are two examples of industry's utilization of the airlift principle (Kanazawa; 1975 and Hines; 1975). However, airlift reactors with liquid recycle are generally not used in industry on a large scale yet because of the lack of know-how in their design and construction. Most airlift reactor designs still operate only at the laboratory scale.

The oxygen volumetric mass transfer coefficient, $k_l a$, indicates how well a gas-liquid system is able to absorb oxygen into the liquid. The ability (k_l) of the liquid phase to transfer oxygen across the specific gas-liquid surface area (a) is reported as the product of the two ($k_l a$). The goal of many airlift investigations is to quantify $k_l a$ so that the resulting information can be used to predict how well an airlift system will be able to maintain its biomass. Extensive studies in specific areas of airlift operations have led to

numerous correlations pairing $k_l a$ with reactor hydrodynamics, distributor design or a limited number of fluid physical properties. Some investigators attempt to enhance the abilities of the liquid phase while others try to increase the surface area (or interfacial area) through which the oxygen must pass. Independent sources tend to report data that seem to be inconsistent. The variables against which $k_l a$ has been correlated do not explain the differences among data from similar systems.

One report (Bello, Robinson and Moo-Young, 1985) has summarized some important operational parameters for three prominent reactor designs. However, the results of the report do not indicate any considerations given to bubble size and changing interfacial area. Also, while the report considered liquid composition as a factor influencing mass transfer, only two media compositions were studied. Further investigations using more varied liquid compositions were recommended.

A goal of the present investigation was to perform airlift operations in one type of reactor studied by Bello et al and to determine how the mass transfer coefficient, $k_l a$, for oxygen is effected by changes in gassing rate. In addition, the interfacial area would be controlled in an attempt to show whether k_l or a was the major contributing factor producing the changes in the $k_l a$ product. Also, three different liquid compositions -- ranging from distilled water to a full plant cell culture media -- would be studied to indicate to what extent mass transfer is effected by liquid composition. The reactor type studied was chosen because it was the most readily available design for the range of operational parameters of interest. The reactor type chosen for the present work was of the single concentric tube design and had gas sparged in the central draft tube.

2 BACKGROUND AND SIGNIFICANCE

Airlift operations lift and suspend biomass, but more importantly supply the aerobic biomass with life-sustaining oxygen. The first application of the airlift principle in fermentation is reported to date back more than 50 years (Onken and Weiland, 1983). Other examples of airlift applications on the industrial scale include the production of fodder yeast from sulphite cellulose waste liquor using reactors with and without liquid flow baffles. Modern day technology has developed methods for producing single cell protein from unconventional carbon sources (Onken and Weiland, 1983) using airlift reactors. The biochemical industry is thus becoming increasingly interested in reactors of the airlift type.

2.1 Bubble Column:

Bubble columns utilize the airlift principle and can be considered airlift reactors. In fact, mass transfer in bubble columns has been studied quite thoroughly. Reports correlating bubble column mass transfer coefficients and mixing characteristics to liquid physicochemical properties, gas holdup and gassing rates are numerous. Schugerl, Lucke and Oels (1977) investigated the effects of individual liquid constituents on $k_l a$ in two connected bubble columns. Both bubble columns were about 4 m high and had diameters of 14 cm. The experiments performed in the columns were continuous liquid flow operations that absorbed oxygen in one column and desorbed oxygen in the other. A relatively wide assortment of alcohol and sugar solutions were studied at various operating parameters and designs. Some of the researchers' relevant conclusions were that in bubble columns with perforated plate spargers (1) 2% glucose had greater mass transfer capabilities than the alcohol/salt solutions studied; (2) both the glucose solutions and the alcohol/salt solutions produced larger $k_l a$ values than pure water systems. Also, the increase in $k_l a$ due to added liquid constituents was due more to a change in interfacial area, a, than an increase in the liquid phase mass transfer coefficient, k_l. A correlation was reported relating $k_l a$ to superficial gas velocity, u_g and mean bubble diameter, D_b

$$k_l a = 0.0023 \left(\frac{u_g}{D_b}\right)^{1.58} \quad (2.1)$$

where superficial fluid velocity is defined by the volumetric fluid flow rate divided by the area through which the fluid passes.

Another group of researchers, Akita and Yoshida (1973) studied a 15.2 cm ID bubble column that was 400 cm in height to determine the effects that liquid physical properties had on gas holdup and $k_l a$ in absorption in aqueous solutions. The resulting correlation was reported in dimensionless form:

$$ShaD = 0.6\ Sc^{0.5}\ Bo^{0.62}\ Ga^{0.31}\ \varepsilon^{1.1} \quad (2.2)$$

$$Sh = k_l D/D_l$$
$$Sc = \mu/(\rho_l D_l)$$
$$Bo = gD^2\rho_l/\gamma$$
$$Ga = gD^3\mu/\rho_l$$

Akita and Yoshida (1974) later studied bubble size, interfacial area and k_l in the same systems to develop empirical correlations for k_l :

$$k_l = 0.5\ g^{5/8}\ D_l^{1/2}\ \rho_l^{3/8}\ \gamma^{-3/8}\ D_b^{1/2} \quad (2.3)$$

$$\frac{u_g}{gD} = 8.887 \left(\frac{\gamma}{gD^2\rho_l}\right)^{-1/8} \left(\frac{\mu_l^2}{gD^3\rho_l^2}\right)^{1/12} \varepsilon^{10/9} \quad (2.4)$$

where D_b is the surface-averaged bubble diameter. Equations 2.2 and 2.3 correlate liquid physical properties, bubble diameter, column diameter and superficial gas velocity to $k_l a$ and k_l, but are limited to bubble column operations for the given column design. These works are examples of numerous reports thoroughly investigating mass transfer in bubble columns.

2.2 Significant Reactor Designs with Controlled Liquid Flow:

More promising airlift reactor designs have been developed that

enhance oxygen transfer to the liquid phase. The airlift fermentor designed with liquid recycle has been the subject of many studies that have revealed its advantages over the bubble column. Better mixing, better heat transfer and higher obtainable rates of mass transfer are among the more prevalent of the benefits of inducing liquid recycle in airlift operations.

Several internal and external loop airlift reactor designs have been developed that produce controlled liquid flow and increase the achievable mass transfer rates over bubble columns by producing controlled liquid flow. In designs of this type, some examples of which are shown in Figure 2.1, the energy of the distributed gas phase is used to force the recycle of the liquid phase. The internal loop or draft tube design uses one or more concentric tubes. Gas is sparged through either the annular space between the tubes or through the center of the innermost tube. For two concentric tubes, the gas is usually dispersed into the area between the center tube and the next larger concentric tube. External loop designs consist of two columns attached at the base and top. Sparging occurs in one of the two columns. Airlift reactors designed with liquid recycle control flow rates by forcing the liquid up through the gassed portion of the reactor (riser) and down through the ungassed portion (downcomer). The types of sparger designs studied include injector nozzles, ejector nozzles, and concentric ring configurations; but common methods of dispersing the gas are with one or more single orifice tubes, a perforated plate or a porous plate.

2.3 Literature Review:

The airlift reactor designs with recycle are reported to have several advantages over the conventional bubble column designs. For example Onken and Weiland (1980) studied an airlift fermentor with an external loop design. A thorough investigation reported gas and liquid velocities, gas holdup, liquid mixing and oxygen transfer coefficients in a 10 m high vessel. For similar gas velocities, Onken and Weiland reported lower volumetric mass transfer coefficients in airlift designs with liquid recycle than in bubble columns. However, they also concluded that airlift reactors can be operated at gas velocities at least two or three times greater than bubble columns. Therefore, it is possible to supply greater amounts of oxygen to the liquid phase even for

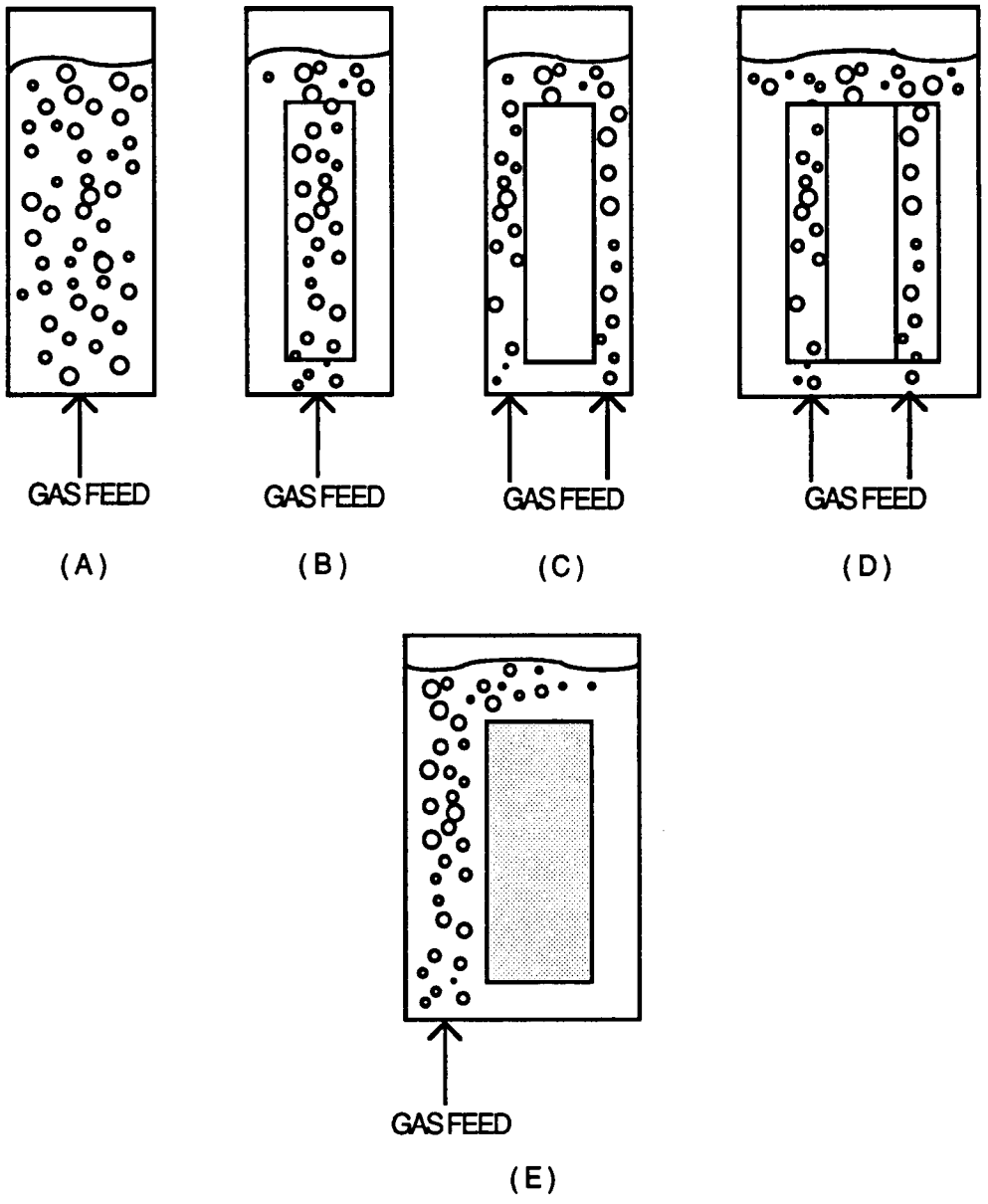

Figure 2.1: Common airlift reactor designs: (a) bubble column, (b) single concentric draft tube (sparging in the central draft tube), (c) single concentric draft tube (sparging in the annulus), (d) double concentric draft tube and (e) external loop.

very tall reactors. In addition, Onken and Weiland concluded that higher liquid velocities achievable in the recycle designs produce greater heat transfer capabilities than those possible in bubble columns.

Sheppard (1978) studied mass transfer and mixing times in concentric draft tube designs of airlift reactors. Gas holdup, mass transfer coefficients and mixing times were measured for two sizes of orifice tubes (DIA = 1.27 mm and DIA = 3.81 mm) in a reactor with four draft tube configurations: no draft tubes (bubble column); single draft tube (sparging in the central tube); single draft tube (sparging in the annulus); and double draft tube (see Figure 2.1). Two advantages of draft tube designs in airlift reactors reported by Sheppard (1978) are: (1) draft tubes in airlift reactors stabilize the liquid circulation patterns and (2) they allow gas rates to exceed the point at which plug flow would normally occur in bubble columns. Using a reactor with a working height of 32 cm, Sheppard concluded that operations using the smaller size orifice increased gas holdup and that the mass transfer coefficients increased correspondingly by 10 to 20 percent. Also, above a superficial gas velocity u_g =1.6 cm/sec the k_la values in the bubble column were lower than the reactors with one or two draft tubes. Sheppard's correlation for k_la in the reactors with the 1.27 mm DIA orifice tube spargers depended only on superficial gas velocity

$$k_la = 33.3\ u_g^2 \qquad (2.4)$$

where k_la is in hr^{-1} and u_g is in cm/s. Use of the smaller diameter orifices also prevented a plateauing effect observed in the mass transfer - gassing rate relation measured in the reactors with 3.81 mm DIA orifice tube spargers.

Sheppard also found that sparger design affected mass transfer. One of the conclusions reached by Schugerl et al in their work with bubble columns was that porous plate distributors produce higher k_la values than perforated plates for pure water as well as culture media. For a given reactor type, indications are that changes in reactor design and dimensions will affect mass transfer characteristics. Numerous researchers have studied various reactor types and designs using different fluid combinations and sparging rates to

determine volumetric mass transfer coefficients under specific conditions. A summary of some of these works is offered in Figure 2.2 and Table 2.1 (Bello, Robinson and Moo-Young, 1985). With regard to aeration rates, all of these workers recorded a direct relationship between mass transfer and superficial gas velocity.

Although this method of reporting is common (k_la versus pneumatic power input or superficial gas velocity) it is evident that it is not reliable for quantitative comparison of k_la values obtained from independent sources. There are inconsistencies among the reported values, even for those of similar reactor type and design. For example, curve 11 (Kastanek; 1976) represents a bubble column with a 0.10 m diameter, a working height between 0.6 m and 1.2 m, and air dispersed in water by a perforated plate. Curve 12 (Yoshida and Akita; 1965) represents a bubble column with a 0.15 m diameter, a working height between 0.9 and 1.82 m, and air dispersed in water by a single orifice. The equipment from which curves 11 and 12 were derived are very similar, but the curves themselves differ greatly. At a gassing power of 0.08 kW/m^3 there is a 60 percent difference in the mass transfer coefficients; at 0.3 kW/m^3 there is a 100 percent difference. The operating or design variables to which these differences are due are not identifiable from the data as presented.

2.4 A More General Approach:

Bello, Robinson and Moo-Young (1985) have included additional operating parameters in relating mass transfer characteristics to reactor type and design to bring the seemingly conflicting reports together. Cross sectional areas of both the riser (A_r) and the downcomer (A_d), as well as the superficial liquid velocity, u_l, are the additional operating parameters of interest. Bello et al worked with three of the previously mentioned airlift reactor types: bubble column, single concentric tube and external loop. Experiments were performed in batch airlift operations with two different liquid compositions: tap water and a coalescence inhibited solution of 0.15 M NaCl. Air or nitrogen was sparged through a perforated plate with 1.02 mm DIA holes designed on a triangular pitch (for the external loop design) or through a ring sparger, containing fifteen 1.02 mm DIA holes (for the

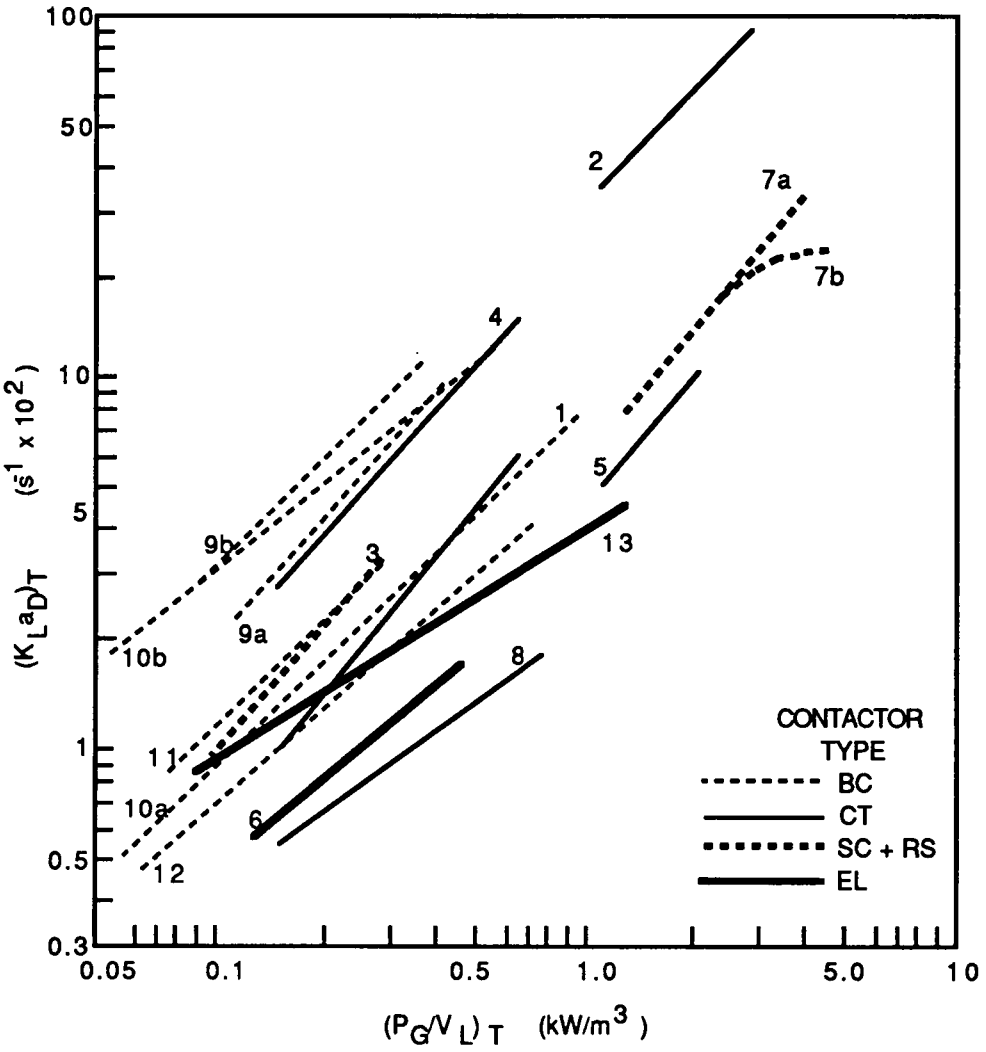

Figure 2.2: Overall volumetric oxygen mass transfer coefficients in airlift contactors and bubble columns. $(P_G/V_L)_T$ is the total pneumatic power input per unit gas-liquid dispersion volume. See Table 2.1 for legend. Source: Bello, Robinson, Moo-Young (1985).

Table 2.1: Summary of Significant Airlift Reactor Investigations[a]

No.	Ref.	Type[b] of Contactor	A_d A_r	D or D_r (m)	$H_d(H_o)$ (m)	Liquid	Type of Sparger
1	El-Gabbani	CT	0.29	0.095	1.65 (1.47)	Water	Ring
2	Fukuda	CT	0.38 - 1.67	0.20	1.82 (1.00)	Na_2SO_3 Solution	Perforated plate
3	Gasner	RS	1.0	0.20x0.30	1.22 (0.71)	Na_2SO_3 Solution	U-shaped
4	Botton et al	CT	1.14	0.19	1.30	Na_2SO_3 Solution	Concentric ring
5	Hatch	CT	1.12	0.30	2.8[c] (2.6)	Ferm'n Medium	Ring
6	Lin et al	EL	0.11	0.15	3.0 (2.87)	Ferm'n Medium	Perforated plate
7	Orazem and Erickson	SC	1.0	0.15	1.22 (1.07)	Na_2SO_3 Solution	Single hole
		SC (two stage)	1.0	0.15	0.66 (0.51) each stage	Na_2SO_3 Solution	Single hole
8	Sinclair and Ryder	CT	3.0	0.15	0.23 (0.18)	Water	Concentric ring
9	Schugerl et al	BC	--	0.14	4	Water	Perforated plate
10	Deckwer et al	BC	--	0.20	7.23	Water	Cross of nozzles
		BC	--	0.15	4.4	Water	Porous plate
11	Kastanek	BC	--	0.10	0.6-1.2	Water	Perforated plate
12	Yoshida and Akita	BC	--	0.15	0.9-1.82	Water	Single hole
13	Onken and Weiland	EL	0.25	0.10	8.5 (8.5)	Water	Porous plate

[a]From Bello, Robinson, Moo-Young (1985)

[b]BC, bubble column; EL, external-loop airlift contactor; CT, concentric-tube airlift contactor; RS, rectangular split airlift contactor; SC, split cylindrical airlift contactor.

[c]Clear liquid height.

concentric tube design). In the concentric tube design the annulus was the riser. A range of downcomer-to-riser cross sectional area ratios was studied: $0.11 \leq A_d/A_r \leq 0.69$ for the external loop reactors and $0.13 \leq A_d/A_r \leq 0.56$ for the concentric tube designs.

Supporting previous reports, Bello et al found a direct relationship between k_la and gassing rate. In addition, they concluded that liquid circulation plays an important part in oxygen transfer to the liquid phase. For specified liquid-phase physicochemical properties, column configuration, sparger type and gassing rate superficial liquid velocity, u_l is established by A_d/A_r. Bello et al also incorporated the total dispersion height in a dimensionless correlation:

$$St = C_1(u_g/u_l)^{C_2}\ (1 + A_d/A_r)^{C_3} \qquad (2.5)$$

where

$$St = \frac{(k_la)_r\, H_d}{(u_l)_r} \qquad (2.6)$$

and $(k_la)_r = k_la$ in the riser

Equations 2.5 and 2.6 were found to best fit the data when C_1, C_2 and C_3 were 1.99, 0.87 and -1, respectively for water and 2.57, 0.92 and -1, respectively for 0.15 kmol/m^3 NaCl. Both sets of the data were represented by an equation with a correlation coefficient of 0.97 and constants C_1, C_2 and C_3 of 2.28, 0.90 and -1, respectively. The data reported by Bello, Robinson and Moo-Young are shown graphically in Figure 2.3. This correlation yields a more general understanding of the interactions of the parameters that govern airlift operations, although it does not include liquid properties explicitly such as viscosity and surface tension. However, Bello et al recommend further investigations into the effects of liquid physicochemical properties.

Liquid circulation rates (e. g. u_l) are not as easily measured as gassing rates and reactor dimensions (e.g. u_g, A_d/A_r). Recognition of the liquid superficial velocity as a relevant factor in mass transfer in airlift reactors with liquid recycle has spurred studies into the empirical measurement as well as the theoretical prediction of liquid circulation rates in these reactors. Jones (1985) has developed a theoretical model for predicting liquid

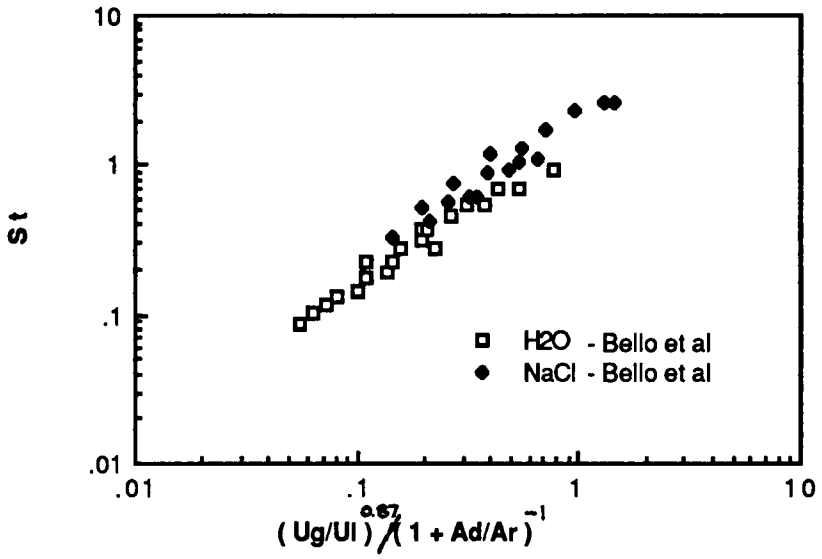

Figure 2.3: Dimensionless correlation of data generated by Bello et al in airlift reactors of concentric tube and external loop designs (Bello, Robinson, Moo-Young, 1980).

circulation velocities in concentric tube airlift reactors. The predicted values were compared with data generated in a single concentric tube airlift reactor with sparging in the central draft tube. The 60 liter reactor had a 25 cm diameter and was operated with five different draft tubes that had diameters of 4.4, 7, 9.6, 12.1 and 14.6 cm. Air was sparged through a perforated plate having twenty-five 2.4 mm DIA holes on a triangular pitch.

Equation 2.7 is the result of Jones' derivation.

$$a_3 v_a^3 + a_2 v_a^2 + a_1 v_a + a_0 = 0 \qquad (2.7)$$

where $$a_0 = -2\frac{P_1}{\rho_1}\left(\log_e\left(1 + \frac{\rho_1 H g}{P_1}\right)\right)\left(\frac{\mu}{1 + \alpha^2}\right)$$

and $$a_1 = 0$$

$$a_2 = v_{sb}$$

$$a_3 = \alpha = A_d/A_r$$

$$v_{sb} = \sqrt{\frac{2\gamma}{\rho_1 D_b} + \frac{g D_b}{2}}$$

The liquid velocity in the central draft tube (riser), v_r can be calculated from a mass balance on the liquid in the vessel. Equating the absolute mass flow rate up the riser ($v_d A_d$) with the absolute mass flow rate down the annulus ($v_a A_r$) results in

$$v_r A_r = v_a A_d \qquad (2.8)$$

or $$v_r = \alpha v_a \qquad (2.9).$$

The absolute liquid velocity in the riser, v_r, is related to the superficial liquid velocity, u_l, by the liquid fraction in the riser: $1 - \varepsilon$, where ε is the gas holdup. In other words,

$$u_l = (1 - \varepsilon) v_r \qquad (2.10).$$

Thus, Jones' (1985) derivation reports the superficial liquid velocity, u_l can be calculated from the absolute liquid velocity in the annulus, the riser and downcomer cross sectional areas, and the gas holdup in the draft tube:

$$u_l = \frac{(1 - \varepsilon)A_d v_a}{A_r} \qquad (2.11).$$

Jones concluded that for an air-water system liquid circulation velocity is dependent on the inlet gas flow rate and the draft-tube diameter. Actual u_l values were measured during airlift operations and compared to those predicted by the model. Jones concluded that the model developed was satisfactory for the small draft-tubes (DIA $\leq$ 12.1 cm) at low gas flow rates (q $\leq$ 400 ml/s), but for higher gas flow rates and larger draft tube diameters the model predicted increasingly excessive liquid circulation.

Bello's empirical correlation -- with the addition of the liquid circulation velocity as a dependent variable -- seems to explain the behavior of airlift reactor mass transfer in terms of operational parameters. Additional similar studies into the effects of liquid physicochemical properties, as recommended by Bello et al, would apparently complete the mass transfer picture. There are, however, other design considerations that affect mass transfer (e. g., sparger design). Specific interfacial area (a) is highly dependent on bubble size. Bello et al did not explain how bubble size and specific interfacial area were effected by changing operational parameters in their work. A method of estimating bubble diameter reported by Treybal (1980) suggests that there may have been a considerable change in the size of the bubbles produced in Bello's work. Using Treybal's (1980) method it is possible to estimate that Bello's bubble size changed by about a factor of two in his experimental flow rate range (Figure 2.4), but the study does not indicate whether considerations have been given to the effects of changing bubble size. For the airlift reactor studies performed by Bello et al it is not known to what extent each of k_l and a effect $k_l a$.

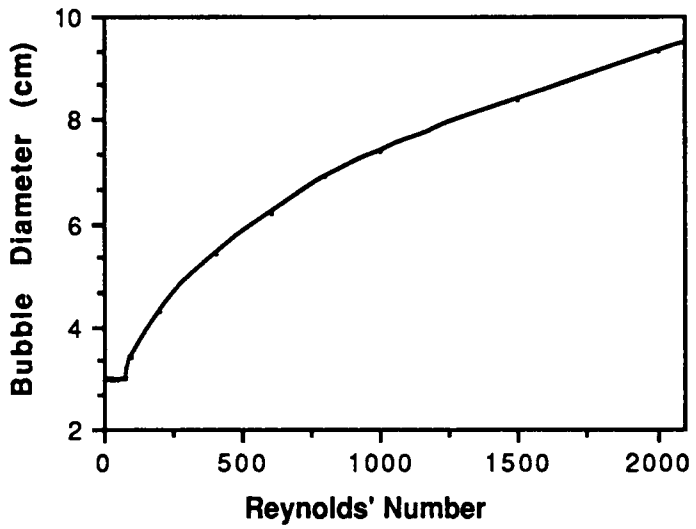

Figure 2.4: Bubble diameter as a function of gassing rate (Reynolds' number) as predicted by Treybal (1980). Calculated bubble diameters are based on an air-water system and an orifice diameter of 1.0 cm.

3 RESEARCH OBJECTIVES

The main purpose of the present work is to measure transient state oxygen mass transfer characteristics in batch operations of a laboratory scale single concentric tube airlift type reactor containing air dispersed in aqueous solutions by a perforated plate. It was intended that volumetric mass transfer coefficients ($k_l a$) for oxygen absorption and desorption be compared to the system's operating parameters and liquid phase physicochemical properties. The study was also designed to determine the extent to which the liquid phase oxygen mass transfer coefficient, k_l, and also the interfacial area, a, change with changes in media composition.

Values for $k_l a$ and a were also determined from airlift operations at selected gas flow rates and fixed liquid compositions. Changes in gas flow rate were produced by changing the number of orifices in the sparger plate while holding constant the pressure gradient across the plate, thereby maintaining constant bubble size. Three gas flow rates were studied for each change in liquid phase composition. The three liquid compositions studied were pure water, five weight percent sugar in water and a complete plant cell growth medium containing sugars, salts and growth hormones.

For a given gassing rate and liquid phase composition $k_l a$ values were calculated from transient oxygen probe response data. The values for a were calculated from photographic measurements of gas holdup and stroboscopic bubble diameter measurements; $k_l a$ values were extracted from those obtained for $k_l a$ and a. In such ways were the mass transfer characteristics of the airlift reactor measured with the physical and chemical variables of the system for comparisons among themselves and to data produced by previous workers.

4 THEORY

4.1 Measuring the Volumetric Mass Transfer Coefficient for Oxygen:

4.1.1 The film theory:

In the study of aerobic fermentation of plant or mammalian cells one of the factors essential to successful production is the supply of oxygen to the living cell. In airlift fermentors without mechanical agitation -- such as bubble columns and concentric tube reactors -- the source that stirs the continuous liquid phase is the same source that supplies the oxygen to the biomass: the dispersed gas phase. The Film Theory models the transfer of oxygen from the bulk gas phase to the biological cell in the following manner: oxygen must diffuse from the bulk of the dispersed gas phase bubble through the theoretical gas film, across the gas-liquid interface, through the theoretical liquid film and finally through the bulk liquid to the biological cell. Through each phase of diffusion the oxygen molecule meets resistance. The driving force for mass transfer is the concentration gradient.

The equation from which an expression for the coefficient k_l is derived relates the steady state flux, N_a, of material a to the concentration gradient, ΔC, in the direction of mass transfer. The proportionality of the two variables is the mass transfer coefficient, k, such that

$$N_a = -k\,\Delta C \qquad (4.1)$$

The resistance to the mass transfer of a is proportional to the inverse of k, 1/k.

In steady state oxygen absorption the flux of oxygen, N_{O_2}, to the gas-liquid interface equals the oxygen flux through the liquid film. Mathematically (Bailey and Ollis, 1986)

$$\begin{aligned} N_{O_2} &= k_l\,(c_l - c_{li}) \quad \text{liquid side} \\ &= k_g(c_g - c_{gi}) \quad \text{gas side} \end{aligned} \qquad (4.2)$$

The interfacial concentrations, c_{gi} and c_{li}, in equations 4.2 are not measurable by available technologies. A means of solving this problem is by using the equilibrium proportionality between liquid phase concentration and gas

phase concentration of pure substances, e. g. Henry's law

$$c_{gi} = m\, c_{li} \tag{4.3}$$

where m is Henry's constant. It has been shown experimentally that interfacial diffusional resistance is nearly always zero in absorption and desorption operations (McCabe and Smith, p. 719, 1976). Therefore, Henry's law still applies for the transient values of gas and liquid phase interfacial concentrations, c_g^* and c_l^*, respectively

$$c_g^* = m\, c_l^* \tag{4.4}$$

If the overall mass transfer coefficient is K_l then the oxygen flux at steady state is (Bailey and Ollis, p. 464, 1986)

$$N_{O_2} = K_l(c_l^* - c_l) \tag{4.5}.$$

Mathematical manipulations of equations 4.2 through 4.5 lead to the following relation:

$$\frac{1}{K_l} = \frac{1}{k_l} + \frac{1}{mk_g} \tag{4.6}.$$

Materials that are sparingly soluble have Henry's constant values much greater than unity. The solubility of oxygen in aqueous solutions at standard temperature and pressure is on the order of only 10 parts per million (ppm). Also, k_g is typically considerably larger than k_l (Bailey and Ollis, p. 464, 1986). Thus,

$$\frac{1}{k_l} \gg \frac{1}{mk_g} \tag{4.7}$$

and

$$\frac{1}{K_l} \cong \frac{1}{k_l} \tag{4.8}.$$

In other words, most of the resistance to mass transfer is in the liquid phase

and K_l can be approximated with k_l. Equation 4.5 then becomes

$$N_{O_2} = k_l (c_l^* - c_l) \qquad (4.9).$$

4.1.2 Methods of measuring dissolved oxygen concentration:

Experimental measurement of mass transfer coefficients is simplified if the oxygen transfer rate per unit volume of reactor, dc_l/dt , is considered instead of the flux per unit interfacial area, N_{O_2}. Determination of k_la is the ultimate goal; this usually requires some method of measuring transient state liquid oxygen concentration, c_l. The sulphite oxidation method has been used extensively in airlift studies to measure liquid phase oxygen concentration. This method depends on the oxidation of sodium sulfite to sulfate in the presence of catalytic metal ions such as Co^{2+} (Bailey and Ollis, p. 470, 1986):

$$SO_3^{2-} + \frac{1}{2}O_2 \quad \rightarrow \quad SO_4^{2-} \qquad (4.10).$$

However, the kinetics of the rate of oxidation of sulfite solutions to sulfate are complex (Bailey and Ollis, p. 470, 1986). The method of experimental measurement requires extracting and analyzing samples of the reactor liquid phase during absorption or desorption.

Another method of measuring liquid phase oxygen concentration has been developed and packaged in a "dissolved oxygen probe." The dissolved oxygen probe utilizes oxygen oxidation and reduction and requires an electrical current. The chemical reaction on which this method is based is (Leeds and Northrup, 1981)

$$O_2 + 4H^+ + 4e^- \leftrightarrow 2H_2O \qquad (4.11).$$

A cathode reduces the oxygen (forward reaction) while an anode simultaneously oxidizes the oxygen (reverse reaction). A third electrode establishes an electrochemical potential that is sustained by a power source. The three electrodes are retained in a gas permeable membrane that allows the apparatus to be submerged in the liquid to be analyzed. Diffusion and

chemical reaction occurs until the oxygen concentrations on both sides of the membrane are equal and balanced. There is no depletion of the liquid phase oxygen concentration since there is no net reaction. The current necessary to sustain this equilibrium can then be converted to a electrical display. The dissolved oxygen probe simplifies the measurement of liquid phase oxygen concentration in that it transmits a continuous signal that may be connected to a recording device even while it is submerged in the liquid phase. Thus, the liquid phase oxygen concentration may be measured quickly and accurately.

Theoretically, as conditions approach those of equilibrium the oxygen concentration in the bulk liquid approaches that at the liquid interface. Consequently, for oxygen absorption with unchanging gas phase oxygen concentration: as elapsed time grows large, a value for c_l^* may be estimated with the dissolved oxygen probe by measuring the value approached by c_l.

4.1.3 Volumetric mass transfer coefficient, k_la:

It is possible to show that k_la values may be extracted from dissolved oxygen concentration vs. time data. A steady state material balance on the oxygen in the liquid phase produces an expression for oxygen absorption to the liquid phase. The time-change in the oxygen concentration in the liquid is the product of the interfacial area and the oxygen flux across that area:

$$\frac{dc_l}{dt} = N_{O_2}a \qquad (4.12).$$

For oxygen absorption $N_{O_2}a = k_la\,(c_l^* - c_l)$. Equation 4.12 then becomes

$$\frac{dc_l}{dt} = k_la\,(c_l^* - c_l) \qquad (4.13).$$

Mathematical manipulation reveals

$$\frac{dc_l}{(c_l^* - c_l)} = k_la\,dt \qquad (4.14).$$

Integrating over the time required to saturate a completely desorbed solution

produces

$$-\ln(c_l^* - c_l) = k_l a \cdot t + \text{constant} \qquad (4.15).$$

Initially (t=0), the bulk liquid oxygen concentration is zero ($c_l = 0$) so the constant in equation 4.15 is $-\ln(c_l^*)$:

$$-\ln(c_l^* - c_l) = k_l a \cdot t - \ln(c_l^*) \qquad (4.16).$$

or

$$-\ln\left(\frac{c_l^* - c_l}{c_l^*}\right) = k_l a \cdot t \qquad (4.17).$$

Equation 4.17 is a linear expression that, when transformed to a coordinate system with time as the abscissa and $-\ln(1-c_l/c_l^*)$ as the ordinate, describes a line of slope $k_l a$.

For oxygen desorption from a saturated liquid phase $N_{O_2} a = k_l a\,(c_l - c_l^*)$. Equation 4.12 then becomes

$$\frac{dc_l}{dt} = k_l a\,(c_l - c_l^*) \qquad (4.18).$$

The mathematical manipulation and integration follow the logic of the absorption case until

$$-\ln(c_l^* - c_l) = k_l a \cdot t + \text{constant} \qquad (4.19).$$

Initially $c_l = c_{lo}$ and the constant in equation 4.19 is $\ln(c_{lo} - c_l^*)$. The resulting linear expression is

$$-\ln\left(\frac{c_l - c_l^*}{c_{lo} - c_l^*}\right) = k_l a \cdot t \qquad (4.20).$$

If pure nitrogen is used to desorb the oxygen, then $c_l^* = 0$. Equation 4.20 simplifies to

$$-\ln\left(\frac{c_l}{c_l^*}\right) = k_l a \cdot t \qquad (4.21).$$

The line described here also has slope $k_l a$ with time as the abscissa and $\ln(c_l/c_{l_0})$ as the ordinate.

It is important to also consider the size of the dissolved oxygen probe response time constant, T, relative to the system response time (e. g. $1/k_l a$). Nakanoh and Yoshida (1976) derived an expression similar to equation 4.20, but included the time constant T:

$$\ln(c_l^* - c_l') = \ln[e^{-k_l a.t} - k_l a \cdot T e^{-t/T}] + \ln[c_l^*/(1-k_l aT)] \quad (4.22)$$

where c_l' is the c_l observed by a dissolved oxygen probe. They worked with an oxygen probe with T < 10 seconds ($1/T > 0.1\ s^{-1}$) and measured $k_l a$ values all less than $0.1\ s^{-1}$. Nakanoh and Yoshida explain that the straight line portion of the curve generated by equation 4.22 is practically parallel to the line generated by equation 4.17. However, if any of their $k_l a$ values had been greater than $0.1\ s^{-1}$, then it would have been necessary to solve equation 4.22 with known values of c_l', t and T.

Thus, the volumetric mass transfer coefficient ($k_l a$) for oxygen may be approximated using a dissolved oxygen meter for both absorption and desorption. To extract the value of k_l it would be necessary to measure the value of the interfacial area per unit volume of reactor.

4.2 Measuring Specific Interfacial Area:

4.2.1 Bubble formation at an orifice:

Gas dispersed into a liquid by a single orifice has been studied extensively by many reporters. Perry (1973) reports three regimes for gas flow through an orifice: (1) single bubble, (2) intermediate and (3) jet. The single bubble regime (Re < 200) produces bubbles in a regular and uniform matter. Bubbles in this regime have a theoretical diameter calculated by equating the bouyant force on the immersed bubble to the force due to surface tension. The resulting equation predicts a bubble diameter independent of gas

flow rate (Treybal, 1980):

$$D_b = \sqrt[3]{\frac{6D_o\gamma}{g\Delta\rho}} \qquad (4.23).$$

According to Perry (1973), the intermediate gas flow regime covers the remainder of the laminar gas flow range, or about from Re = 200 to Re = 2100. Treybal (1980) gives a complicated correlation that can be used to estimate the lower bound of this regime; it equates the gas flow rate at the orifice to fluid properties and orifice diameter. In this regime, as gas flow rate increases the bubbles tend to increase in size and form in chains, but are still fairly uniform in size at constant gas flow rate. Perry (1973) mentions a range of gas flow rates over which bubble size decreases in size owing to liquid currents that shear the bubble prematurely and produce a minimum bubble size at some particular gas rate. Bubble size in the upper part of this regime is dependent primarily on orifice size and liquid properties. For air-water systems operating in the intermediate regime, Treybal(1980) reports

$$D_b = 0.0287\ D_o^{1/2} Re_o^{1/3} \qquad (4.24)$$

where D_b and D_o are in meters; and for other gases and liquids

$$D_b = Q_o^{0.4} \sqrt[5]{\frac{72\rho_l}{\pi^2 g\Delta\rho}} \qquad (4.25).$$

For most gases and liquids $\rho_l >> \rho_g$ or $\Delta\rho = \rho_l$. It is interesting to note that with this consideration equation 4.25 simplifies to

$$D_b = 1.49 g^{-0.2} Q_o^{0.4} \qquad (4.26).$$

According to equation 4.26 -- in contrast to Perry's report -- bubble diameter is not significantly affected by fluid properties.

The jet regime is the third gas flow rate range reported by Perry.

Turbulent gas flow occurs in this range of Reynolds numbers (Re > 10 000). As the gas flow rate increases the emerging gas stream takes on the appearance of a continuous jet. The dispersed phase actually consists of irregularly shaped bubbles with a random size distribution and rapid swirling motion. Reports in this regime are contradictory; bubble size is difficult to measure experimentally and theoretically hard to predict.

The single-bubble and intermediate regimes include the full range of gassing rates for which flow is laminar. Another work (Leibson et al) studied the complete laminar flow range (for single submerged orifices in an air-water bubble column) and developed a correlation of bubble diameter as a function of orifice diameter and Reynolds number:

$$D_b = 0.18\ D_o^{1/2} Re_o^{1/3} \qquad (4.27).$$

4.2.2 Rise path and velocity:

In a stagnant liquid, as a single bubble leaves the dispersing orifice it is initially spherical but deforms and accelerates in a manner depending on its size. The terminal velocity achieved by the bubble occurs when the bouyant force on the bubble equals the drag force. Treybal(1980) reports four methods for estimating the terminal rise velocity of bubbles in liquids. The methods are separated by bubble size: (1) $D_b < 0.7$ mm; (2) $0.7 < D_b < 1.4$ mm; (3) 1.4 mm $< D_b < 6$ mm; and (4) $D_b > 6$ mm. In the first region the rising bubbles are spherical and behave like rigid spheres. The terminal velocity for these bubbles can be estimated using

$$V_t = \frac{g D_b^2 \Delta \rho}{18 \mu_l} \qquad (4.28)$$

As the diameter of the bubbles in regions three and four increases the bubbles begin to deform and oscillate under the dynamic forces. The bubbles have a random distribution of shapes and tend to rise following a zigzag or helical path at a terminal velocity that, for low viscosity liquids, can be approximated by (Treybal, 1980)

$$V_t = \sqrt{\frac{2\gamma g_c}{D_b \rho_l} + \frac{g D_h}{2}} \qquad (4.29).$$

Region two acts as a transition region between one and three. The gas within bubbles of this size tends to circulate as the bubbles rise allowing the bubble to 'slip' easier through the liquid and achieve a higher terminal velocity. Treybal does not give a correlation for bubbles with sizes in the second region, but suggests a linear relationship between terminal velocity and bubble diameter in the range between the upper-diameter bound of region one and the lower-diameter bound of region three.

4.2.3 Coalescence:

Many bubble columns and most airlift reactors use a number of submerged orifices to disperse the gas phase. A problem arises when predicting or measuring bubble sizes in systems with numerous orifices in that bubbles from adjacent orifices will tend to interact; also, nearby bubbles may cause liquid turbulence that interferes with a rising bubble. One result of these interactons is that two or more bubbles may join (coalesce) or split (redistribute) into a different number of bubbles of different size. Systems with designs that result in coalescence and redistribution are studied with the goal of determining the mean or effective diameter of the dispersed gas bubbles. Rise velocities of swarms of bubbles tend to be smaller than those of single bubbles because of crowding (Treybal; 1980).

Several methods have been developed for predicting mean bubble diameter for bubble swarms either from theoretical equations or empirical correlations. The Sauter mean bubble diameter D_{sm} represents a surface-averaged value for the bubble diameter (Bailey and Ollis, 1986, p. 482):

$$D_{sm} = \frac{\sum m_j D_j^3}{\sum m_j D_j^2} \qquad (4.30)$$

Estimating D_{sm} using this equation requires counting and measuring each bubble dispersed in the liquid phase. Other researchers have reported correlations for D_{sm} in terms of pneumatic gassing power (P/V), fluid

properties (eg. ρ_g, ρ_l, μ_l and γ) and gas holdup, ε. For example, Calderbank (1958) reported a correlation for gas dispersed in a liquid electrolyte:

$$D_{sm} = 2.25 \frac{\gamma^{0.6}}{\rho_l (P/V)^{0.4}} \varepsilon^{0.4} \left(\frac{\mu_g}{\mu_l}\right)^{0.25} \qquad (4.31).$$

Similar correlations have been developed for gases in viscous liquids, gases in alcohol solutions and other systems as a means of estimating the average bubble diameter.

An airlift reactor with more than one sparger orifice does not always produce bubble coalescence and redistribution. Designs placing orifices close together coupled with operating gassing rates in the jet regime will result in bubble interactions. If adjacent orifices are separated and gassing rates are in the intermediate regime then coalescence and redistribution are preventable. To prevent interactons among bubbles, Treybal (1980) recommends adjacent and horizontal orifices be separated by at least thrice the bubble diameter.

4.2.4 Stroboscopic size measurements:

Under controlled conditions bubble-size distribution can be narrowed to the extent that mean bubble diameter may be estimated by the size of the spherical bubble immediately downstream of the sparging orifice. One method of estimating bubble diameter was used by Leibson et al (1956), who studied bubble formations in single submerged orifices in a 20.5 cm ID bubble column operating in an air-water system. Leibson's method used utilized the 'fairly uniform' formation of bubbles in the intermediate gas flow regime. A narrow distribution of bubble sizes allowed the mean bubble diameter to be estimated by the size of the spherical bubble immediately downstream of the dispersing orifice. At intermediate gas flow rates, Leibson et al used stroboscopic equipment to visibly "stop" the motion of the bubble forming at the orifice. This technique assumes that the flash frequency required to "stop" the bubble is numerically equivalent to the bubble formation rate. Therefore, the gas flow rate through the orifice (q) is equal to the product of the bubble formation frequency (f) and the mean bubble volume (v_b). Leibson et al state this equality in the form:

$$v_b = \frac{q}{f} \qquad (4.32).$$

The average bubble diameter of the spherical bubble can be calculated directly using equation 4.33.

$$D_b = \sqrt[3]{\frac{6v_b}{\pi}} \qquad (4.33).$$

Leibson et al mentioned minute bubbles besides the regularly formed bubbles but assumed the volume and surface contributions of these were negligible.

One consideration of stroboscopic measurement of bubble diameter concerns matching the bubble formation frequency with the stroboscopic flash frequency. There is a probability of error associated with the frequency at which the bubbles appear to be stopped. Further references to this frequency will be made in terms of the "stop frequency, f_s." As the bubbles being dispersed at formation rate, f, leave the orifice they accelerate until the achieve terminal velocity V_t. At any height greater than that point at which V_t has been reached the distance, z, between any two successive bubbles is f/V_t for regular and uniform bubble formation. At stop frequencies $f_s \leq f$ the apparent distance, z_a between bubbles will be equal to z. If $f_s > f$ then $z_a < z$. The following equation applies:

$$z_a = \frac{f}{f_s} z \qquad (4.34).$$

As f_s increases, that value of f_s that last produces $z_a = z$ satisfies $f_s = f$. Hence, studies using stroboscopic techniques to measure mean bubble diameter should investigate this area to assess the validity of the results.

4.2.5 Interfacial area:

In mass transfer studies the goal of estimating the mean bubble diameter is to use it in calculating the surface area through which mass transfer occurs. The interfacial area per unit volume (specific interfacial

area), a, is the ratio of the interfacial area to the total volume of the reactor (liquid and gas). For a single spherical bubble this ratio can be symbolized mathematically:

$$a_b = \frac{s_b}{v_b} \tag{4.35}$$

where $$s_b = \pi D_b^2 \tag{4.36}$$

and $$v_b = \frac{\pi}{6} D_b^3 \tag{4.37}$$

or $$a_b = \frac{6}{D_b} \tag{4.38}.$$

The transition from single bubble volume to total reactor volume is performed by multiplying a_b by the gas holdup, ε:

$$a = \varepsilon \cdot a_b \tag{4.39}$$

or $$a = \frac{6\varepsilon}{D_b} \tag{4.40}$$

The result is the specific interfacial area per unit reactor volume.

For nonspherical bubbles a different equation for a_b must be used. For example, deforming bubbles may take on the shape of an oblate spheroid. The surface area of an oblate spheroid bubble is represented by the equation (Beyer, W.H., 1978)

$$s_b = 2\pi A^2 + \left(\frac{\pi B^2}{e}\right) \ln\left(\frac{1+e}{1-e}\right) \tag{4.41}$$

where $$v_b = \frac{4}{3} AB^3,$$

$$e = \frac{\sqrt{A^2-B^2}}{A}$$

ln = logarithm base 2.71828

The variables a_b and a would be calculated using the same methods as for the spherical bubble (equations 4.35 and 4.39). Mathematical application of these equations to bubbles is not plausible because experimental measurement of A and B would be difficult at least and would only be applicable to oblate spheroid

bubbles. Other equations would be needed to calculate a_b for other variously shaped bubbles. It would then be necessary to use a surface-averaging method like the Sauter mean bubble method.

4.3 Liquid Physicochemical Properties:

Many of the reports in the available literature (Bello et al, 1980; Akita and Yoshida, 1973,1965) relate mass transfer coefficients as well as bubble diameters to liquid physicochemical properties among other things (e.g. operational parameters). Liquid properties such as density, viscosity and surface tension can be found in most of these correlations. Several techniques have been developed for measuring each of these properties. Liquid density is, of course, the simplest to measure: a quantity of the liquid under study is measured for volume and mass, the quotient of these producing the desired value. Values for liquid viscosity and surface tension, however, are not as easily measured.

4.3.1 Viscosity:

For steady laminar fluid flow viscosity, μ, is defined as the proportionality constant that relates the flow-driving force per unit area to the change in flow velocity in the direction normal to flow. In fact, Newton's law of viscosity states that the shear force per unit area, τ_{yx}, is proportional to the negative of the local velocity gradient (Bird, Stewart and Lightfoot, 1960). Mathematically,

$$\tau_{yx} = -\mu \frac{dv_x}{dy} \tag{4.42}$$

Hagen and Poiseuille developed an equation using Newton's law of viscosity. The equation describes steady state laminar flow of an incompressible Newtonian fluid in a "very long" tube of length L and radius R. The result is the Hagen-Poiseuille equation (Bird, Stewart, Lightfoot; 1960):

$$\mu = \pi \frac{\Delta P R^4}{8QL} \tag{4.43}.$$

Liquid viscosity may therefore be empirically measured in long thin tubes using this equation as long as the asumptions of the Hagen-Poiseuille derivation apply.

4.3.2 Surface tension:

Surface tension is a measure of the surface free energy of a material. A body of liquid at constant temperature and pressure will seek the equilibrium state of lowest free energy. In the absence of external forces this liquid will seek the conformation of minimum surface area. According to Shoemaker et al (1970) the free energy, G, of a system having variable surface areas A_1, A_2, . . .A_i can be expressed

$$G= \quad G_h + \Sigma\gamma_i A_i \tag{4.44}$$

where γ_i is the surface tension of surface i. Shoemaker et al report the following derivation:

> "Let a liquid with surface tension γ_1 be in contact with a solid with surface tension γ_2, with which it has an interfacial tension γ_{12}. Under what circumstances will a liquid film freely spread over the solid surface and 'wet' it? This will happen if, in creating liquid-solid interface and an equal area of liquid surface at the expense of an equal area of solid surface, the free energy of the entire system decreases:
>
> $$\gamma_1 + \gamma_{12} - \gamma_2 < 0 \tag{16}$$
>
> If we have a vertical capillary tube which dips into a liquid, a film of the liquid will tend to run up the capillary wall if condition (16) is obeyed. Then, in order to reduce the surface of the liquid, the meniscus will tend to rise in the tube. It will rise until the force of gravity on the liquid in the capillary above the outside surface $\pi r^2(h + r/3)\rho g$, exactly counterbalances the tension at the circumference, which is $2\pi rg$. . . .Thus we obtain
>
> $$\gamma_1 = \quad \frac{1}{2}(h + \frac{r}{3})\, r\, \rho\ g" \tag{4.45}$$

However, if conditions are such that equation 4.45 does not apply, then the value for h will not be consistently the same for repetitive measurements. It is necessary when measuring surface tension using a vertical capillary tube to allow the liquid column to approach its equilibrium height from both above and below this position. Shoemaker et al assure that equation 4.45 is "almost certainly valid" for aqueous solutions in carefully cleaned glass capillary tubes.

Methods are available for measuring the volumetric mass transfer coefficient as well as the interfacial area of oxygen dispersed in aqueous solutions. Liquid density, viscosity and surface tension are three of the most prevalent properties found in correlations of airlift reactor studies pairing mass transfer and liquid physicochemical properties. A simple laboratory scale experimental apparatus may be used to measure each of the liquid physicochemical properties as described above.

5 MATERIALS AND METHODS

5.1 Materials:

Preliminary experiments in a bubble column of rectangular cross sectional area (12.6 cm x 13.9 cm) were performed using a single orifice tube to disperse the gas phase in one liter of liquid (~5.7 cm working height above the orifice). Four orifice sizes (0.028, 0.036, 0.056 and 0.066 cm) were studied in each of four liquid compositions over a range of gas flow rates (up to 1.35 ml/sec) to determine the orifice size and Reynolds number range necessary to produce a desired bubble size. A General Radio Company strobotac (1531 AB) measured the bubble formation rate immediately downstream of the orifice at each gas flow rate. The liquid compositions studied were distilled water (H2O), five weight percent sucrose in distilled water (SUC) and Wild Carrot Media 4 (WCM-4) with a pH of 4.5 (Table 5.1). For a given liquid composition and sparger orifice size the mean bubble diameter was calculated using equations 4.32 and 4.33 for increasing rates of gas flow until bubble formation at the orifice became too erratic for stroboscopic measurement. Thus, a plot of bubble diameter versus gas flow rate (or Reynolds number) was generated for each liquid composition. The results of these experiments were used to guide the design of the orifice plates of the airlift fermentor (see Appendix I).

Airlift operations were performed in a single concentric draft tube airlift reactor (Figure 5.1). The reactor was made of a 39.2 cm long plexiglas tube with an inner diameter of 14 cm. The draft tube had an inner diameter of 6.35 cm, a wall thickness of 0.64 cm and was suspended by six plexiglas cylindrical pegs (DIA = 0.95 cm). Nitrogen from a tank or air from a compressor passed through a 0.023 cm DIA choke orifice, into the sparger plenum, through the perforated plate and into the liquid. The sparger (Figure 5.2) was a 4.4 cm long plexiglas tube with a 6.35 cm inner diameter. The plenum was filled with spherical glass beads (mean DIA = .62 cm) to reduce its volume and to disperse the gas flow equally among the plate orifices. Gas was dispersed through the central draft tube by one of three 0.16 cm thick aluminum perforated plate spargers (five, nine or 19 orifices @ 0.066 cm DIA).

Table 5.1: Components of Wild Carrot Medium (pH =4.5)*

Component	Concentration	
	mg/L	mM
ammonium chloride, NH_4Cl	320.04	6.00
magnesium sulfate, $Mg_4SO{\cdot}7H_2O$	185	0.75
calcium chloride, $CaCl_4$	166	1.50
potassium phosphate, dibasic, K_2HPO_4	87.1	0.50
disodium EDTA	18.6	0.05
ferrous sulfate, $FeSO_4{\cdot}7H_2O$	13.6	0.05
manganous sulfate, $MnSO_4{\cdot}H_2O$	7.0	0.04
zinc sulfate, $ZnSO_4{\cdot}7H2O$	4.0	0.01
boric acid, H_3BO_3	2.4	0.04
ammonium molybdate, $(NH_4)_6Mo_7O_{24}{\cdot}4H2O$	0.01	8.0E-06
potassium iodide, KI	0.38	2.0E-03
cupric sulfate, $CuSO_4{\cdot}5H_2O$	0.015	6.0E-05
thiamine HCl	3.0	9.0E-03
2,4-dichlorophenoxyacetic acid	2.5	0.01
sucrose	20,000	58.43
potassium succinate	3885.8	20.0

*The WCM-4 components and mixing equipment were generously donated by Dr. D. K. Dougall of the University of Tennessee, Knoxville Botany Department.

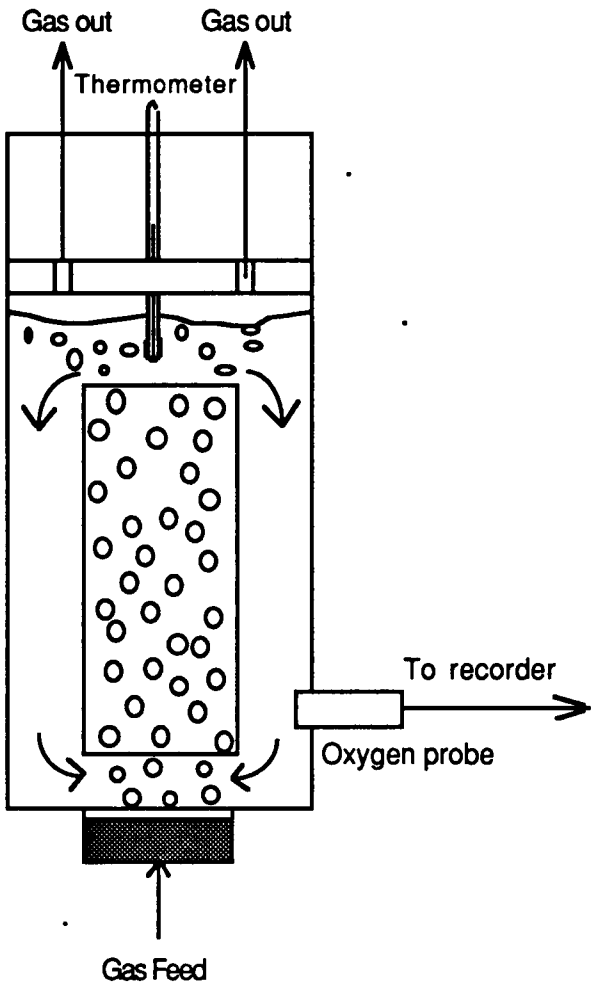

Figure 5.1: Single concentric tube airlift reactor used to study transient state batch oxygen absorption and desorption operations.

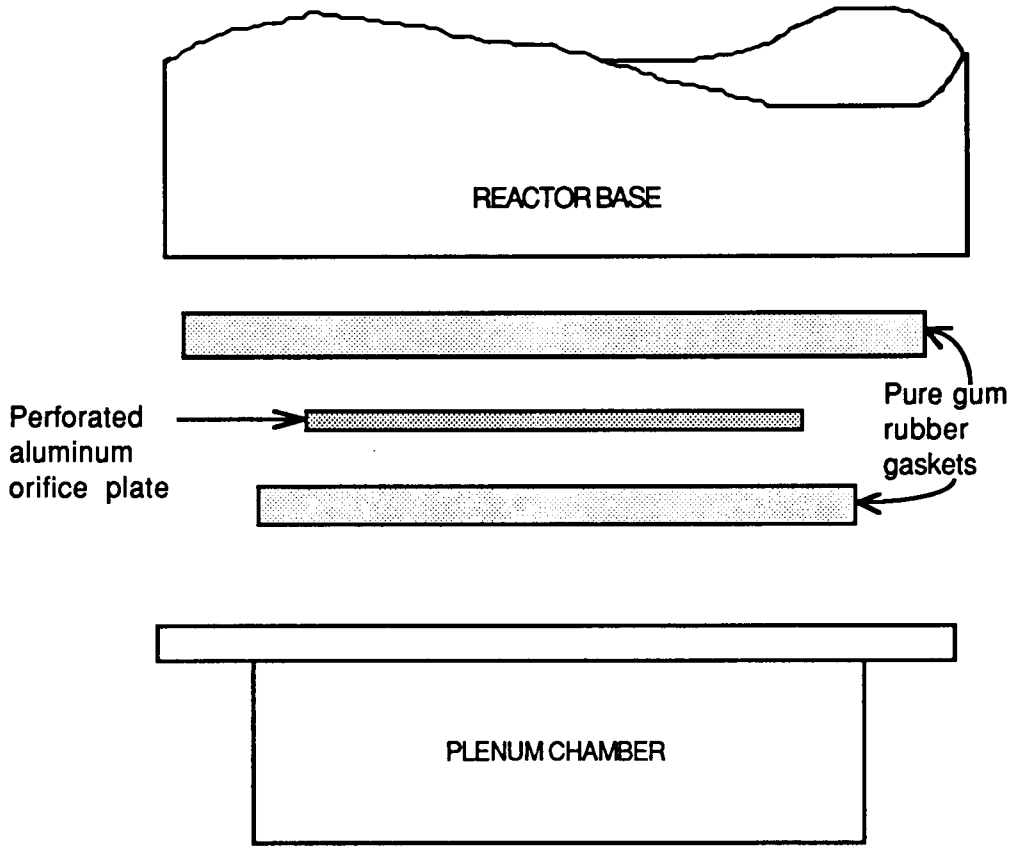

Figure 5.2: Design of sparger used in the airlift reactor studies. The perforated plate had five, nine or 19 orifices each with diameter 0.066 cm. The plenum chamber was filled with glass beads (mean DIA = 0.62 cm).

Three gas flow rates were studied for each of three liquid composition. The change in total gas flow rate was accompanied by a proportional change in the number of orifices in the perforated plate. Thus, the gas flow rate through each orifice -- and the Reynolds' number at each orifice -- was held relatively constant for a given liquid composition. For the distilled water (H2O) the gas flow rate through an orifice was approximately 0.98 ml/sec. Thus, for the H2O solution three perforated plates with five, nine and 19 orifices were used to produce three total gas flow rates of about 4.9 ml/sec, 8.8 ml/sec and 18.6 ml/sec, respectively. The gas flow rate through an orifice for the SUC and WCM-4 solutions were approximately 1.28 ml/sec and 1.35 ml/sec, respectively. The number of orifices per perforated plate was designed based on the operating Reynolds' number, the orifice diameter and the desired total gas flow rates (0.1 to 0.4 vvm).

Treybal (1980) recommends separating adjacent orifices by at least thrice the bubble diameter to prevent interference among bubbles. Therefore, orifices on a perforated plate were arranged according to the bubble diameters likely to be produced at the selected orifice Reynolds' numbers. The results of the orifice plate design are shown in Figure 5.3. The orifices on the five- and nineteen-orifice plates were arranged on a triangular pitch while those on the nine-orifice plate were arranged on a circular pitch. The sparger was bolted to the base of the reactor with six equally spaced 3/16 inch bolts. Two pure gum rubber gaskets (0.35 cm thick) seated the perforated orifice plate to the reactor and the sparger.

A General Radio Company strobotac (1531 AB) measured the bubble formation rate of each orifice. Photographs taken with a NIKON camera (55 mm) were used to measure the number of bubbles suspended in the liquid phase. Dissolved oxygen liquid concentration was measured by a general purpose electrode connected to a Leeds and Northrup 7932 portable dissolved oxygen meter. The probe electrode was supported 8.2 cm (at the center line) from the base of the reactor. Output from the probe was in parts per million (ppm) and was recorded on a Heath single pen strip chart recorder (SR-205).

The response time of the electrode/probe apparatus was measured using two beakers of distilled water. The electrode was submerged in a beaker of distilled water. Nitrogen was sparged through a length of rubber tubing into

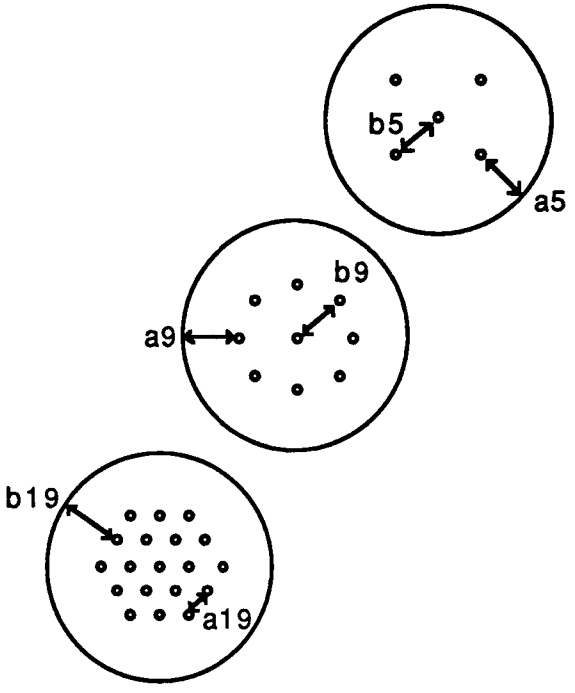

Figure 5.3: Perforated plate orifice design used for airlift reactor operations. Dimensions in centimeters: a5 =1.90, b5 = 2.54, a9 = 1.90, b9 = 2.54, a19 = 1.43, b19 = 1.90.

the stirred water until the probe meter displayed 0.00 ppm dissolved oxygen in the liquid. The electrode was then "instantaneously" moved to and submerged in a beaker of distilled water that had been vigorously stirred for a sufficiently long time (about 20 minutes) to reach its equilibrium dissolved oxygen concentration. The amount of time for the electrode to measure 95 percent of the total concentration change (t_{95}) was measured as approximately 30 seconds.

The reactor had a clear liquid working height of 20.2 cm (2300 ml) and was held at approximately 25°C (±1.5°C). Three gassing rates were studied for each liquid composition. For a given liquid composition bubble diameter was controlled by increasing the number of perforated plate orifices in proportion to the gassing rate, thereby maintaining a relatively constant gas Reynolds' number at each orifice and insuring that gas bubble size remained essentially constant as the gas flow rate increased.

5.2 Volumetric Mass-Transfer Coefficient (k_la):

The liquid-phase mass transfer coefficient product (k_la) was calculated from transient oxygen probe response data at a given gassing rate and liquid phase composition. Appendix II contains the details of the collected data and the relevant calculations. As nitrogen was sparged through the reactor (desorption) the probe measured the decreasing dissolved oxygen concentration in the liquid phase until a reasonable approximation of steady state was reached. When the reading became steady the sparging gas was changed to air (absorption) and the probe output was recorded until a new steady state approximation was reached. An experimental run for a given liquid composition and gassing rate was complete when the oxygen had been alternately desorbed and absorbed twice. The chart recorder had been previously calibrated (to 0.46 inches per ppm) and the chart output rate was known (e. g. 0.2 inches per min). Digitizing computer software (CALCOMP) was used to translate the chart recorder output to coordinates of oxygen ppm vs. time. The chart recorder output was then replotted according to equation 4.17 with expected results for absorption similar to Figure 5.4.

The initial nonlinear section of Figure 5.4 is due to the response time lag of the system. The best fit line through the linear portion of Figure 5.4 has

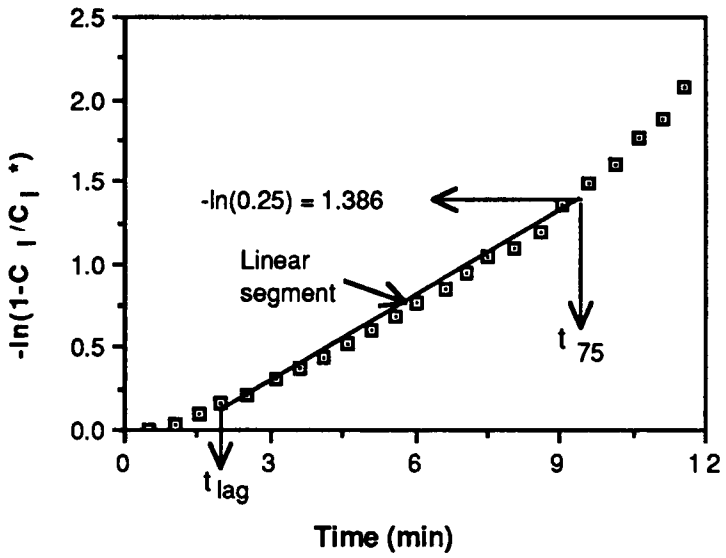

Figure 5.4: Expected results of plotting the chart recorder output for absorption using the format of equation 4.17.

slope equal to k_la. The slope k_la was measured from the end of the response lag time of the system to t_{75}. The variable t_{75} is defined in this work as that time at which 75 percent of the total response change in dissolved oxygen concentration has occurred. Thus, for a given liquid composition and gassing rate the volumetric liquid phase mass transfer coefficient was calculated and averaged for all absorption runs and separately for all desorption runs.

5.3 Interfacial Area:

5.3.1 Bubble diameter:

The interfacial area per unit volume, or specific interfacial area, was calculated as a function of the bubble diameter and the gas holdup using equation 4.40. Bubble formation in the gas flow regime studied -- Perry's intermediate regime (Re < 2100) -- is uniform and regular. Therefore, it can be assumed that the bubble size distribution was narrow and the average bubble size can be represented by the bubble immediately downstream of (above) the sparger orifice. The present work studied Reynolds' numbers from 120 to 180 and assumed a narrow bubble distribution, but held the Reynolds' number constant for a given liquid composition. The bubble diameter used in this work refers to the diameter of the spherical bubble immediately above the sparger orifice. For the airlift reactor as well as the bubble column operations the strobotac measured the bubble formation rate (f) for a given orifice gas flow rate (q). Equations 4.32 and 4.33 were then used to calculate bubble diameter.

Tests were performed to ensure that the bubble formation rate measured by the strobotac was not a multiple of the actual bubble formation rate. There was an inverse relationship between the strobotac stop frequency and the visible distance between successively formed bubbles. The strobotac frequency at which this inverse relation ended was the frequency chosen as the actual bubble formation rate.

5.3.2 Gas holdup:

The Nikon camera was used to take three pictures of the number of bubbles suspended in the liquid phase during oxygen absorption and

desorption. The photographs were developed by Thompson Photo Products. The bubbles in each photograph were counted by hand. The average number for the three photos was used in equations 5.1a and 5.1b to calculate gas holdup, ε:

$$V_g = V_b \cdot N_b$$
$$= \frac{q}{f} \times N_O \times N_b \qquad (5.1a)$$

$$\varepsilon = \frac{V_g}{V_g + V_l} \qquad (5.1b)$$

Bubble diameter and gas holdup were then used in equation 4.40 to calculate specific interfacial area for the absorption or desorption run. The resulting two values for the absorption run were averaged, as were the two values for the desorption run.

5.3.3 Liquid phase mass transfer coefficient:

Thus, the overall mass transfer coefficient and the interfacial area were both independently measured. The quotient of the two values is the liquid phase oxygen mass transfer coefficient, k_l . This value was calculated using equation 5.2,

$$k_l = \frac{k_l a}{a} \qquad (5.2).$$

Equation 5.2 was the last equation needed to calculate the mass transfer variables. Some of the liquid physicochemical properties were also measured.

5.4 Liquid Physicochemical Properties:

For each of the liquid compositions (H2O, SUC or WCM-4) the liquid density, viscosity and surface tension were measured. The mass of a given volume of liquid was measured and both quantities were recorded. The liquid density was calculated as the quotient of the two measured values. The liquid viscosity was measured with an apparatus built to utilize the Hagen-Poiseuille

equation (eq. 4.43). The apparatus is shown in Figure 5.5. An 84.6 cm long glass capillary tube (ID = 0.0614 cm) was secured horizontally to the base of a vertical cylinder. The cylinder (ID = 6.35 cm) was filled with the liquid to be measured such that the driving force for flow was the hydrostatic pressure due to the head of liquid. The flowing liquid exited the base of the cylinder, passed through a 1 cm long section of TYGON tubing (ID = 0.5 cm) and entered the capillary tube. Hot concentrated nitric acid was used to clean the capillary tube, which was stored in distilled water at room temperature when not in use. Liquid leaving the capillary tube was collected in a ten milliliter graduated cylinder. The time required to collect a volume of liquid was measured as was the volume collected. Each experiment was performed three times for each liquid composition. The viscosity was calculated as the average of the three values obtained when the measured quantities were used in equation 4.43. Calibration of the viscosometer capillary tube diameter was based on the literature value of the viscosity of distilled water at 298 K ($\mu \cong 0.009$ g/cm sec).

The surface tension of each liquid was measured with the apparatus shown in Figure 5.6. The 38.2 cm long vertical precision bore capillary tube, purchased from Lab Glass, Incorporated, had an inner diameter of 0.0203 cm. The capillary tube was partially immersed vertically in the liquid. A column of liquid climbed the inside of the tube until the force of gravity equalled the force due to the surface tension. The column was allowed to approach its equilibrium height several times from above and below. If the equilibrium heights were not independent of the direction of approach then the apparatus was disassembled, the capillary tube was washed in hot concentrated nitric acid and the experiment was repeated. When not in use the capillary tube was stored in distilled water at room temperature. The height of the column of liquid was measured using an R-18J cathetometer purchased from Sargent-Welch. The liquid density, column height and the capillary tube inner radius were used in equation 4.45 to calculate the surface tension. This procedure was used for each of the three liquid compositions studied.

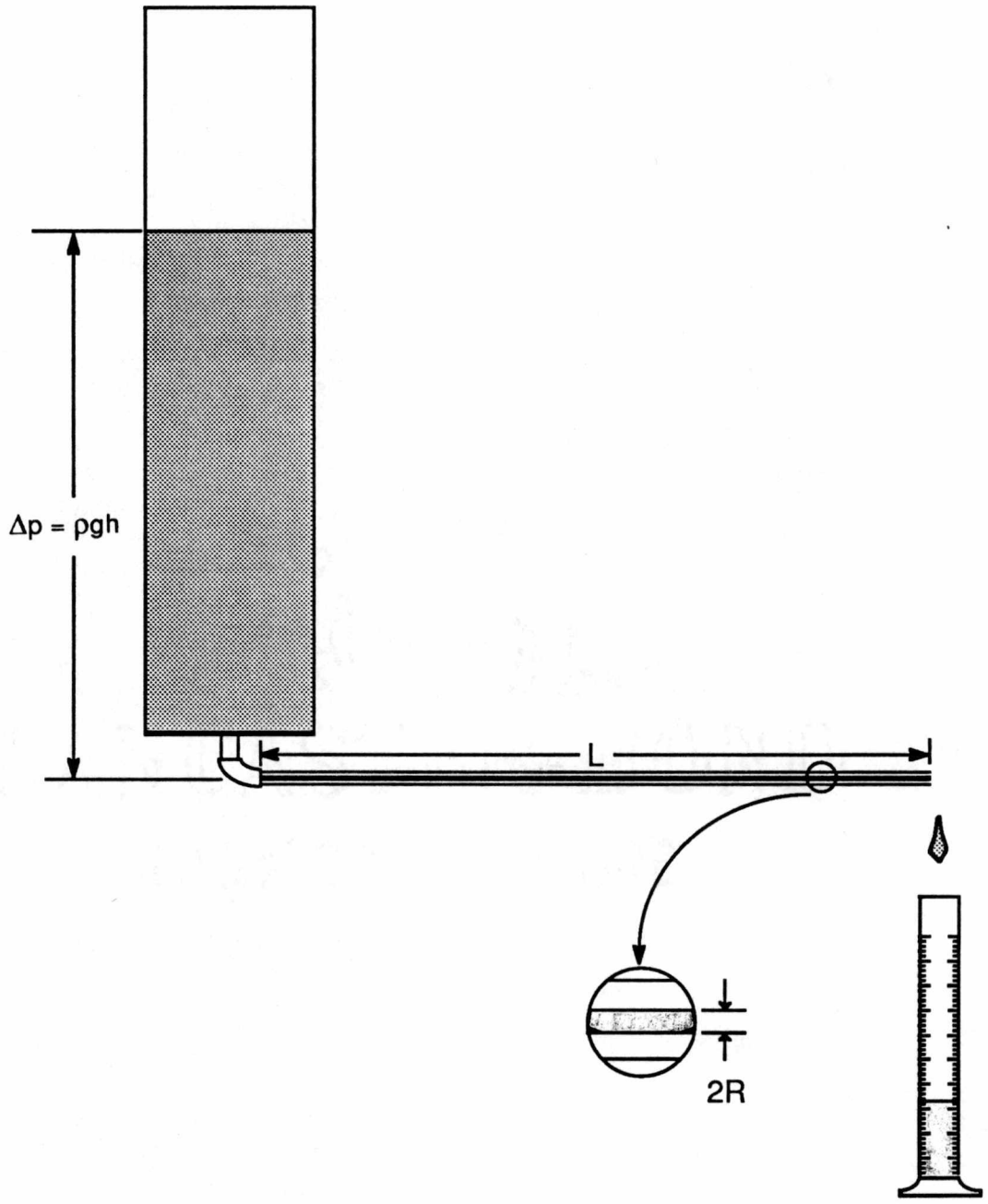

Figure 5.5: Apparatus used for measuring viscosities of aqueous solutions (H2O, SUC and WCM-4) according to the Hagen-Poiseuille equation 4.43.

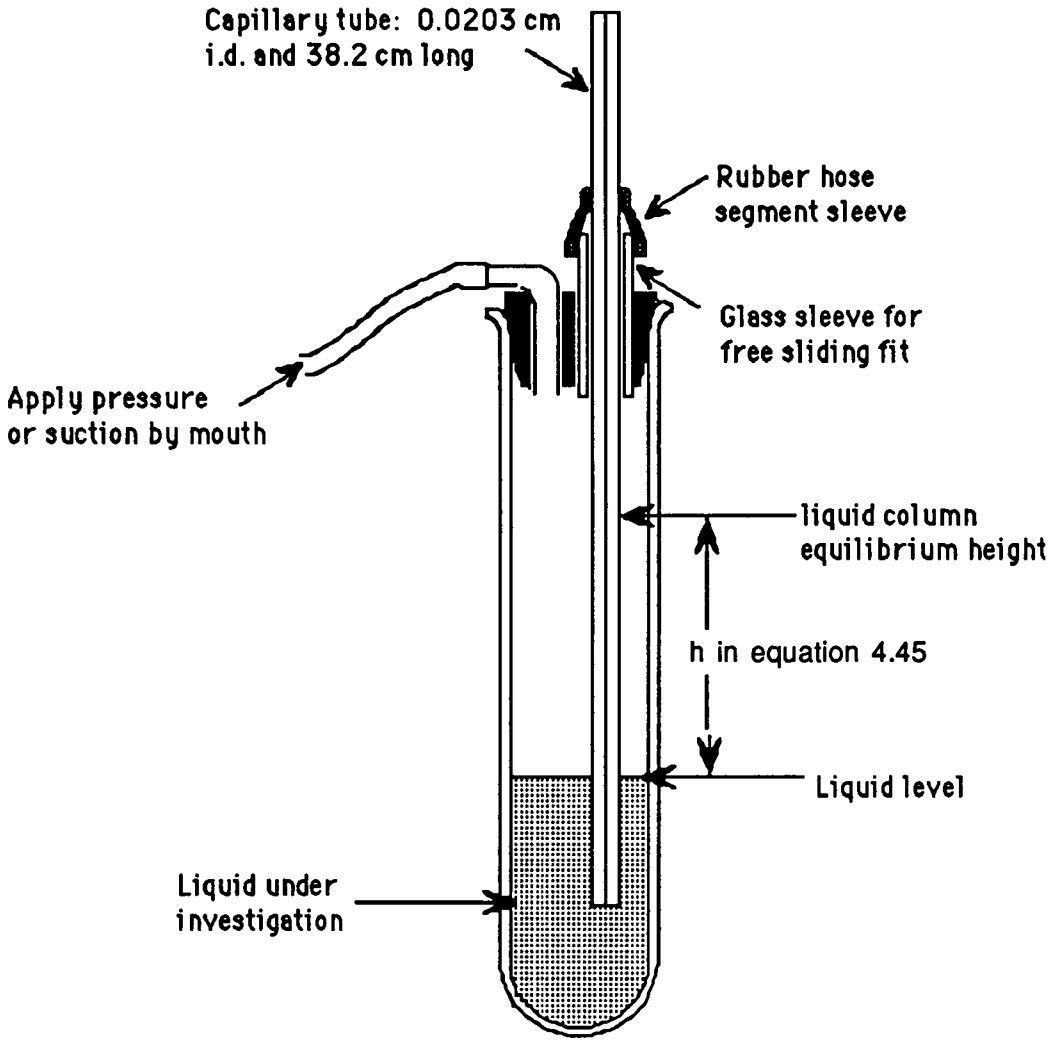

Figure 5.6: Apparatus for measuring surface tension by the method of capillary rise. A Sargent-Welch cathetometer was used to measure h.

6 RESULTS AND DISCUSSION

6.1 Liquid Physicochemical Properties:

Mass transfer rates in a single concentric tube airlift reactor were studied for a variety of liquid compositions and a range of gas flow rates. The volumetric mass transfer coefficient, k_la, and also the specific interfacial area, a, were determined for conditions that controlled the bubble size of the dispersed gas phase. Prior to the airlift reactor investigations, some of the physicochemical properties of the liquids were measured to compare to the data that would be generated in the airlift reactor.

A table of the measured liquid physicochemical properties is shown in Table 6.1. The properties of all three liquid compositions -- distilled water (H2O), five weight percent sucrose (SUC) and Wild Carrot Media 4 (WCM-4) -- were measured at approximately the same temperature (24.5 ° C to 25.5 ° C). Total difference in densities among solutions were about two percent. Liquid viscosity increased 23 percent from H2O to WCM-4 and seven percent from WCM-4 to SUC. Surface tension increased less than one percent for the three solutions.

The increase in viscosity from H2O to WCM-4 to SUC may be attributed partly to the increase in dissolved sugar concentration (zero percent, two weight percent and five weight percent, respectively). The large ionic concentration of the WCM-4 solution (pH = 4.5) may have contributed to the liquid viscosity and surface tension. The differences in densities were not significant.

In fact, the differences among all measured liquid physicochemical properties was not appreciable to the extent that a correlation derived with them would be indicative of actual mass transfer/liquid property interactions. Such a correlation would be more a measure of the accuracy of experimental procedure and the sensitivity of the apparatus used. Therefore, speculations on the effects of liquid physicochemical properties on mass transfer characteristics in the airlift reactors in this work are restricted to qualitative analysis.

Table 6.1: Measured Physicochemical Properties of Liquids[a] Studied in Airlift Reactor Experiments.

Liquid	$\rho \left(\frac{g}{cm^3}\right)$	$\mu \left(\frac{g}{cm \cdot sec}\right)$	$\gamma \left(\frac{dyne}{cm}\right)$	T (°C)
H2O	0.99	0.0090	72.1	25.0
SUC	1.01	0.0119	72.4	24.5
WCM-4	1.00	0.0111	72.7	24.5
Air or N_2[b]	1.21 $x10^{-3}$	0.00018	-	25.0

[a]H2O = distilled water; SUC = five wt percent sucrose; WCM-4 = wild carrot cell media (pH = 4.5).

[b]The gas densities were based on the ideal gas law at 25°C and one atmosphere; the gas viscosities were taken from a nomograph given by McCabe and Smith (1976).

6.2 Bubble Column Results:

One goal of the mass transfer investigations was to sparge the gas into the liquid phase under conditions that would control the size of the dispersed gas phase bubble. There was not, however, sufficient information available on the operating conditions necessary to produce uniform and regular formation of bubbles from a perforated plate sparger in a concentric tube airlift reactor. It was necessary to generate bubble diameter data using a system of less complicated design: a single submerged orifice in a bubble column.

The goal of studying single orifice bubble formation in the bubble column was to measure diameters of bubbles dispersed in various liquid compositions for a range of gas flow rates and orifice sizes. The results were used in the airlift operations to control bubble size during mass transfer. The regular and uniform formation of bubbles was necessary that stroboscopic methods could be used to measure bubble diameters. For a given liquid composition, bubble diameters were calculated for increasing gas flow rates until irregular and nonuniform bubble formation was observed.

Gas flow rate effects on bubble size were similar for all liquid compositions studied. Equating bubble bouyant force to the force due to surface tension (single bubble regime - Perry, 1973) predicts bubble diameters independent of gas flow rate (equation 4.23). In the range of gas flow rates that designate the single bubble regime bubble diameters were found to vary directly with gas flow rate (see Figure 6.1). For the smaller orifice sizes studied (diameters of 0.028 cm and 0.036 cm) bubble formation became erratic at the beginning of the intermediate gas flow regime, and thus there is no bubble diameter information in this regime. For the larger orifice sizes studied (0.056 cm and 0.066 cm) bubble diameters in the intermediate gas flow regime were approximately constant for increasing gas flow until erratic bubble formation prevented bubble size measurement. The bubble diameter and orifice diameter varied directly, for a given liquid composition but as orifice diameter increased, the effect of D_o on D_b became less until a change from D_o = 0.056 cm to D_o = 0.066 cm produced negligible change in bubble diameter. It was

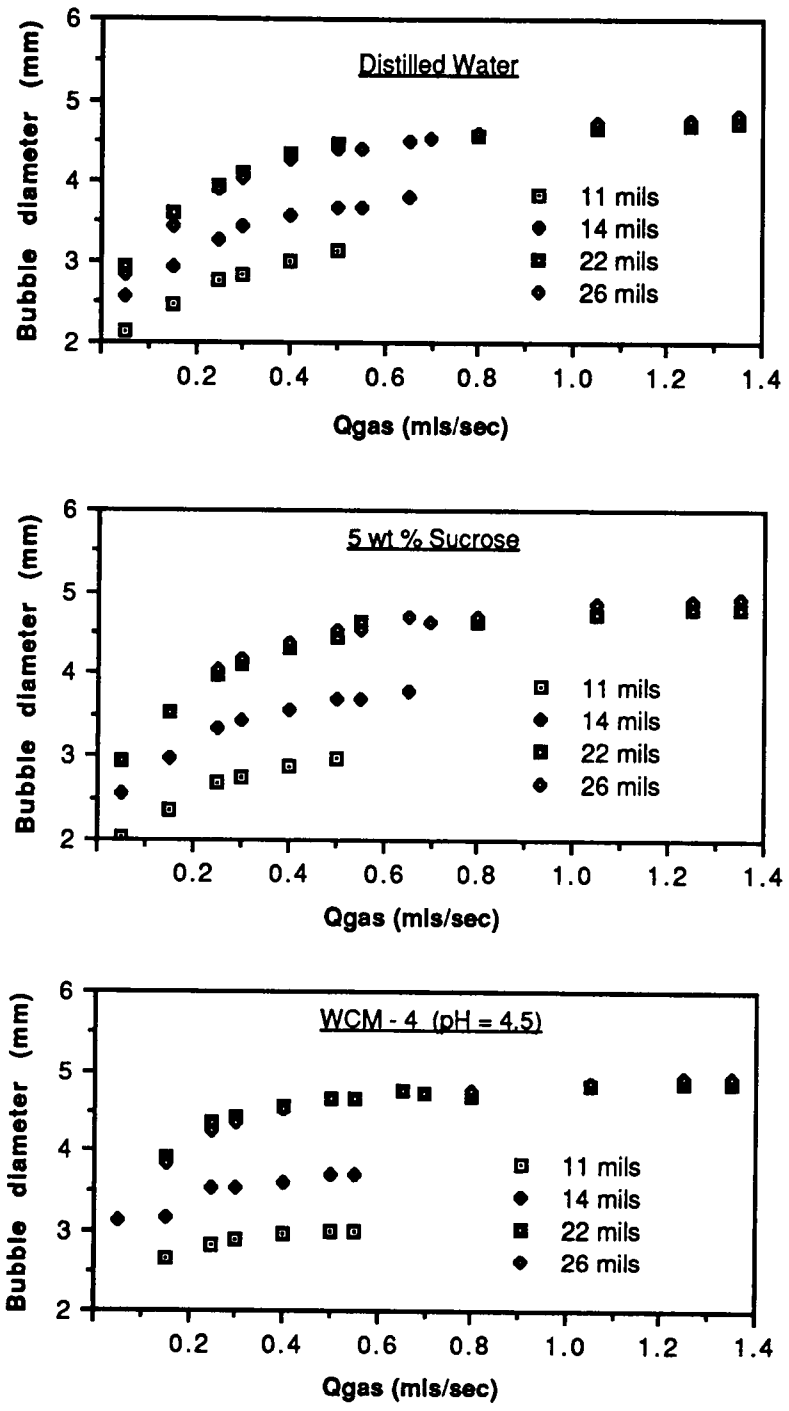

Figure 6.1: Bubble diameter as a function of orifice size, liquid composition and volumetric gas flow rate. System: single submerged orifice in a bubble column. Orifice diameters measured were: 11, 14, 22 and 26 mils (0.028, 0.036, 0.056 and 0.066 cm, respectively).

concluded therefore that, for a given liquid composition and gas flow in the intermediate regime, the 0.066 cm diameter orifice would produce relatively constant bubble diameters for the widest range of gas flow rates in the intermediate gas flow regime (Perry, 1973). Figure 6.2 is a summary of the bubble diameter as a function of gas flow rate using the 0.066 cm diameter orifice. It was concluded that for each liquid solution studied the single submerged orifice in the bubble column would produce a bubble with a relatively constant diameter at the gas flow rates ranging from ~ 1 ml/sec to ~ 1.35 ml/sec. Sparging air through the 0.066 cm diameter orifice in this range of gas flow rates produced bubbles with diameters 0.47 cm, 0.49 cm and 0.49 cm for the H2O, SUC and WCM-4 liquid solutions, respectively.

6.3 Airlift Reactor Results:

6.3.1 Volumetric mass transfer coefficient, $k_l a$:

The experimental work with the single submerged orifice in the bubble column generated data on bubble formation that was used to design the sparger perforated plates and to determine gas flow rates for use in the operation of the airlift reactor. For a given liquid in the airlift reactor, three gas flow rates were studied. At each gas flow rate oxygen was absorbed to, as well as desorbed from, the liquid phase twice. The volumetric mass transfer coefficient, $k_l a$, for oxygen and the specific interfacial area were calculated at each gas flow rate. The resulting values were compared to data produced in other works.

In the single concentric tube airlift reactor nitrogen was sparged through the perforated plate and into the liquid phase until the dissolved oxygen meter display read "00.0" ppm. The gas composition was then changed from nitrogen to air. THe absorption process was thus begun. A typical output of the chart recorder is shown in Figure 6.3. The period of time (system response lag time) between the change in gas feed composition and the initial response of the dissolved oxygen meter varied inversely with the gassing rate. It can be assumed that the lag time was at least in part a result of the gas lines and sparger volume through which the initial change in gas composition had to pass to reach the liquid phase. However, at least 30 seconds of the lag time

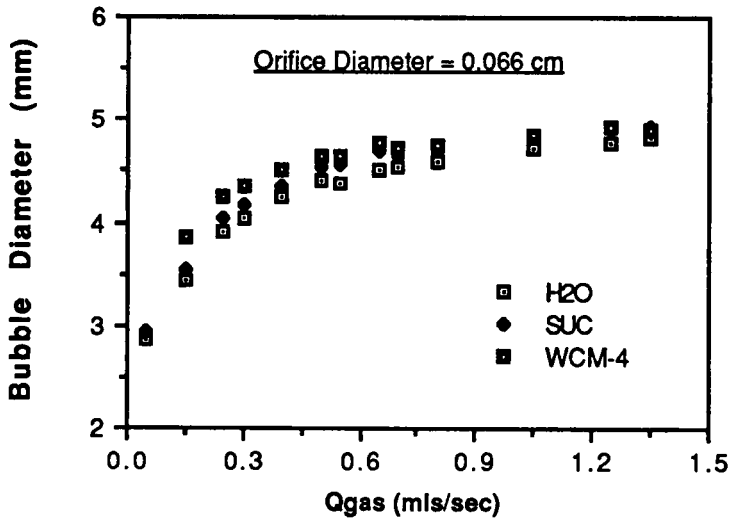

Figure 6.2: Gas flow rate through a single orifice (0.066 cm DIA) in a bubble column: bubble diameter (mm) vs. gas flow rate (ml/s) for three liquid compositions: distilled water, five weight percent sucrose, WCM-4 (pH = 4.5).

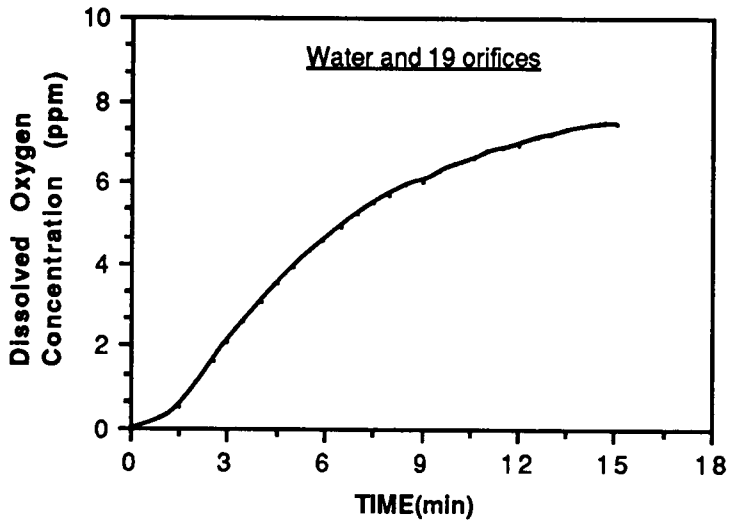

Figure 6.3: A typical curve representing dissolved oxygen profile data collected during absorption to the liquid in the airlift reactor. System: Air-water and 19 orifices at a gas flow rate of 0.98 ml/s per orifice.

may be attributed to the dissolved oxygen meter, because the characteristic response time of the meter (t_{95}) was 30 seconds. That is, when the electrode was "instantaneously" transferred from a liquid completely stripped of oxygen to a liquid completely aerated with oxygen it took the measuring apparatus about 30 seconds to register 95 percent of the change in dissolved oxygen concentration.

Figure 6.4 represents three typical sets of data. Each data set is a dissolved oxygen profile for oxygen absorption to distilled water. The data differ by gas flow rate and the number of orifices per perforated plate. The distilled water experiments were designed to operate at about 1 ml/s per orifice. Therefore, the five-, nine- and 19-orifice plates had total gas flow rates of about five, nine and nineteen ml/s, respectively. There are two things immediately evident in Figure 6.4. As oxygen absorption occurs the bulk liquid dissolved oxygen concentration increases and approaches a final value asymptotically. Also, the time required to reach the asymptote varies inversely with the total gas flow rate (and, in this case, with the number of orifices in the perforated plate). Indications are that the final oxygen concentration (c_l^*) is not exactly constant with varying gassing rate. The value for c_l^* was therefore approximated for each absorption run as well as each desorption run to account for fluctuations in temperature, pressure and other operating conditions.

The asymptotic behavior of the oxygen concentration profile indicates that the dissolved oxygen bulk liquid concentration is approaching the interfacial liquid concentration. The time required to reach the asymptote indicates the system's ability to transfer oxygen to the liquid phase. If the required time of a system is relatively small, then one would speculate that k_la for that system is relatively large. Quantification of k_la for each of the systems is the end to which equations 4.17 and 4.21 are applied. Figure 6.5 is a typical representation of equation 4.17.

A quick perusal of the figure reveals that it is not a straight line. The nonlinearity in the initial time span may be partly attributed to the system response time lag, t_{lag}. As time grows large, however, the curve becomes nonlinear and the ordinate values begin to approach infinite rather quickly. It is likely that the problem here lies in the model used to predict mass

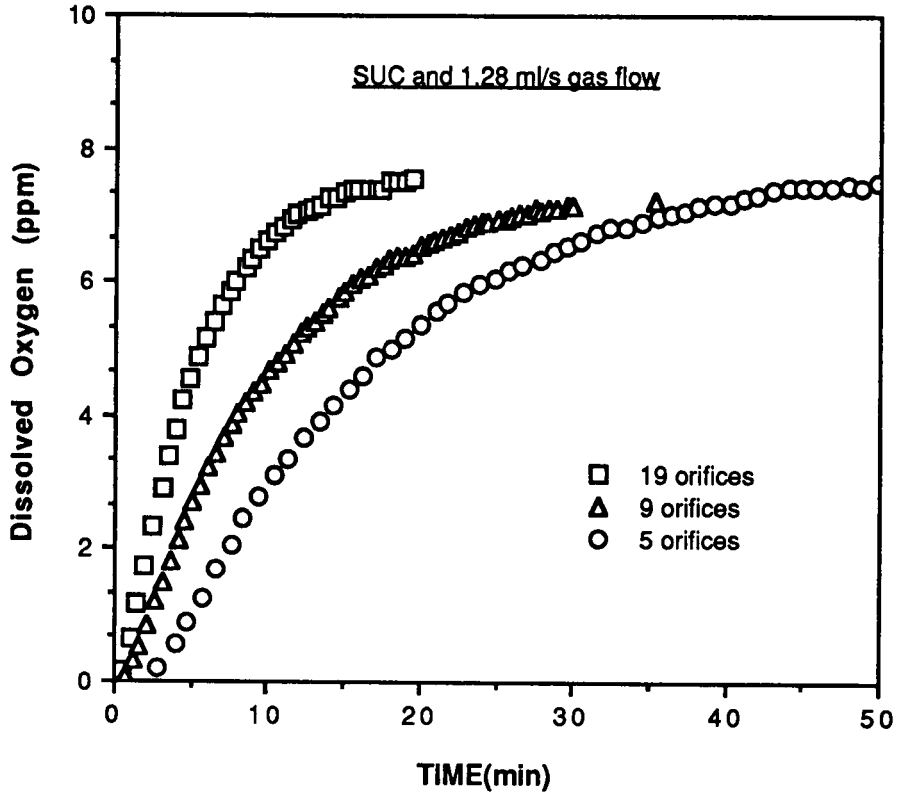

Figure 6.4: Three typical sets of dissolved oxygen profile data collected with the oxygen probe for absorption to five wt percent sucrose (SUC) at 1.28 ml/s gas flow per orifice. The total gas flow rate was varied proportionately with the number of orifices in the perforated plate: 19 orifices, 24.5 ml/s; 9 orifices,11.52 ml/s; 5 orifices, 6.4 ml/s.

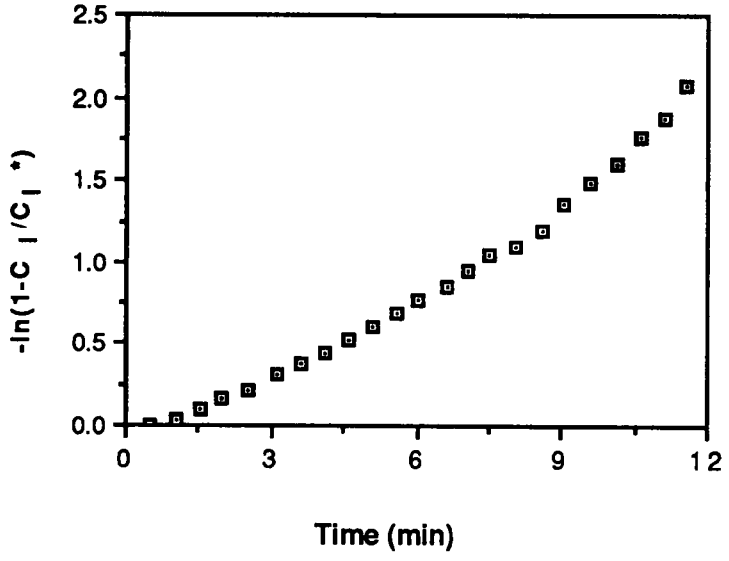

Figure 6.5: Unsteady oxygen transfer to the liquid phase in the laboratory draft tube reactor: Dimensionless ordinate as a function of time in the format of equation 4.17.

transfer behavior, specifically the two-film or two-resistance theory. As equilibrium is approached conditions may change that invalidate one or more of the assumptions on which the model is based causing the model to break down. Therefore, to extract the value of k_la from the semilog plot it is necessary to consider only the linear portion of the curve. The part of the curve considered in this work is the portion occurring after t_{lag} and before t_{75} (the time at which the dissolved oxygen electrode has reached 75 percent of the total dissolved oxygen change. Mathematically, at t_{75} in an absorption run $c_l = 0.75\ c_l^*$ and substituting into the left-hand side of equation 4.17.

$$-\ln\left(\frac{c_l^* - 0.75c_l^*}{c_l^*}\right) = -\ln(0.25) \cong 1.39 \qquad (6.1).$$

Similarly, for a desorption run at t_{75}, $c_l = 0.25\ c_l^*$ and equation 4.21 becomes

$$-\ln\left(\frac{0.25\ c_l^*}{c_l^*}\right) = -\ln(0.25) \cong 1.39 \qquad (6.2).$$

Thus, the portion of the semilog plot considered for measuring the value of k_la for either absorption or desorption is the portion with abscissa greater than t_{lag} and ordinate less than or equal to 1.39. Figure 6.6 shows a typical plot of the linear portion of the curves representing equations 4.17 and 4.21. In the present case Figure 6.6 represents two absorption and two desorption response curves for air or nitrogen sparged through a nine-orifice perforated plate into distilled water. A linear regression analysis on the data yields an equation in the form of y = m+bt where y is the ordinate and t is the abscissa. The constant 'm' is associated with t_{lag} . The constant b is the overall mass transfer coefficient, k_la for oxygen. The equations shown in Figure 6.6 yield two values for oxygen absorption into the system, $k_la = 0.1167\ min^{-1}$ and $k_la = 0.0936\ min^{-1}$, and two values for oxygen desorption from the system, $k_la = 0.1116\ min^{-1}$ and $k_la = 0.1214\ min^{-1}$. The average of the first two values ($k_la = 0.1052\ min^{-1}$) was considered a good estimate of the absorption k_la for that system; similarly with the average of the second two values ($k_la = 0.1165\ min^{-1}$) for the desorption k_la for that system.

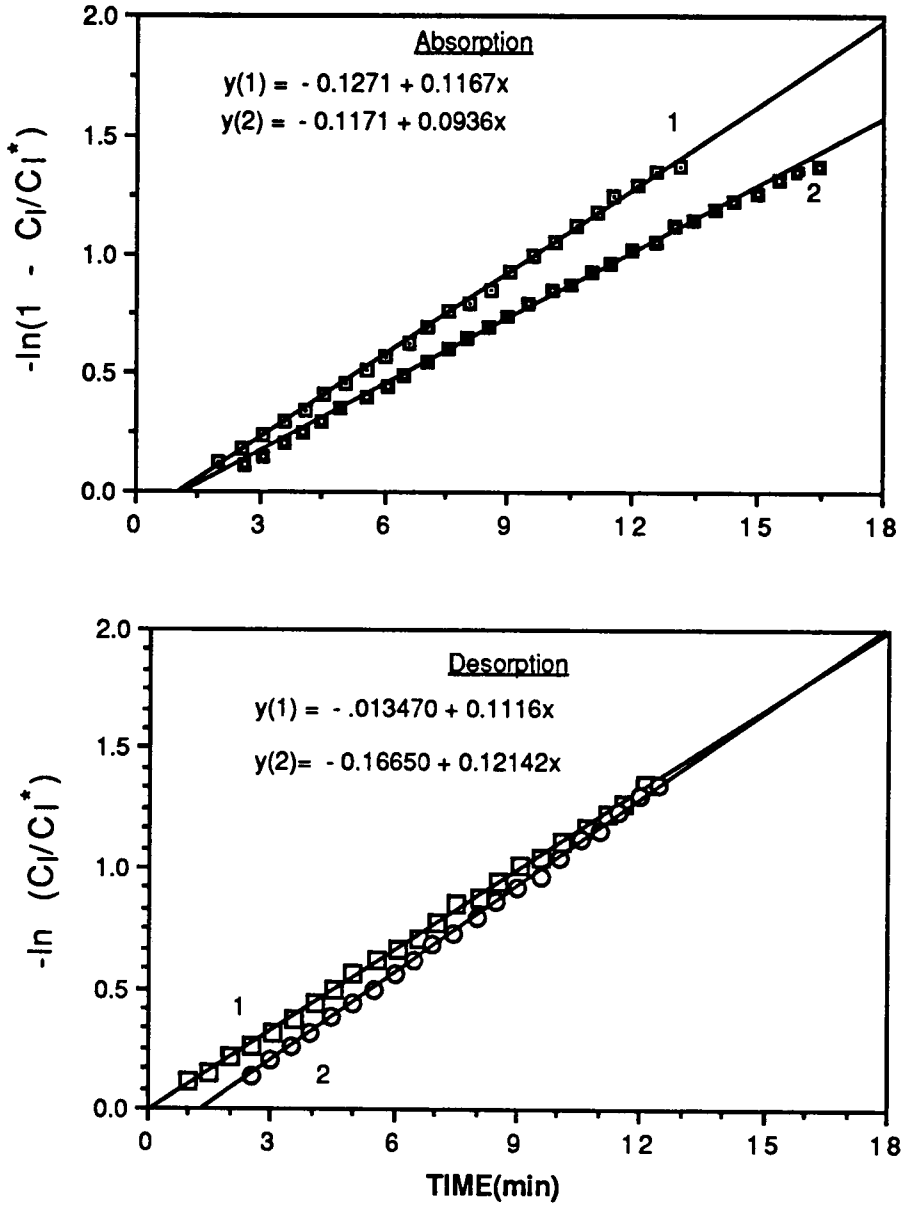

Figure 6.6: Linear segments of absorption and desorption dissolved oxygen profile data reduced to conform to equations 4.17 and 4.21, respectively. System: Air-water, nine orifices

Table 6.2 is a summary of the absorption and desorption k_la's for oxygen measured in the concentric tube airlift reactor for a range of gassing rates and liquid compositions. The average absorption and average desorption values in Table 6.2 are plotted against the corresponding vvm values in Figure 6.7. The vvm values are the total volumetric gas flow rate on a minute basis divided by the reactor liquid volume (gas volume per minute per unit liquid volume). For all three liquid compositions studied, there seems to be a direct relationship between the average k_la values and the gassing rate (vvm). A regression analysis on the data in Figure 6.7 produced equations relating k_la to vvm for absorption

$$k_la = 0.336\ vvm^{0.917} \tag{6.3}$$

and for desorption

$$k_la = 0.41\ vvm^{0.889} \tag{6.4}.$$

A comparison of the data producing equations 6.3 and 6.4 is shown in Figure 6.8. The values for the desorption k_la's were consistently greater than those for the absorption k_la's averaging about 27 percent greater but were as little as 13 percent greater for H2O and five orifices and as much as 61 percent greater for WCM-4 and five orifices. Although the absolute differences in the two curves in Figure 6.7 diverge from 0.0132 min^{-1} (at 0.1 vvm) to 0.0563 min^{-1} (at 0.7 vvm), on a percent basis the difference between the two curves decreases from 33 percent (at 0.1) vvm to 23 percent (at 0.7 vvm). All systems studied produced k_la values for oxygen absorption that averaged significantly less than the k_la values for oxygen desorption.

The average absorption and average desorption values in Table 6.2 are also plotted against the corresponding superficial gas velocity values (u_g) in Figure 6.9. A regression analysis on the data in Figure 6.9 produced equations relating k_la to u_g for absorption

$$k_la = 0.282\ u_g^{0.916} \tag{6.5}$$

Table 6.2: Average $k_l a$,Values Based on Experimental Data.

$k_l a$ (1/min)	H2O[a]	SUC	WCM-4
5 orifices:			
A1[b]	0.0489	0.0711	0.0529
A2	0.0561	0.0679	0.0532
N2	0.0609	0.0826	0.0839
N3	0.0574	0.0903	0.0873
Air Average:	0.0525	0.0695	0.0531
Nit. Average:	0.0592	0.0865	0.0856
Average All:	0.0558	0.0780	0.0693
9 orifices:			
A1	0.1167	0.1059	0.1169
A2	0.0936	0.1212	0.1106
N2	0.1214	0.1463	0.1489
N3	0.1214	0.1549	0.1584
Air Average:	0.1052	0.1136	0.1138
Nit. Average:	0.1214	0.1506	0.1537
Average All:	0.1133	0.1321	0.1337
19 orifices:			
A1	0.1766	0.2106	0.2111
A2	0.1945	0.2157	0.2282
N2	0.2095	0.2542	0.2863
N3	0.2150	0.2438	0.2874
Air Average:	0.1856	0.2132	0.2197
Nit. Average:	0.2123	0.2490	0.2869
Average All:	0.1989	0.2311	0.2533

[a]Gas flow rate per orifice: H2O, 0.98 ml/s; SUC, 1.28 ml/s; WCM-4, 1.35 ml/s.

[b]A1 = first oxygen run; A2 = second oxygen run; N2 = first nitrogen run; N3 = second nitrogen run.

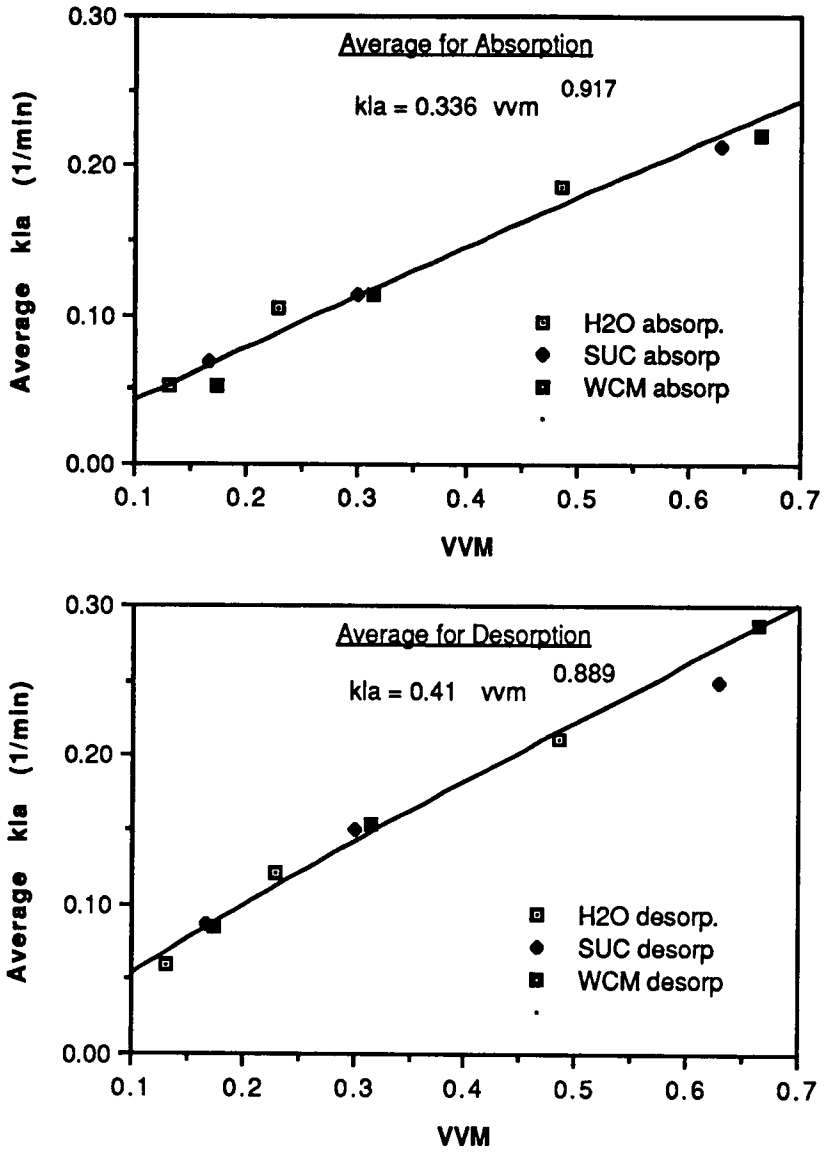

Figure 6.7: Average absorption and average desorption k*l*a values plotted individually against gassing rate (vvm).

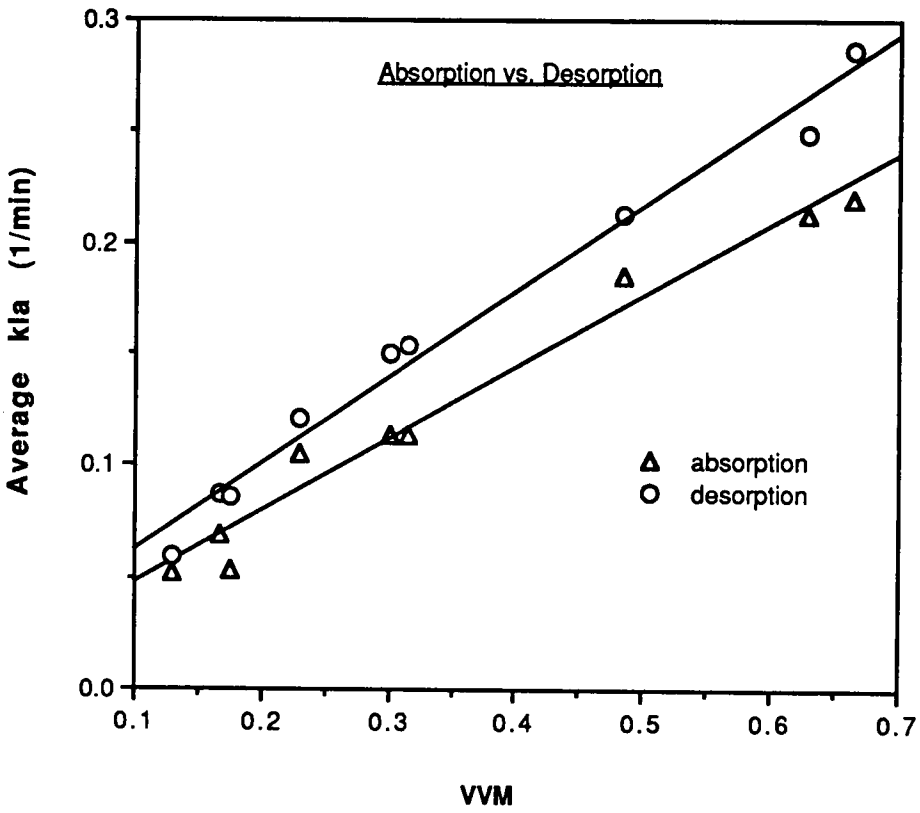

Figure 6.8: Comparison of absorption $k_l a$ for oxygen vs. gassing rate (vvm) and desorption $k_l a$ for oxygen vs. gassing rate (vvm) for distilled water (H20), 5 wt % sucrose (SUC), and wild carrot cell media (WCM-4).

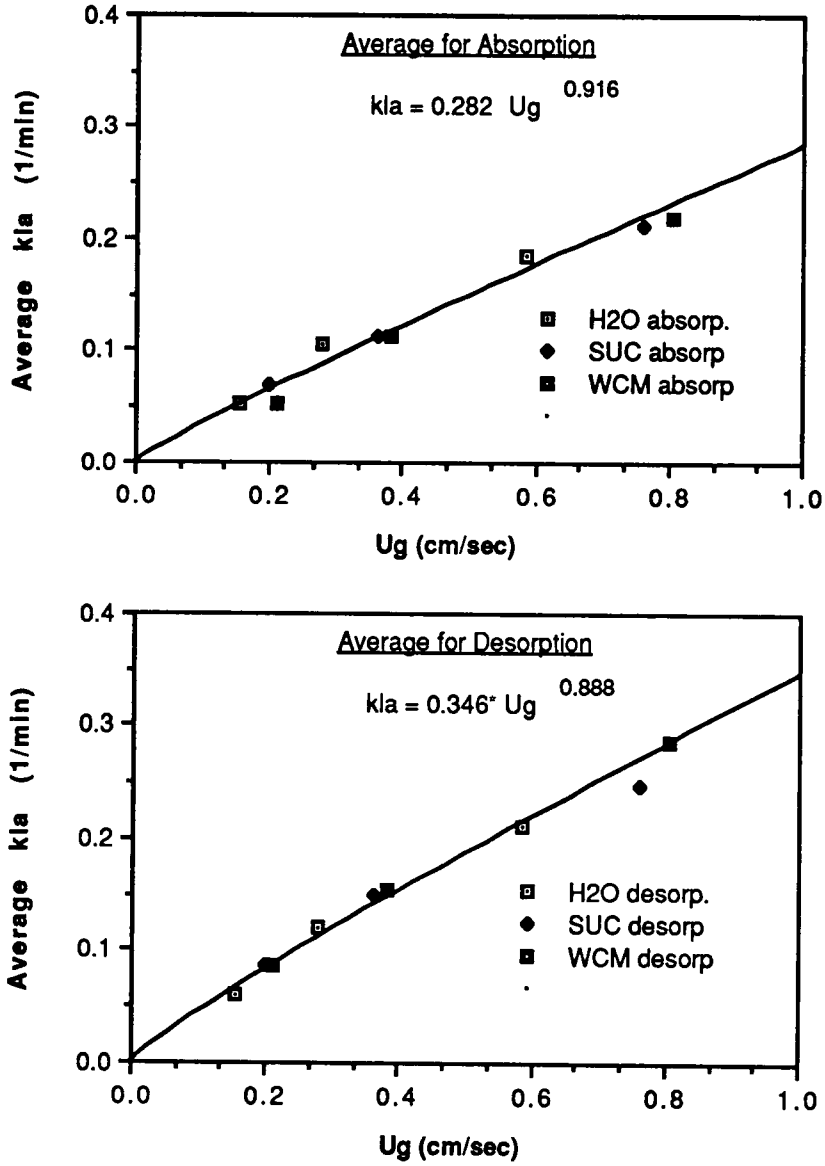

Figure 6.9: Average k$_l$a for absorption and average k$_l$a for desorption as functions of superficial gas velocity for distilled water (H20), 5 wt % sucrose (SUC) and wild carrot cell media (WCM-4). Ug = (volumetric gas flow rate)/(draft tube cross sectional area).

and for desorption

$$k_l a = 0.346\ u_g^{0.888} \tag{6.6}$$

where $k_l a$ is in min^{-1} and u_g is in cm/sec.

The trends in this figure are the same as for Figure 6.7 because both relate $k_l a$ to gassing rate, but relating $k_l a$ to superficial gas velocity (u_g) permits a comparison of the data generated in this work to that reported by Sheppard (1978).

Sheppard studied mixing and oxygen absorption in four designs of an airlift reactor: a bubble column, a single concentric tube airlift reactor with sparging in the annulus, a single concentric tube airlift reactor with sparging in the central tube, and a double concentric tube airlift reactor (see Figure 2.1). Sheppard produced a correlation fitting his $k_l a$ data to superficial gas velocity:

$$k_l a = 33.3\ u_g^2 \tag{6.7}$$

where $k_l a$ is in hr^{-1} and u_g is in cm/sec. The data generated in this work are summarized with Sheppard's data and on Sheppard's coordinates in Figure 6.10. The reactor types in Sheppard's work and that for the present work are all internal loop designs, but Sheppard studied more concentric tube configurations and a larger working volume. Also, the sparger used for the correlation given above (equation 6.7) consisted of orifice tubes each with a 0.127 cm diameter. If applied to the range of gas flow rates studied in the present work, equation 6.7 underpredicts by 74 percent $k_l a$ at the lower u_g extreme (0.157 cm/s) and overpredicts by 64 percent $k_l a$ at the upper extreme (0.805 cm/s). Equations 6.5 and 6.7 converge at a superficial gas velocity of about 0.54 cm/sec and $k_l a = 0.16\ min^{-1}$. While the present work found an approximately linear proportionality between $k_l a$ and gassing rate, Sheppard reported $k_l a$ proportional to the square of u_g.

In an attempt to clarify the relationship between $k_l a$ and gassing rate alone (u_g), regression analyses were performed on Sheppard's data together

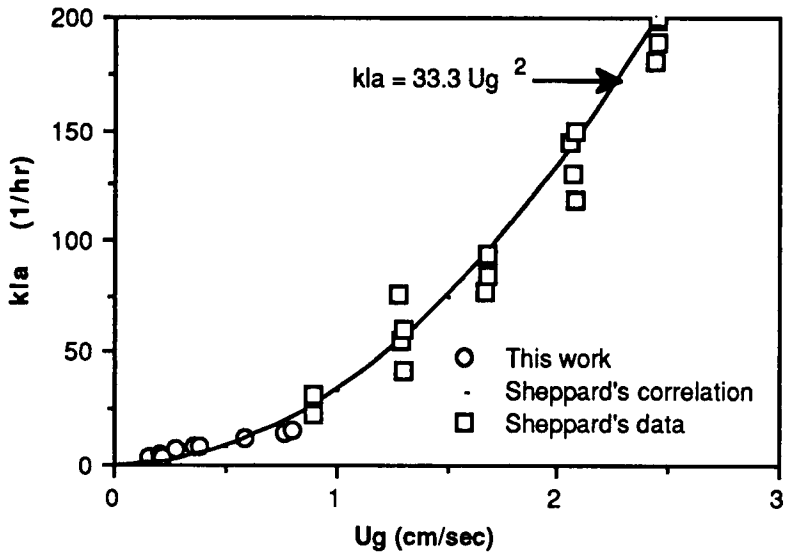

Figure 6.10: Comparison of data in the present work with all those produced by Sheppard (1978) on Sheppard's coordinates. Sheppard's reported correlation relates $k_l a$ to the square of the superficial gas velocity.

with the data presented in this work. In order to compare analogous information, the data of the present work was analysed with the data only from Sheppard's single concentric outer tube reactor configuration (see figure 2.1). Power law, exponential and polynomial model regressions were all performed on the data to determine the best applicable equation for incorporating the single-bubble and intermediate gassing regimes into one model. As is evident from the correlation coefficients in figures 6.11 through 6.13 the resulting equations did not fit the data well. Of the models analysed the best fit was with the cubic analysis (figure 6.13) with a correlation coefficient of 0.981. An alternative was to analyse the single-bubble and intermediate gassing regimes separately.

Figure 6.14 shows the result of performing a linear regression analysis on each of the two sets of data. The resulting equations generate two distinctly different lines, each representing a correlation between k_la and u_g for the respective gassing regime. The figure appears to support the theory that the two gassing regimes should be investigated separately. However, the apparent discontinuity between gassing regimes may be due to differences in sparger configuration, reactor dimensions or other operational parameters. For example, Sheppard studied two orifice diameters (1.27 and 3.81 mm DIA) with gassing rates ranging into the jetting bubble regime (turbulent gas flow, $u_g >$ 0.75 cm/s). The present work studied orifice diameters up to 0.66 mm and laminar gas flow in the single bubble regime ($u_g \leq 0.75$ cm/s). While it is difficult to estimate the range of Sheppard's bubble sizes it is clear that both the orifice size and gassing rate directly affect the bubble formed at the orifice. The specific interfacial area, and the product k_la, are directly affected by the bubble size. The difficulty in fitting both data sets with a single model may therefore be due to the different orifice diameters and gassing rates studied.

Other investigators (e. g. Bello, Robinson and Moo-Young) include more independent variables in their mass transfer correlations to better explain the factors that effect k_la.

The data generated in the present work were also compared to those reported by Bello, Robinson and Moo-Young (1985). Bello, Robinson and Moo-Young worked with a bubble column, an external loop airlift reactor and a

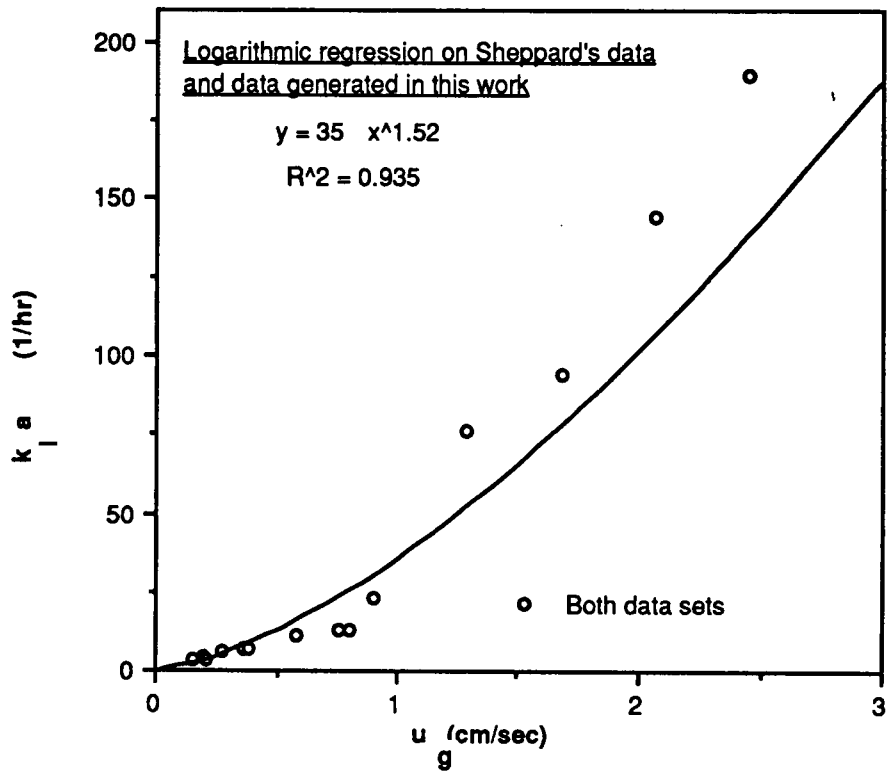

Figure 6.11: Comparison of data in the present work with those produced by Sheppard (1978) on Sheppard's coordinates. The power law model on the data included Sheppard's data from only his single concentric outer tube reactor configuration.

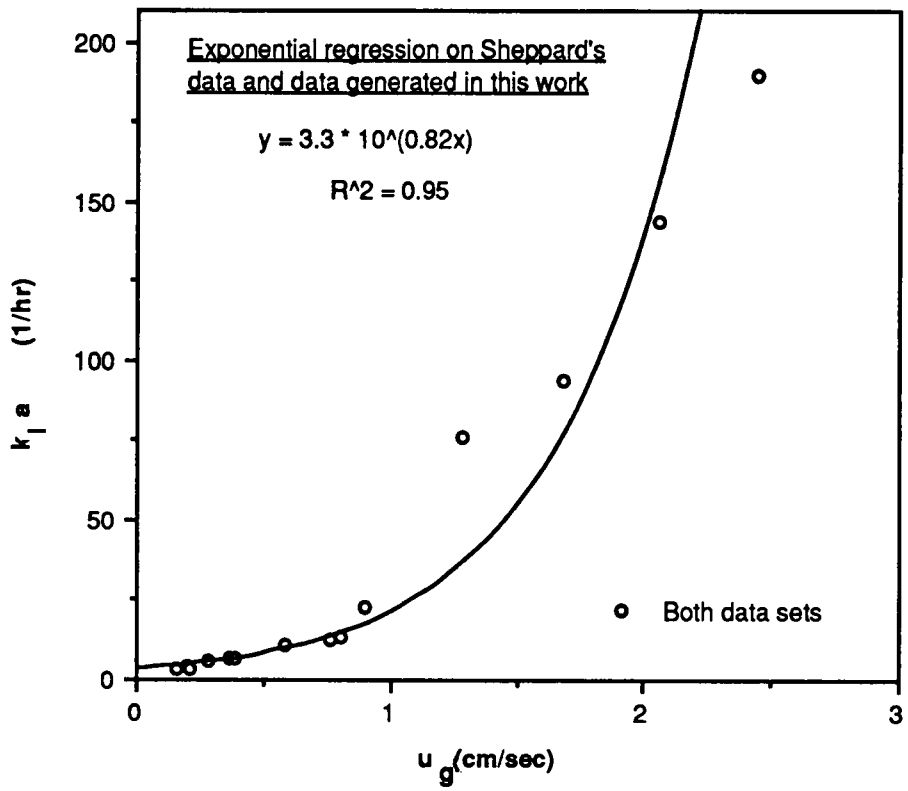

Figure 6.12: Comparison of data in the present work with those produced by Sheppard (1978) on Sheppard's coordinates. The exponential model on the data included Sheppard's data from only his single concentric outer tube reactor configuration.

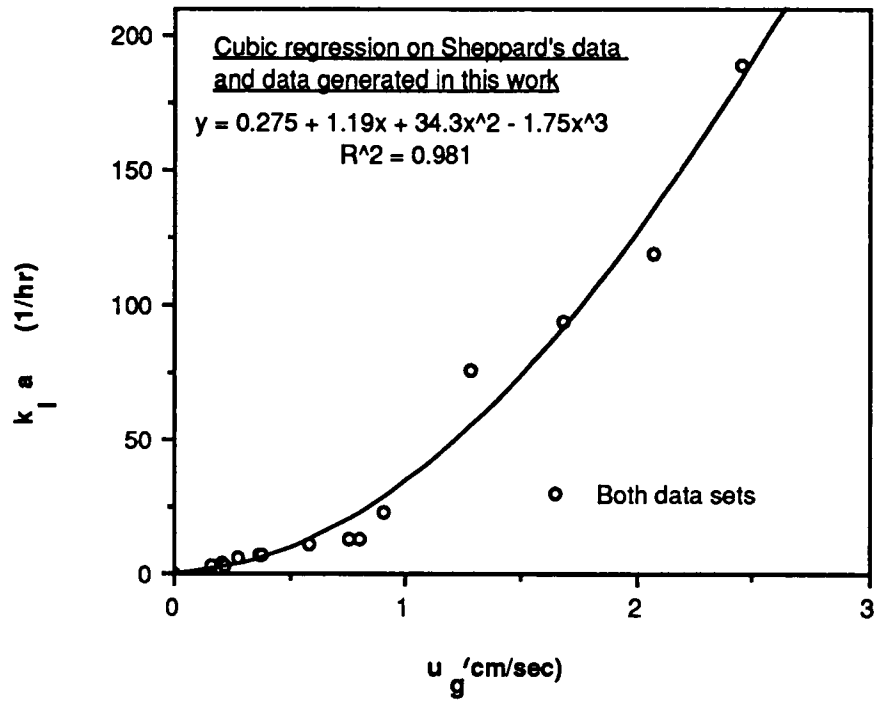

Figure 6.13: Comparison of data in the present work with those produced by Sheppard (1978) on Sheppard's coordinates. The cubic model on the data included Sheppard's data from only his single concentric outer tube reactor configuration.

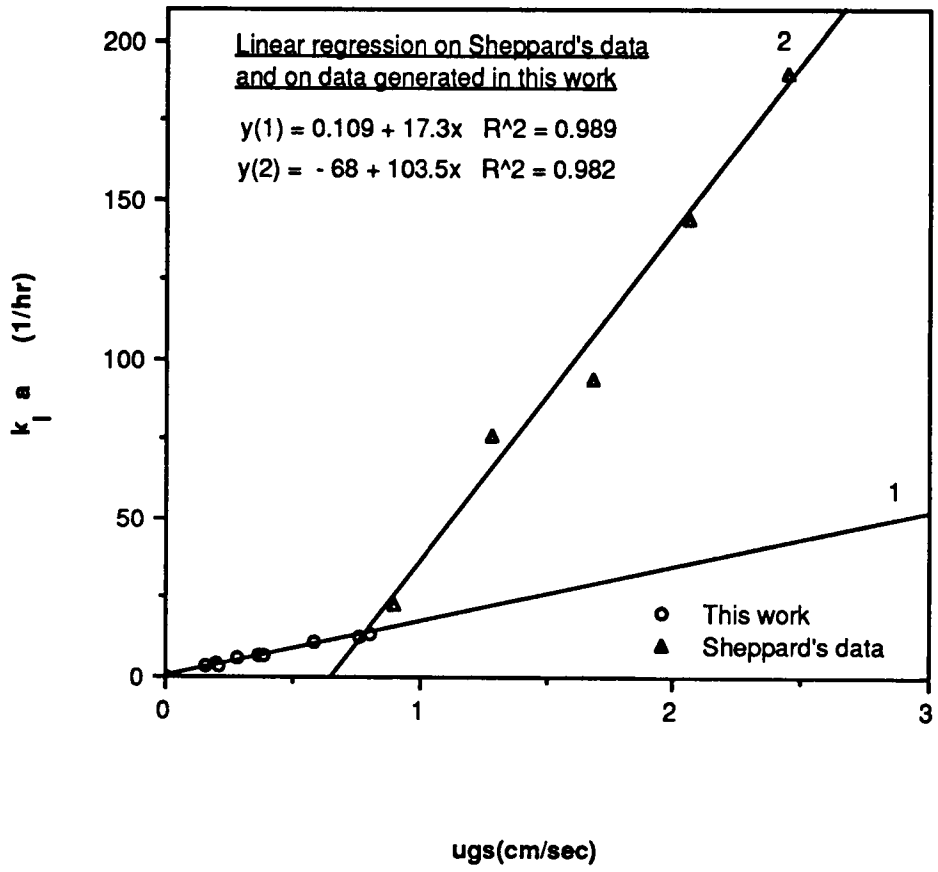

Figure 6.14: Comparison of data in the present work with those produced by Sheppard (1978) on Sheppard's coordinates. The linear model on Sheppard's data was performed on data from his single concentric outer tube reactor configuration.

single concentric tube airlift reactor with sparging in the annulus (see Figure 2.1) and reported mass transfer characteristics as a function of reactor design and gassing velocity as well as superficial liquid velocity (equation 2.5). The variables measured in the work of Bello et al were also measured in the present work, except for the superficial liquid velocity. Therefore, in order to compare the two investigations it was necessary to estimate u_l. To that end, the cubic equation (2.7) developed by Jones (1985) was utilized. For draft tubes with diameters less than 12.1 cm and gas flow rates less than 40 ml/s the superficial liquid velocities predicted by Jones' model did not differ appreciably from measured values of u_l. The operational parameters of the present work fell within the limits established in Jones' investigation.

For each absorption run the design characteristics and operating parameters as well as the properties of the liquid being studied in the airlift reactor were substituted into Jones' cubic equation (2.7). The cubic root of Jones' equation was equal to the absolute liquid velocity in the annular space of the concentric tube airlift reactor. There was only one real, positive root for each absorption run. The superficial liquid velocity, u_l, in the central draft tube was then calculated using equation 2.11. The resulting value of u_l was the final variable needed to manipulate the data to fit the coordinate system developed by Bello et al. The abscissa and ordinate were plotted according to equation 6.8:

$$\frac{(k_l a)_r H_d}{(u_l)_r} = C_1 \left(\frac{u_g}{u_l}\right)^{C_2} \left(1 + \frac{A_d}{A_r}\right)^{C_3} \qquad (6.8)$$

with C_2 and C_3 equal to 0.87 and -1, respectively. A summary of the results are shown in Figure 6.15 with the data reported by Bello et al. A linear regression on the data of this work in Figure 6.15 extrapolates well below the data reported by Bello et al. It appears that the two sets of data in Figure 6.15 do not agree. However, the experimental work of Bello et al was in an airlift reactor of external loop design and a reactor of the concentric tube design (with sparging in the annulus). Reynolds' numbers at the orifice ranged at least from Re = 400 to Re = 9000. The present work studied a concentric tube airlift reactor with sparging in the central tube and Reynolds numbers at the orifice

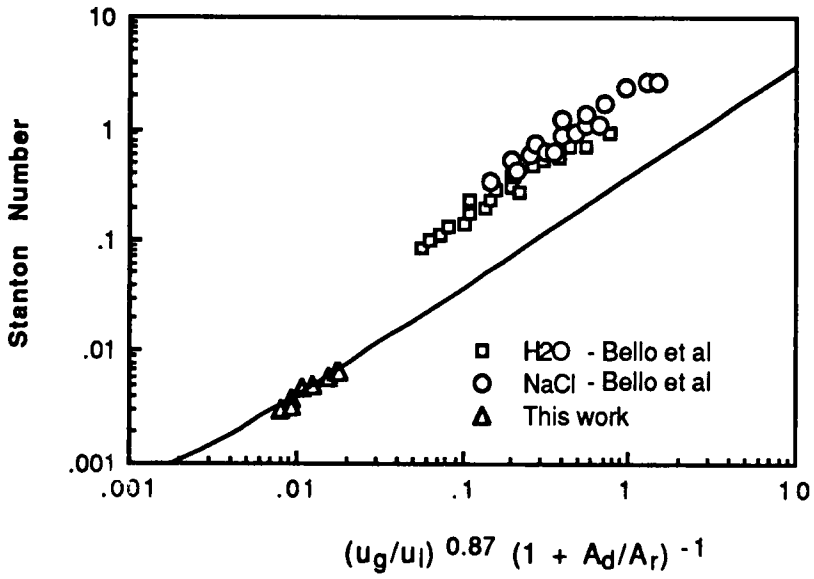

Figure 6.15: Summary of Bello, Robinson and Moo-Young's data and the data generated in the present work on the coordinates developed by Bello, Robinson and Moo-Young.

ranging from Re = 120 to Re = 180. Thus, the difference in the data in Figure 6.15 may be the effects of different sparging configurations as well as lower gas phase turbulence generated in the present work.

As with Sheppard's correlation the difference in the data of this work and those of Bello et al may be due to the different ranges of bubble size studied. The sparging orifices in Bello's investigation had 1.02 mm inner diameter. At comparable gassing rates Bello's sparger would produced significantly larger bubbles than those studied in the present work. Bello et al did not report the bubble sizes generated in their work, but the gas Reynolds' numbers studied suggest that the range of bubble diameters produced was also greater than that of the present work. The differences in sparging orifice size and gassing rates may have contributed to the disparity between the dimensionless data generated in the present work and those reported by Bello et al (Figure 6.15).

6.3.2 Specific interfacial area:

It was intended that the behavior of the liquid phase mass transfer coefficient k_l be separated from that of the specific interfacial area, a. To that end, the specific interfacial area was also measured during the oxygen absorption and desorption experiments so that the k_l values could be extracted from the values of k_la and a. The bubble volume, V_b was measured from the bubble formation rate and the stroboscopic stop frequency, q and f, respectively in equation 4.32. Equation 4.33 produced the bubble diameter, D_b. The gas holdup, ε, was calculated from equations 5.1a and 5.1b and the measured number of bubbles, N_b.

Some workers report k_la as a function of gas holdup. Reactors with large height to diameter ratios (L/D) that can accomodate many bubbles suspended in the liquid phase result in a fairly wide range of relatively large gas holdups. Airlift operations in the jetting-bubble regime also produce relative large gas holdups. The small L/D ratio of the laboratory scale airlift reactor and the low gassing rates studied in this work resulted in very small gas holdups ranging from 0.191 percent to 0.477 percent. A value for gas holdup was necessary, however, with the bubble diameter to calculate specific

interfacial area. Equation 4.40 was used for this purpose. A summary of the values produced for specific interfacial area is shown in Table 6.3. There was not an appreciable difference between the interfacial areas for absorption and desorption (less than 11 percent difference for all cases) so a summary of the average interfacial areas for the absorption and the desorption runs is shown in Figure 6.16. Average interfacial area has been related to gassing rate in this figure. The figure indicates that interfacial area varies directly with the gassing rate (vvm), similar to the volumetric mass transfer coefficient. Aside from this relationship there are no clear trends. There appears to be no appreciable difference in the distilled water (H2O) and the wild carrot media (WCM-4) data, although the data are very limited. However, there is an increase in values for 5 weight percent sucrose (SUC) that is on the order of 25%. Greater interfacial areas can be the result of decreasing bubble diameters found in more viscous solutions. Therefore the increase in specific interfacial area as a result of changes in liquid composition suggested by Figure 6.16 may be due to the greater viscosity measured in the SUC solution (~0.119 g/cm sec).

The liquid phase mass transfer coefficient, k_l, was calculated from the quotient of k_la and a ($k_l = k_la/a$). For an approximately constant gassing rate there was not an appreciable change in k_la with changing liquid composition (see Figure 6.7). There was a slight increase in specific interfacial area for a change to the SUC solutions (Figure 6.16). A plot of apparent k_l versus gassing rate would be expected to produce apparent k_l values smaller for the SUC solutions than for the H2O or WCM-4 solutions. The data in Figure 6.17 summarizes the behavior of the apparent liquid phase mass transfer coefficient, k_l. Figure 6.17 may be interpreted as described above, but for the most part no definite trends are indicated.

Table 6.3: Interfacial Area Based on Airlift Reactor Experimental Bubble Diameter

area (1/cm)	H2O	SUC	WCM-4
5 orifices:			
A1	0.0218	0.0301	0.0206
A2	0.0208	0.0306	0.0219
N2	0.0219	0.0284	0.0181
N3	0.0212	0.0293	0.0264
Air Average:	0.0213	0.0303	0.0212
Nit. Average:	0.0216	0.0288	0.0222
Average All:	0.0214	0.0296	0.0217
9 orifices:			
A1	0.0328	0.0426	0.0378
A2	0.0330	0.0461	0.0357
N2	0.0323	0.0448	0.0352
N3	0.0351	0.0426	0.0352
Air Average:	0.0329	0.0444	0.0368
Nit. Average:	0.0337	0.0437	0.0352
Average All:	0.0333	0.0440	0.0360
19 orifices:			
A1	0.0484	0.0642	0.0496
A2	0.0471	0.0641	0.0521
N2	0.0458	0.0653	0.0526
N3	0.0491	0.0635	0.0523
Air Average:	0.0477	0.0642	0.0509
Nit. Average:	0.0474	0.0644	0.0524
Average All:	0.0476	0.0643	0.0516

[a]Gas flow rate per orifice: H2O, 0.98 ml/s; SUC, 1.28 ml/s; WCM-4, 1.35 ml/s.

[b]A1 = first oxygen run; A2 = second oxygen run; N2 = first nitrogen run; N3 = second nitrogen run.

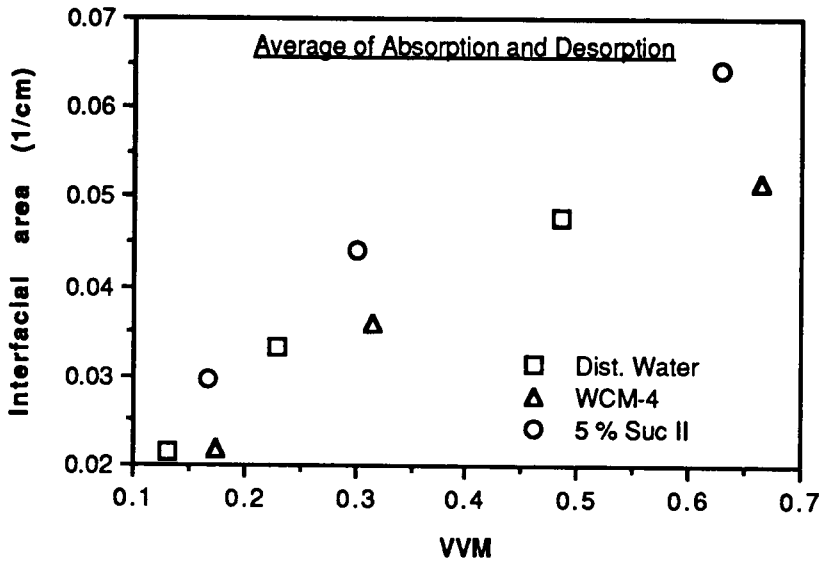

Figure 6.16: Summary of interfacial area vs gassing rate (vvm) as calculated from data generated in the airlift reactor experiments.

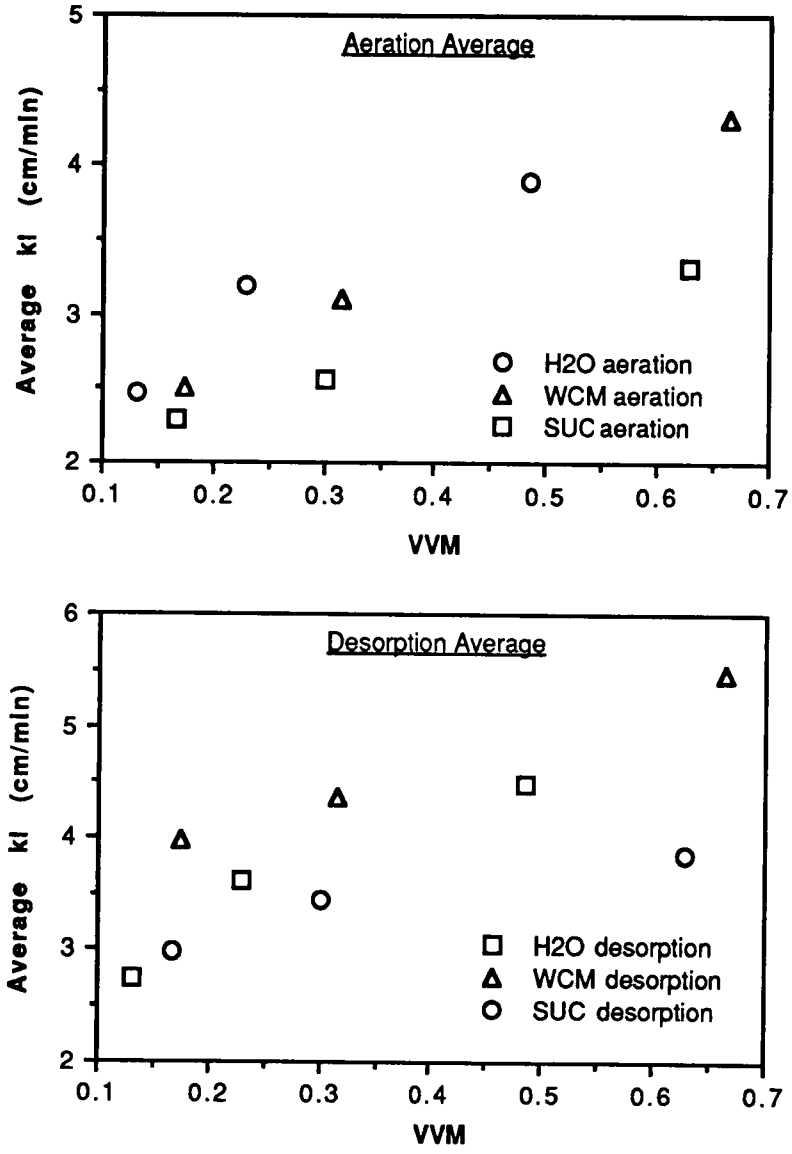

Figure 6.17: Summary of liquid phase mass transfer coefficients, k_l. vs. gassing rate (vvm) for oxygen absorption and desorption in H2O, SUC and WCM-4 solutions.

7 CONCLUSIONS

The following conclusions are a result of the airlift investigatons performed in the present work.

1. The values obtained for the overall volumetric mass transfer coefficient for oxygen desorption (ranging 0.0574 to 0.2874 min^{-1}) were consistently greater than those for the absorption (ranging 0.0489 to 0.2282 min^{-1}). The desorption k_la values averaged about 27 % greater than the absorption k_la values, but the percent difference between the two ranged from 13% to 61%. Although the absolute values of the average k_la versus vvm curves for absorption and desorption diverge from a difference of 0.0132 min^{-1} (at 0.1 vvm) to a difference of 0.0563 min^{-1} (at 0.7 vvm), the percent difference in the two curves decreases from 33% at 0.1 vvm to 23 % at 0.7 vvm. Thus, for the systems studied the k_la values for oxygen absorption were on the average significantly less than the k_la values for oxygen desorption.

2. The volumetric mass transfer coefficients, k_la for oxygen absorption and desorption were studied in three different aqueous solutions for gassing rates ranging from 0.13 vvm (superficial gas velocity, u_g = 0.157 cm/sec) to 0.67 vvm (u_g = 0.805 cm/sec). The overall volumetric mass transfer coefficients for oxygen measured for the given gassing rates in these experiments were not appreciably affected by changes in liquid composition ranging from distilled water to five weight percent sucrose to wild carrot media.

3. Although the data presented by Sheppard (1978) were produced in the same type of reactor as the data presented in this work, the volumetric mass transfer coefficients predicted by extrapolating his correlation into the lower gassing range of this work are as much as 74 percent different from the present values. While several mathematical models have been explored to correlate the present k_la data and those produced by Sheppard with only the gassing rate, it is necessary to include other variables --such as design and fluid parameters -- when predicting or modelling mass transfer in airlift reactors.

4. When plotted in terms of the Bello et al. correlation (1985), the data of this work are in a much lower range of dimensionless gassing rate and extrapolate well below but parallel to their data. The reason for this lack of agreement is attributed to the differences in gassing configurations and bubble sizes and possibly to the lower liquid phase turbulence generated in this work. Bello et al. studied a bubble column, an external loop reactor and a single concentric tube airlift reactor sparged in the annulus. The present work investigated mass transfer in a single concentric tube airlift reactor sparged in the central draft tube. Bello et al. studied gassing rates and orifice sizes producing orifice Reynolds numbers from about Re = 400 to 9000; and this work studied orifice Reynolds numbers from Re = 120 to 180.

5. The disparities between the data produced in the present work and those presented by Sheppard and by Bello et al. suggest that a complete model predicting airlift reactor mass transfer behavior may necessitate two correlations: one for the situation in which liquid flow is predominantly laminar and one for the situation producing transition-to-turbulent liquid flow. It is expected that the former would correspond to the superficial gas velocities in the present work of less than 0.75 cm/s; the latter would correspond to those superficial gas velocities greater than 0.75 cm/s.

6. The small height to diameter ratio of the airlift reactor studied in the present work together with the relatively low gassing rates produced gas holdup values less than 0.5 percent. As a consequence, this work was not able to produce any quantitive information correlating the behavior of $k_l a$ for oxygen with gas holdup in the airlift reactor.

7. The specific interfacial bubble area varied directly with the gassing rate. Aside from this relationship, scatter in the data was such that there appeared to be no appreciable difference in the interfacial area data for the distilled water and the wild carrot media, although the data are very limited. However, there is an increase in specific interfacial area values for 5 weight percent sucrose that is on the order of 25% larger than for the case with water

or wild carrot media and may be the result of the relatively large viscosity measured for this solution (~ 0.119 g/cm sec).

8. Although the specific interfacial area was greatest for the five weight percent sucrose solutions the volumetric mass transfer coefficient was not appreciably different for this liquid composition. The apparent liquid phase mass transfer coefficient was, therefore, least in the five weight percent sucrose solutions. The data support the described behavior, but do not indicate a clear relationship between the liquid phase mass transfer coefficient and the composition of the liquid phase.

The following conclusions apply to operations of a single submerged orifice in a bubble column:

9. For a single submerged orifice of a given diameter in a bubble column, the diameter of the essentially spherical bubble immediately above the dispersing orifice increases with increasing gas flow rate and approaches asymptotically a diameter dependent on the size of the dispersing orifice (and also on the liquid composition). However, this behavior applies only for volumetric gas flow rates up to 1.35 ml/sec, orifice diameters up to 0.066 cm and the liquid compositions studied in the present work.

10. Similarly, in a bubble column containing a given liquid composition (for the system studied): at a fixed gas flow rate, bubble diameter increases with orifice diameter from 0.028 cm to 0.056 cm and remains approximately constant from 0.056 cm to 0.066 cm.

11. For the full range of gassing rates studied, an increase in volumetric mass transfer coefficient was attributed more to an increase in specific interfacial area than an increase in liquid phase mass transfer coefficient.

8 SUGGESTED AREAS OF STUDY

The study of mass transfer in airlift reactors has encompassed various reactor types and design configurations as well as a wide range of operational parameters and fluid compositions. Recent investigations have concentrated on airlift reactor types with liquid recycle. The present work studied mass transfer in one airlift reactor type: the single concentric tube airlift reactor with gas dispersed in the central draft tube.

Three gassing rates for each of three liquid compositions were studied to determine the volumetric mass transfer coefficient as well as the specific interfacial area for oxygen in absorption and desorption operations of the airlift reactor. The resulting data were compared to data and correlations produced by reporters working with reactors of design similar to the concentric tube airlift reactor (e. g. Bello, Robinson and Moo-Young, 1985; and Sheppard, 1978). However, the present investigation encompasses only part of the operational parameters and fluid compositions that should be studied to elucidate the mass transfer characteristics of the reactor type studied. Therefore, further investigations are recommended in the following areas:

1. A greater range of gassing rates should be studied. The present work studied gassing rates in the single-bubble gas flow regime, but many investigators choose conditions that produce greater turbulence in the reactor. Further investigations should concentrate, in part, on generating continuous data using gassing rates that produce liquid flow ranging from the more laminar to the more turbulent regimes.

2. More information in dimensionless form such as the coordinates reported by Bello et al (1985) might explain the apparent inconsistencies in independent investigations in reactors of similar type and design. Also, mass transfer investigations in different reactor designs (e.g. external loop, single concentric tube, double concentric tube, etc.) should be performed to produce information relating, in the same equation, the volumetric mass transfer coefficients, design characteristics and operational parameters for each reactor.

3. The changes in volumetric mass transfer coefficients for oxygen due to changes in medium properties do not appear to be appreciable. In addition, there is limited, undocumented evidence that oxygen transfer into media with living cells produces higher volumetric mass transfer coefficients for oxygen. The phenomenon may be due to living cells trapped in the gas-liquid interface. Airlift operation studies should therefore be performed with a wider range of liquid physicochemical properties including the addition of plant or mammalian cells.

4. Specific interfacial area estimations are restricted by the technique used to measure bubble diameter. Further investigations in the laminar gas flow regime should therefore include means of estimating or measuring increasing interfacial area due to oscillations in the shape of the rising gas bubble.

The result of studies in the recommended areas should produce data relating a wider range of fluid properties, operational parameters and sparger/reactor design dimensions to mass transfer characteristics in airlift reactors of many related significant types. The ultimate goal is to develop a general mass transfer model that can be used to predict the conditions required to produce a specific biomass or its by-products.

BIBLIOGRAPHY

BIBLIOGRAPHY

Aiba, S., Humphrey, A.E., Millis, N.F., **Biochemical Engineering**, Second edition, Academic Press, Inc. (1973) pp. 163-194.

Akita, K., Yoshida, F., **Ind. Eng. Chem. Process Des. Develop.**, 12(1):76- 80 (1973).

Alvarez-Cuenca, M., Neremberg, M.A., **AIChE Journal.**, 27(1):66 (1981).

Bailey, J.E., Ollis, D.F., **Biochemical Engineering Fundamentals**, Second edition, McGraw-Hill, Inc. (1986) p.473

Bello, R.A., Robinson, C.W., Moo-Young, M.,**Biotech. and Bioeng.** 27:369-381,(1985).

Bird, R.B., Stewart, W.E., Lightfoot, E.N., **Transport Phenomena**, John Wiley and Sons, Inc. (1960) p. 48.

Botton, R.D., Cosserat, D., Charpentier, J.C., **Chem. Eng. J.** 20:87 (1980)

Calderbank, P.H., **Trans. Inst. Chem. Eng.**, 36:443, 1958.

Chakravarty, M., Begum, S., Singh, H.D., Barvali, J.N., Iyengar, M.S.,**Biotech. and Bioeng. Symp. No. 4** (1973) pp.363-378

Deckwer, W.D., Burckhart, R., Zoll, G., **Chem. Eng. Sci.**, 29:2177 (1974)

El-Gabbani, D.E.D.H., "Hydrodynamic and Mass Transfer Characteristics of an Airlift Contactor", M.A.Sc. Thesis, University of Waterloo, Ontario (1977)

Fukuda, H., Shiotani, T., Okada, W., Morikawa, H., **J. Ferment. Technol.**, 56:619 (1978)

Gasner, L.L., **Biotech. and Bioeng.** 16:1179 (1974)

Goldberg, I., **Single Cell Protein**, Springer-Verlag, Berlin, (1975) p.87.

Hatch, R.T., "Experimental and Theoretical Studies of Oxygen Transfer in the Airlift Fermentor:, Doctoral Thesis, MIT, Cambridge, Massachusetts (1973)

Hines, D.A., Bailey, M., Ousby, J.C., Roesler, F.C., "The ICI Deep Shaft Aeration Process for Effluent Treatment", **Int. Chem. Eng. Symp. Ser. No. 41, D1** (1975).

Jones, A.G., "Liquid Circulation in a Draft-Tube Bubble Column", **Chemical Engineering Science**, 40(3):449-462

Kanazawa, M., "The Production of Yeast from N-Paraffins", Tannenbaum, S.R., Wang, D.I.C. (eds): **Single Cell Protein II**. Cambridge, Massachusetts, MIT Press, (1975), p.438.

Kastanek, F., ***Coll. Czech. Chem. Commun.***, 41:3709 (1976).

Kawagoe, M., Robinson, C.W. (unpublished data).

Leeds and Northrup Company, Operation and Service Manual, D.B. 3572, 1981

Leibson, I., Holcomb, E.G., Cacoso, A.G., J.J. Jacmic, "Rate of Flow and Mechanics of Bubble Formation from Single Submerged Orifices, **AIChE Journal** 2(3):296-306, 1956

Lin, C.H., Fang, B.S., Wu, C.S., Fang, H.Y., Kuo, T.F., Hu, KC.Y., **Biotech. and Bioeng.** 18:1557 (1976).

Margaritis, A., Wallace, J.B., **Biotechnology**, (May 1984), pp. 447-453.

Nakanoh, M., Yoshida, F., "Gas Absorption by Newtonian and Non-Newtonian Liquids in a Bubble Column, **Ind. Eng. Chem. Process Des. Dev.** 19:190-195, 1980

Onken, U., Weiland, P., **European J. Appl. Microbiol. Biotechnol.** 10:31-40 (1980)

Onken, U., Weiland, P., **Advances in Biotechnology**, Vol. 1, **Scientific and Engineering Principles**, M. Moo-Young, C.W. Robinson, C. Vezina (eds), (Pergamon Press, Toronto, 1981), p. 559.

Orazem, M.E., Erickson, L.E., **Biotech. and Bioeng.** 21:69 (1979)

Perry, R.H., Chilton, C.H., **Chemical Engineers' Handbook**, McGraw-Hill, Inc. (1973) p. 18-68.

Schugerl, K., Lucke, J., Oels, V., **Advances in Biochemical Engineering**, Vol. 7, T.K. Ghose, A. Fiechter, N. Blakebrough (eds) (Springer Verlag, Berlin, 1977), pp. 1-84.

Sheppard, J.D.J., "Mixing and Oxygen Transfer Characteristics of an Airlift Fermentor", M.S. Thesis, University of Western Ontario, Ontario, Canada (1978).

Shoemaker, D.P., Garland, C.W., Steinfeld, J.I., **Experiments in Physical Chemistry**, Third Edition, McGraw-Hill, Inc. (1970?), pp. 353-364.

Sinclair, C.G., Ryder, D.N., **Biotech. and Bioeng.** 17:375 (1975)

Treybal, R.E., **Mass Transfer Operations**, Third edition, McGraw-Hill, Inc. (1980), p. 141.

Yoshida, F., Akita, K., **AIChE Journal.** 11:9 (1965).

APPENDICES

APPENDIX I

APPENDIX I

The following pages contain raw data collected during the bubble column experiments. The pages are labelled to indicate from which particular experiment each data set was collected. The stop frequency, f_s, was measured at each gas flow rate, Q. The mean bubble diameter D_b was calculated from the measured data using the method described in section 4.2.4. For each liquid composition and orifice size, three sets of data were collected at each flow rate for each liquid composition and orifice size. The average of the three data points was the mean bubble diameter.

The data generated in the bubble column -- bubble diameter as a function of gassing rate, orifice size and liquid composition -- were used to design the perforated plates for the airlift reactor. An outline of the method used to design the orifice diameter and number of orifices in the perforated plates follows the raw data and a summary of the bubble column results.

Bubble Column Experiment

System -- Liquid: Distilled Water Orifice Diameter: 11 mils
Gas: Air

Gauge (-)	Q (ml/s)	Time(hr:min): 7:10 f_s (s^{-1})	Time(hr:min): 7:10 D_b mm	Time(hr:min): 7:22 f_s (s^{-1})	Time(hr:min): 7:22 D_b mm	Time(hr:min): ? f_s (s^{-1})	Time(hr:min): ? D_b mm
1	0.05	565	2.13	630	2.05	560	2.13
2	0.15	1120	2.44	1170	2.41	1100	2.46
2.5	0.25	1330	2.74	1300	2.76	1280	2.77
3	0.3	1440	2.83	1450	2.82	1410	2.85
4	0.4	1620	3.00	1580	3.02	1610	3.00
5	0.5	1700	3.18	1750	3.14	1770	3.13
6	0.55						
7	0.65						
8	0.70						
10	0.80						
15	1.05						
20	1.25						
23	1.35						

Liquid: height (above orifice): 5.7 cm
volume: 2 L
temperature (C) 25

Bubble Column Experiment

System -- Liquid: Distilled Water Orifice Diameter: 14 mils
Gas: Air

Gauge (-)	Q (ml/s)	Time(hr:min): 7:40 f_s (s^{-1})	Time(hr:min): 7:40 D_b mm	Time(hr:min): 7:50 f_s (s^{-1})	Time(hr:min): 7:50 D_b mm	Time(hr:min): 8:05 f_s (s^{-1})	Time(hr:min): 8:05 D_b mm
1	0.05	343	2.51	336	2.53	325	2.56
2	0.15	592	3.02	643	2.94	645	2.94
2.5	0.25	660	3.45	750	3.31	770	3.28
3	0.3	800	3.44	810	3.43	820	3.42
4	0.4	950	3.58	970	3.55	960	3.57
5	0.5	1070	3.71	1090	3.68	1090	3.68
6	0.55	1200	3.68	1200	3.68	1200	3.68
7	0.65	1270	3.82	1305	3.78	1300	3.79
8	0.70						
10	0.80						
15	1.05						
20	1.25						
23	1.35						

Liquid: height (above orifice): 5.7 cm
volume: 2 L
temperature (C) 24

Bubble Column Experiment

System -- Liquid: Distilled Water Orifice Diameter: 22 mils
Gas: Air

Gauge (-)	Q (ml/s)	Time(hr:min): f_s (s^{-1})	Time(hr:min): D_b mm	Time(hr:min): f_s (s^{-1})	Time(hr:min): D_b mm	Time(hr:min): f_s (s^{-1})	Time(hr:min): D_b mm
1	0.05	218	2.92	215	2.94	216	2.93
2	0.15	380	3.50	356	3.58	352	3.59
2.5	0.25	426	4.00	435	3.97	444	3.94
3	0.3	465	4.13	455	4.16	475	4.10
4	0.4	553	4.29	536	4.33	532	4.34
5	0.5	600	4.49	610	4.47	604	4.48
6	0.55						
7	0.65						
8	0.70						
10	0.80	900	4.59	900	4.59	920	4.56
15	1.05	1100	4.70	1100	4.70	1125	4.67
20	1.25	1280	4.74	1280	4.74	1300	4.71
23	1.35	1390	4.73	1380	4.73	1390	4.73

Liquid: height (above orifice): 6.0 cm
volume: 2 L
temperature (C) 24

Bubble Column Experiment

System -- Liquid: Distilled Water Orifice Diameter: 26 mils
Gas: Air

Gauge (-)	Q (ml/s)	Time(hr:min): f_s (s^{-1})	D_b mm	Time(hr:min): f_s (s^{-1})	D_b mm	Time(hr:min): f_s (s^{-1})	D_b mm
1	0.05	267	2.73	227	2.88	235	2.85
2	0.15	412	3.41	400	3.44	405	3.43
2.5	0.25	480	3.84	450	3.93	457	3.91
3	0.3	505	4.01	495	4.04	497	4.04
4	0.4	610	4.15	575	4.23	565	4.26
5	0.5	675	4.32	645	4.39	640	4.40
6	0.55	750	4.31	710	4.39	710	4.39
7	0.65	800	4.46	765	4.52	770	4.51
8	0.70	840	4.49	820	4.53	820	4.53
10	0.80	930	4.54	910	4.57	900	4.59
15	1.05	1100	4.70	1070	4.74	1080	4.73
20	1.25	1230	4.80	1230	4.80	1250	4.77
23	1.35	1310	4.82	1300	4.84	1315	4.82

Liquid: height (above orifice): 5.7 cm
volume: 2 L
temperature (C) 26

Bubble Column Experiment

System -- Liquid: 5 wt % Sucrose Orifice Diameter: 11 mils
Gas: Air

Gauge (-)	Q (ml/s)	Time(hr:min): f_s (s^{-1})	Time(hr:min): D_b mm	Time(hr:min): f_s (s^{-1})	Time(hr:min): D_b mm	Time(hr:min): f_s (s^{-1})	Time(hr:min): D_b mm
1	0.05	640	2.04	600	2.09	650	2.03
2	0.15	1250	2.36	1250	2.36	1250	2.36
2.5	0.25	1420	2.68	1400	2.69	1420	2.68
3	0.3	1560	2.76	1590	2.74	1560	2.76
4	0.4	1850	2.87	1850	2.87	1840	2.87
5	0.5	2080	2.97	2120	2.95	2080	2.97
6	0.55						
7	0.65						
8	0.70						
10	0.80						
15	1.05						
20	1.25						
23	1.35						

Liquid: height (above orifice): 5.7 cm
volume: 2 L
temperature (C) 25

Bubble Column Experiment

System -- Liquid: 5 wt % Sucrose Orifice Diameter: 14 mils
Gas: Air

Gauge (-)	Q (ml/s)	Time(hr:min): 8:00 f_s (s^{-1})	8:00 D_b mm	Time(hr:min): 8:20 f_s (s^{-1})	8:20 D_b mm	Time(hr:min): 8:30 f_s (s^{-1})	8:30 D_b mm
1	0.05	325	2.56	350	2.50	326	2.56
2	0.15	625	2.97	620	3.00	610	2.99
2.5	0.25	720	3.36	750	3.31	730	3.34
3	0.3	815	3.42	820	3.42	810	3.43
4	0.4	950	3.58	970	3.55	970	3.55
5	0.5	1060	3.72	1090	3.68	1090	3.68
6	0.55	1170	3.71	1195	3.69	1195	3.69
7	0.65	1295	3.79	1300	3.79	1305	3.78
8	0.70						
10	0.80						
15	1.05						
20	1.25						
23	1.35						

Liquid: height (above orifice): 5.7 cm
volume: 2 L
temperature (C) 25

Bubble Column Experiment

System -- Liquid: 5 wt % Sucrose Orifice Diameter: 22 mils
Gas: Air

Gauge (-)	Q (ml/s)	Time(hr:min): f_s (s^{-1})	Time(hr:min): D_b mm	Time(hr:min): f_s (s^{-1})	Time(hr:min): D_b mm	Time(hr:min): f_s (s^{-1})	Time(hr:min): D_b mm
1	0.05	222	2.91	222	2.91	216	2.93
2	0.15	375	3.52	377	3.51	370	3.53
2.5	0.25	422	4.01	413	4.04	410	4.05
3	0.3	453	4.16	455	4.16	450	4.17
4	0.4	522	4.37	525	4.36	525	4.36
5	0.5	585	4.53	586	4.53	580	4.54
6	0.55	640	4.54	640	4.54	636	4.55
7	0.65	690	4.68	686	4.69	686	4.69
8	0.70	760	4.65	750	4.67	760	4.65
10	0.80	835	4.71	840	4.70	840	4.70
15	1.05	1000	4.85	1000	4.85	1000	4.85
20	1.25	1150	4.91	1150	4.91	1150	4.91
23	1.35	1220	4.94	1220	4.94	1230	4.93

Liquid: height (above orifice): 5.7 cm
volume: 2 L
temperature (C) 25

Bubble Column Experiment

System -- Liquid: 5 wt % Sucrose Orifice Diameter: 26 mils
Gas: Air

Gauge (-)	Q (ml/s)	Time(hr:min): 5:45 f_s (s^{-1})	5:45 D_b mm	Time(hr:min): 5:55 f_s (s^{-1})	5:55 D_b mm	Time(hr:min): 6:05 f_s (s^{-1})	6:05 D_b mm
1	0.05	222	2.91	222	2.91	216	2.93
2	0.15	375	3.52	377	3.51	370	3.53
2.5	0.25	422	4.01	413	4.04	410	4.05
3	0.3	453	4.16	455	4.16	450	4.17
4	0.4	522	4.37	525	4.36	525	4.36
5	0.5	585	4.53	586	4.53	580	4.54
6	0.55	640	4.54	640	4.54	636	4.55
7	0.65	690	4.68	686	4.69	686	4.69
8	0.70	760	4.65	750	4.67	760	4.65
10	0.80	835	4.71	840	4.70	840	4.70
15	1.05	1000	4.85	1000	4.85	1000	4.85
20	1.25	1150	4.91	1150	4.91	1150	4.91
23	1.35	1220	4.94	1220	4.94	1230	4.93

Liquid: height (above orifice): 5.7 cm
volume: 2 L
temperature (C) 25

Bubble Column Experiment

System -- Liquid: WCM-4 (pH=4.5) Orifice Diameter: 11 mils
Gas: Air

Gauge (-)	Q (ml/s)	Time(hr:min): f_s (s^{-1})	Time(hr:min): D_b mm	Time(hr:min): f_s (s^{-1})	Time(hr:min): D_b mm	Time(hr:min): f_s (s^{-1})	Time(hr:min): D_b mm
1	0.05						
2	0.15	980	2.55	980	2.55	860	2.67
2.5	0.25	1200	2.83	1200	2.83	1200	2.83
3	0.3	1350	2.89	1360	2.89	1340	2.90
4	0.4	1700	2.95	1720	2.94	1680	2.96
5	0.5	1940	3.04	2000	3.01	2000	3.01
6	0.55	2180	3.02	2180	3.02	2180	3.02
7	0.65						
8	0.70						
10	0.80						
15	1.05						
20	1.25						
23	1.35						

Liquid: height (above orifice): 5.7 cm
volume: 2.5 L
temperature (C) 25

Bubble Column Experiment

System -- Liquid: WCM-4 (pH=4.5) Orifice Diameter: 14 mils
Gas: Air

Gauge (-)	Q (ml/s)	Time(hr:min): 2:25 f_s (s^{-1})	D_b mm	Time(hr:min): - f_s (s^{-1})	D_b mm	Time(hr:min): - f_s (s^{-1})	D_b mm
1	0.05	105	3.73	137	3.41	175	3.14
2	0.15	500	3.18	510	3.18	505	3.18
2.5	0.25	630	3.51	625	3.52	610	3.55
3	0.3	740	3.53	730	3.55	730	3.55
4	0.4	910	3.63	900	3.64	910	3.63
5	0.5	1050	3.73	1040	3.74	1050	3.73
6	0.55	1160	3.72	1150	3.73	1150	3.73
7	0.65						
8	0.70						
10	0.80						
15	1.05						
20	1.25						
23	1.35						

Liquid: height (above orifice): 5.8 cm
volume: 2.5 L
temperature (C) 22

Bubble Column Experiment

System -- Liquid: WCM-4 (pH=4.5) Orifice Diameter: 22 mils
Gas: Air

Gauge (-)	Q (ml/s)	Time(hr:min): f_s (s^{-1})	Time(hr:min): D_b mm	Time(hr:min): f_s (s^{-1})	Time(hr:min): D_b mm	Time(hr:min): f_s (s^{-1})	Time(hr:min): D_b mm
1	0.05						
2	0.15	275	3.90	250	4.03	270	3.93
2.5	0.25	340	4.31	337	4.32	330	4.35
3	0.3	375	4.43	375	4.43	380	4.41
4	0.4	460	4.56	465	4.54	460	4.56
5	0.5	535	4.67	535	4.67	545	4.64
6	0.55	595	4.65	590	4.66	590	4.66
7	0.65	655	4.76	650	4.77	650	4.77
8	0.70	740	4.69	750	4.67	730	4.71
10	0.80	940	4.70	830	4.72	840	4.70
15	1.05	1010	4.84	1020	4.82	1020	4.82
20	1.25	1190	4.85	1180	4.87	1180	4.87
23	1.35	1260	4.89	1280	4.86	1270	4.87

Liquid: height (above orifice): 5.7 cm
volume: 2.5 L
temperature (C) 25

Bubble Column Experiment

System -- Liquid: WCM-4 (pH=4.5) Orifice Diameter: 26 mils
Gas: Air

Gauge (-)	Q (ml/s)	Time(hr:min): 4:25 f_s (s^{-1})	Time(hr:min): 4:25 D_b mm	Time(hr:min): 4:32 f_s (s^{-1})	Time(hr:min): 4:32 D_b mm	Time(hr:min): 4:40 f_s (s^{-1})	Time(hr:min): 4:40 D_b mm
1	0.05						
2	0.15	285	3.86	285	3.86	280	3.88
2.5	0.25	355	4.25	350	4.27	350	4.27
3	0.3	395	4.36	395	4.36	390	4.37
4	0.4	475	4.51	470	4.52	465	4.54
5	0.5	545	4.64	540	4.65	540	4.65
6	0.55	600	4.64	590	4.66	595	4.65
7	0.65	650	4.77	655	4.76	650	4.77
8	0.70	730	4.71	730	4.71	730	4.71
10	0.80	820	4.74	820	4.74	820	4.74
15	1.05	1000	4.85	1000	4.85	1000	4.85
20	1.25	1140	4.92	1140	4.92	1140	4.92
23	1.35	1240	4.91	1240	4.91	1240	4.91

Liquid: height (above orifice): 5.7 cm
volume: 2.5 L
temperature (C) 24.5

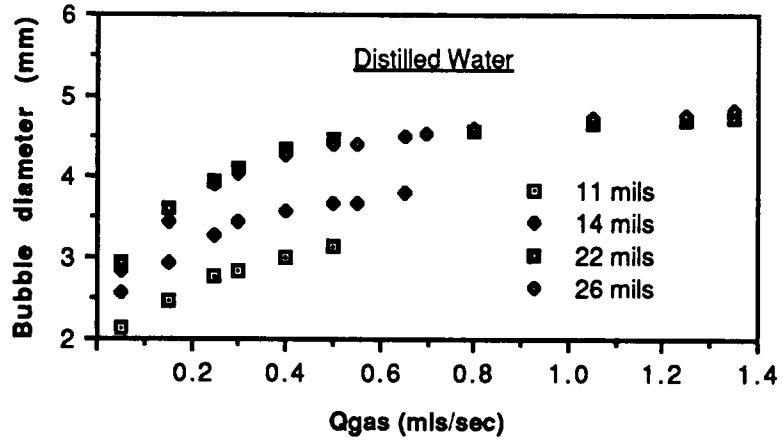

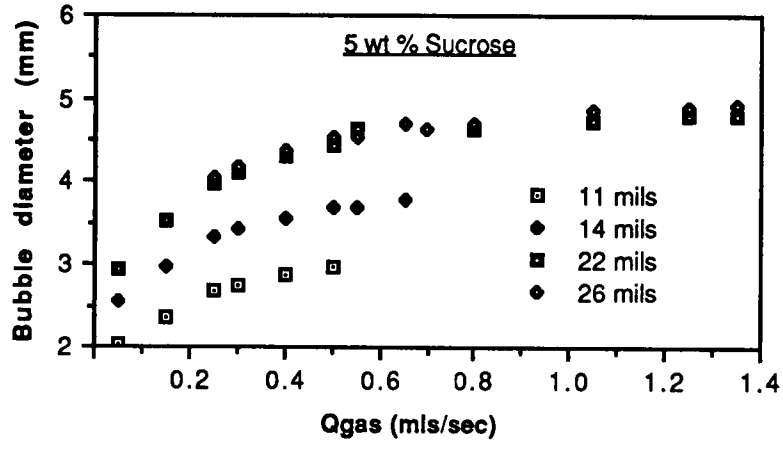

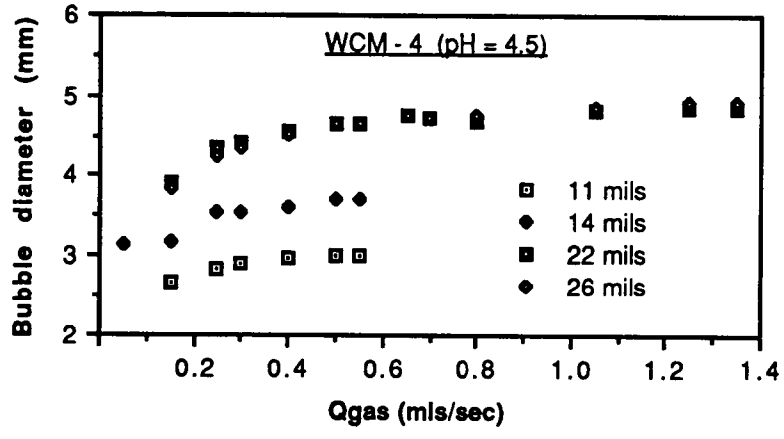

Bubble diameter as a function of orifice size, liquid composition and volumetric gas flow rate. System: single submerged orifice in a bubble column. Orifice diameters measured were: 11, 14, 22 and 26 mils (0.028, 0.036, 0.056 and 0.066 cm, respectively).

Design of Airlift Reactor Perforated Plate

Goal: To determine what orifice plate design would be most efficient for producing the given operational parameters.

Given: (1) Gas flow rate (vvm) will be increased while increasing the number of holes in the orifice plate such that the Reynolds number at each orifice will remain constant.

(2) The desired vvm are 0.1, 0.2 and 0.4 necessitating three orifice plates, one for each vvm.

(3) Each orifice on each plate should be at least thrice the bubble diameter from every adjacent orifice to minimize bubble-bubble interaction (e.g. coalescence) -- as recommended by Treybal.

(4) The inner draft tube outer diameter is 6.35 cm (2.5 in) so all orifices must fall within that diameter by the distance necessary to minimize bubble interaction with the draft tube inside wall.

Designing a plate to meet operational the given item (3) requires prior knowledge of bubble size. Use the data generated in the bubble column experiments and the method outlined below.

(1) Establish an operational Reynolds number (e.g. Re $\leq$ 2100)
(2) Establish an orifice diameter
(3) Calculate the volumetric gas flow rate per orifice
(4) Establish a range of vvm (e.g. 0.1 to 0.4)
(5) Establish a liquid volume (e.g. 1 liter)
(6) Calculate the total volumetric gas flow rate required to meet each vvm given the liquid volume
(7) Calculate the number of orifices required to meet the total volumetric flow rate
(8) Estimate average bubble diameters (for different liquid solutions)
(9) Calculate the minimum distance between adjacent orifices
(10) Determine the pitch of the orifice design (e.g. circular or triangular).

APPENDIX II

APPENDIX II

The following pages contain raw data collected during the operation of the airlift reactor. Included are the strip chart recording of the liquid phase dissolved oxygen concentration and tabulated information on the number of dispersed gas bubbles suspended in the liquid phase during absorption and desorption. The preliminary pages contain information that distinguish the raw data into groups and reference them to each other.

Reduced data on the oxygen absorption and desorption in the airlift reactor are also included. The reduced data summarize the dimensionless liquid phase oxygen concentration as a function time, the calculated gas holdup and other intermediate calculated values of relevant parameters in the airlift reactor operations.

EXPERIMENTAL AIRLIFT OPERATION

Data to be used to calculate overall mass-transfer coefficient ($k_l a$), interfacial area, (a) and liquid-phase mass-transfer coefficient (k_l).

Date: 6/3

Orifice plate: Number of orifices: 5

NO GAS FLOW

Liquid Composition: Dist. H_2O
Liquid Temperature: 24.5°C
Liquid Height (from outside bottom of reactor): 20.1 cm
Liquid Volume (including that in manometer): 2300 mls

Draft tube: Distance from outside bottom of reactor to bottom of draft tube: 2.5 cm
Distance from top of draft tube to top of liquid: 2.5 cm

Reactor Lid: Distance from top of liquid to bottom of lid: 2.5 cm

CAMERA

FILM: ☒ B & W ☐ Color TYPE: ☒ TMAX 100 400 TX 135-36
SHUTTER SPEED: 250 ☐ OTHER: _____

LIGHTING: ☒ 2 Flood lamps @ ~ 6 cm from opposites of reactor wall
☐ OTHER: _____
APERTURE SETTING: 16

GAS FLOW NOT EQUAL TO ZERO*

IF STRIPPING WITH NITROGEN THEN ESTABLISH A STEADY BASELINE (ABOUT 20 MINUTES)

Gas Flow: Gauge Reading: 1.3 PSIG
Flow Rate: 4.9 mls/sec

Gas Composition: N_2

Dissolved Oxygen: Beginning ppm: ?

Exposure label (take three data points): 6/3M _____ _____

Bubble size: Strobe light RPM (take three data points): 770 770 _____

MAKE SURE THE FLASH-BUBBLE RATIO IS ONE-TO-ONE

Number of sparger orifices producing bubbles: 5

Label this length of strip chart output: N1 * Liquid Temp.: 25°C

Final Dissolved oxygen ppm*: 00.0

* Mark this on the strip chart output, also

(1)

(2)

6/3

GAS FLOW NOT EQUAL TO ZERO*

Gas Flow: Gauge Reading: 1.3 PSIG
Flow Rate: 4.9 mls/sec

Gas Composition: AIR

Dissolved Oxygen: Beginning ppm: 00.0

Exposure label (take three data points): 6/3N 6/3O 6/3P

Bubble size: Strobe light RPM (take three data points): 780 780 770

MAKE SURE THE FLASH-BUBBLE RATIO IS ONE-TO-ONE

Number of sparger orifices producing bubbles: 5

Label this length of strip chart output: A1 . Liquid temp. 25°C

Final Dissolved oxygen ppm*: 8.7

GAS FLOW NOT EQUAL TO ZERO*

Gas Flow: Gauge Reading: 1.3 PSIG
Flow Rate: 4.8 mls/sec

Gas Composition: N_2

Dissolved Oxygen: Beginning ppm: 8.7

Exposure label(take three data points): 6/3Q 6/3R 6/3S

Bubble size: Strobe light RPM (take three data points): 770 770 770

MAKE SURE THE FLASH-BUBBLE RATIO IS ONE-TO-ONE

Number of sparger orifices producing bubbles: 5

Label this length of strip chart output: N2 . Liquid temp: 25°C

Final Dissolved oxygen ppm*: 00.0

COMMENT: Liquid comp: dist. H_2O

(3)

GAS FLOW NOT EQUAL TO ZERO*

Gas Flow: Gauge Reading: 1.3 PSIG
Flow Rate: 4.9 mls/sec

Exposure 6/3 "T" is WASTED. Due to A Qgas being wrong A2 was redone

Gas Composition: AIR

Dissolved Oxygen: Beginning ppm: 00 0

Exposure label (take three data points): 6/3 U 6/3 V 6/3 W

Bubble size: Strobe light RPM (take three data points): 770 770 780

MAKE SURE THE FLASH-BUBBLE RATIO IS ONE-TO-ONE

Number of sparger orifices producing bubbles: 5

Label this length of strip chart output: A2 .

Liquid temp: 24.5°C

Final Dissolved oxygen ppm*: 8.3

GAS FLOW NOT EQUAL TO ZERO*

Gas Flow: Gauge Reading: PSIG
Flow Rate: mls/sec

Gas Composition:

Dissolved Oxygen: Beginning ppm:

Exposure label(take three data points): 6/3 X 6/3 Y 6/3 Z

Bubble size: Strobe light RPM (take three data points): 780 780 780

MAKE SURE THE FLASH-BUBBLE RATIO IS ONE-TO-ONE

Number of sparger orifices producing bubbles: 5

Label this length of strip chart output: N3 .

Liquid temp: 25°C

Final Dissolved oxygen ppm*: 00.5 BUT C* = 00.0 (SAME N_2)

COMMENT: E 6/3 T IS NOT A RELEVANT PICTURE.
Liquid comp.: dist. H_2O

* Mark this on the strip chart output, also

EXPERIMENTAL AIRLIFT OPERATION

Data to be used to calculate overall mass-transfer coefficient ($k_l a$), interfacial area, (a) and liquid-phase mass-transfer coefficient (k_l).

Date: 6/3

Orifice plate: Number of orifices: 9

NO GAS FLOW

Liquid Composition: Dist. H_2O
Liquid Temperature: 25° C
Liquid Height (from outside bottom of reactor): 20.3 cm
Liquid Volume (including that in manometer): 2300 mls

Draft tube: Distance from outside bottom of reactor to bottom of draft tube: 2.5 cm
Distance from top of draft tube to top of liquid: 2.5 cm

Reactor Lid: Distance from top of liquid to bottom of lid: 2.5 cm

CAMERA

FILM: ☒ B & W ☐ Color TYPE: ☒ TMAX TMY 135-24 ASA 40
SHUTTER SPEED: 250 ☐ OTHER:_____

LIGHTING: ☒ 2 Flood lamps @ ~ 6 cm from opposites of reactor wall
☐ OTHER:_____

APERTURE SETTING: 16

GAS FLOW NOT EQUAL TO ZERO*

IF STRIPPING WITH NITROGEN THEN ESTABLISH A STEADY BASELINE (ABOUT 20 MINUTES)

Gas Flow: Gauge Reading: 3.9 PSIG
Flow Rate: 8.8 mls/sec

Gas Composition: N_2

Dissolved Oxygen: Beginning ppm: 8.2

Exposure label (take three data points): 6/3 A _____ _____

Bubble size: Strobe light RPM (take three data points): 1160 1160 1170

MAKE SURE THE FLASH-BUBBLE RATIO IS ONE-TO-ONE

Number of sparger orifices producing bubbles: 9

Label this length of strip chart output: N1 • Liquid Temp.: 24.5 °C

Final Dissolved oxygen ppm*: 00.0

* Mark this on the strip chart output, also

(1)

(2)

GAS FLOW NOT EQUAL TO ZERO*

Gas Flow: Gauge Reading: 3.9 PSIG
Flow Rate: 8.2 mls/sec

Gas Composition: AIR

Dissolved Oxygen: Beginning ppm: 00.0

Exposure label (take three data points): 6/3B 6/3C BETWEEN 6/3C & 6/3D

Bubble size: Strobe light RPM
(take three data points):
1170 1170 1170

MAKE SURE THE FLASH-BUBBLE RATIO IS ONE-TO-ONE

Number of sparger orifices producing bubbles: 9

Liquid Temp: 25°C

Label this length of strip chart output: A1 *

Final Dissolved oxygen ppm*: 8.1

GAS FLOW NOT EQUAL TO ZERO*

Gas Flow: Gauge Reading: 3.9 PSIG
Flow Rate: 8.3 mls/sec

Gas Composition: N_2

Dissolved Oxygen: Beginning ppm: 8.1

Exposure label(take three data points): 6/3D 6/3E 6/3F

Bubble size: Strobe light RPM
(take three data points):
1170 1170 1170

MAKE SURE THE FLASH-BUBBLE RATIO IS ONE-TO-ONE

Number of sparger orifices producing bubbles: 9

Liquid Temp: 25°C

Label this length of strip chart output: N2 *

Final Dissolved oxygen ppm*: 00.0

COMMENT: Liquid comp: dist. H_2O

* Mark this on the strip chart output, also

(1)

(3)

GAS FLOW NOT EQUAL TO ZERO*

Gas Flow: Gauge Reading: 3.9 PSIG
Flow Rate: 8.8 mls/sec

Gas Composition: AIR

Dissolved Oxygen: Beginning ppm: 00.0

Exposure label (take three data points): 6/3G 6/3H 6/3I

Bubble size: Strobe light RPM (take three data points): 1160 1160 1160

MAKE SURE THE FLASH-BUBBLE RATIO IS ONE-TO-ONE

Number of sparger orifices producing bubbles: 9

Label this length of strip chart output: A2 . Liquid temp. 24.5°C

Final Dissolved oxygen ppm*: 8.9 (kinda high)

GAS FLOW NOT EQUAL TO ZERO* NEW ROLL OF FILM: **

Gas Flow: Gauge Reading: 3.9 PSIG
Flow Rate: 8.8 mls/sec

Gas Composition: N_2

Dissolved Oxygen: Beginning ppm: 8.9

Exposure label(take three data points): 6/3J 6/3K 6/3L

Bubble size: Strobe light RPM (take three data points): 1170 1170 1170

MAKE SURE THE FLASH-BUBBLE RATIO IS ONE-TO-ONE

Number of sparger orifices producing bubbles: 9

Label this length of strip chart output: N3 . Liquid Temp: 25°C

Final Dissolved oxygen ppm*: 00.0

COMMENT: ** Tri-x Pan (ISO 400) TX 135-36
Liquid comp: dist. H_2O

* Mark this on the strip chart output, also

EXPERIMENTAL AIRLIFT OPERATION

Data to be used to calculate overall mass-transfer coefficient ($k_l a$), interfacial area, (a) and liquid-phase mass-transfer coefficient (k_l).

Date: 6/2

Orifice plate: Number of orifices: 19

NO GAS FLOW

Liquid Composition: Dist. H_2O
Liquid Temperature: 25.5 °C
Liquid Height (from outside bottom of reactor): 20.4 cm
Liquid Volume (including that in manometer): 2300 mls

Draft tube: Distance from outside bottom of reactor to bottom of draft tube: 2.5 cm
Distance from top of draft tube to top of liquid: 2.5 cm

Reactor Lid: Distance from top of liquid to bottom of lid: 2.5 cm

CAMERA

FILM: ☒ B & W ☐ Color TYPE: ☒ TMAX 135-24
SHUTTER SPEED: 250 ☐ OTHER:_____

LIGHTING: ☒ 2 Flood lamps @ ~ 6 cm from opposites of reactor wall
☐ OTHER:_____
APERTURE SETTING: 16

GAS FLOW NOT EQUAL TO ZERO*

IF STRIPPING WITH NITROGEN THEN ESTABLISH A STEADY BASELINE (ABOUT 20 MINUTES)

Gas Flow: Gauge Reading: 14.5 PSIG
Flow Rate: 18.6 mls/sec

Gas Composition: N_2

Dissolved Oxygen: Beginning ppm: 7.9

Exposure label (take three data points): 6/2A 6/2A _____
OOPS
TWO EXPOSURES OF 6/2A

Bubble size: Strobe light RPM (take three data points): MAKE SURE THE FLASH-BUBBLE RATIO IS ONE-TO-ONE
1420 _____ _____

Number of sparger orifices producing bubbles: 19

Label this length of strip chart output: N1 * Liquid Temp.: 26.5 °C

Final Dissolved oxygen ppm*: 00.0

* Mark this on the strip chart output, also

6/2

GAS FLOW NOT EQUAL TO ZERO*

Gas Flow: Gauge Reading: 14.5 PSIG
Flow Rate: 18.6 mls/sec

Gas Composition: Air

Dissolved Oxygen: Beginning ppm: 00.0

Exposure label (take three data points): 6/2B 6/2C 6/2D

Bubble size: Strobe light RPM (take three data points): 1450 1462 1470

MAKE SURE THE FLASH-BUBBLE RATIO IS ONE-TO-ONE

Number of sparger orifices producing bubbles: 19

Label this length of strip chart output: A1 *

Liquid Temp: 26°C

Final Dissolved oxygen ppm*: 8.3

GAS FLOW NOT EQUAL TO ZERO*

Gas Flow: Gauge Reading: 14.5 PSIG
Flow Rate: 18.6 mls/sec

Gas Composition: N_2

Dissolved Oxygen: Beginning ppm: 8.3

Exposure label(take three data points): 6/2E 6/2F 6/2G

Bubble size: Strobe light RPM (take three data points): 1470 1470 1470

MAKE SURE THE FLASH-BUBBLE RATIO IS ONE-TO-ONE

Number of sparger orifices producing bubbles: 19

Label this length of strip chart output: N2 *

Liquid Temp: 26°C

Final Dissolved oxygen ppm*:

COMMENT: Liquid comp: dist. H_2O

* Mark this on the strip chart output, also

6/2

GAS FLOW NOT EQUAL TO ZERO*

Gas Flow: Gauge Reading: 14.5 PSIG
Flow Rate: 18.6 mls/sec

Gas Composition: AIR

Dissolved Oxygen: Beginning ppm: 00.0

Exposure label (take three data points): 6/2 H 6/2 I 6/2 J

Bubble size: Strobe light RPM (take three data points): 1460 1460 1460

MAKE SURE THE FLASH-BUBBLE RATIO IS ONE-TO-ONE

Number of sparger orifices producing bubbles: 19

Label this length of strip chart output: (A2) . Liquid Temp.: 26°C

Final Dissolved oxygen ppm*: 8.5

GAS FLOW NOT EQUAL TO ZERO*

Gas Flow: Gauge Reading: 14.5 PSIG
Flow Rate: 18.6 mls/sec

Gas Composition: N_2

Dissolved Oxygen: Beginning ppm: 8.5

Exposure label(take three data points): 6/2 K 6/2 L 6/2 M

Bubble size: Strobe light RPM (take three data points): 1460 1460 1465

MAKE SURE THE FLASH-BUBBLE RATIO IS ONE-TO-ONE

Number of sparger orifices producing bubbles: 19

Label this length of strip chart output: N3 . Liquid Temp: 26°C

Final Dissolved oxygen ppm*: 00.1*

COMMENT: * Stopped before reaching 00.0 because running low on N_2
Liquid comp.: dist. H_2O

* Mark this on the strip chart output, also

EXPERIMENTAL AIRLIFT OPERATION

Data to be used to calculate overall mass-transfer coefficient ($k_l a$), interfacial area, (a) and liquid-phase mass-transfer coefficient (k_l).

Date: 7/7

Orifice plate: Number of orifices: 5

NO GAS FLOW

Liquid Composition: 5 % sucrose
Liquid Temperature:
Liquid Height (from outside bottom of reactor):
Liquid Volume : 2300 mls

Draft tube: Distance from outside bottom of reactor to bottom of draft tube:
Distance from top of draft tube to top of liquid:

Reactor Lid: Distance from top of liquid to bottom of lid:

CAMERA

FILM: ☒ B & W ☐ Color TYPE: ☒ TMAX TMY 125-36
SHUTTER SPEED: 250 ☐ OTHER:_____

LIGHTING: ☒ 2 Flood lamps @ ~ 6 cm from opposites of reactor wall
☐ OTHER:_____
APERTURE SETTING: 16

GAS FLOW NOT EQUAL TO ZERO*

IF STRIPPING WITH NITROGEN THEN ESTABLISH A STEADY BASELINE (ABOUT 20 MINUTES)

Gas Flow: Gauge Reading: PSIG
Flow Rate: mls/sec

Gas Composition: N_2

Dissolved Oxygen: Beginning ppm: ?

Exposure label (take three data points): ___ ___ ___

Bubble size: Strobe light RPM (take three data points): ___ ___ ___

MAKE SURE THE FLASH-BUBBLE RATIO IS ONE-TO-ONE

Number of sparger orifices producing bubbles: 5

Label this length of strip chart output: N1 * Liquid Temp.: 24.5 °C

Final Dissolved oxygen ppm*: 00.0

* Mark this on the strip chart output, also

Date: 7/7

GAS FLOW NOT EQUAL TO ZERO*

Gas Flow: Gauge Reading: 25 PSIG
Flow Rate: 6.4 mls/sec

Gas Composition: AIR

Dissolved Oxygen: Beginning ppm: 00.0

Exposure label (take three data points): 7/7A 7/7B 7/7C

Bubble size: Strobe light RPM (take three data points): 1160 1160 1160

MAKE SURE THE FLASH-BUBBLE RATIO IS ONE-TO-ONE

Number of sparger orifices producing bubbles: 5

Label this length of strip chart output: A1 *

Final Dissolved oxygen ppm*: 7.9 Liquid Temp.: 23.5 °C

Heat to 25°C

GAS FLOW NOT EQUAL TO ZERO*

Gas Flow: Gauge Reading: 25 PSIG
Flow Rate: 6.4 mls/sec

Gas Composition: N_2

Dissolved Oxygen: Beginning ppm: 7.7

Exposure label(take three data points): 7/7D 7/7E 7/7F

Bubble size: Strobe light RPM (take three data points): 1350 1350 1350

MAKE SURE THE FLASH-BUBBLE RATIO IS ONE-TO-ONE

Number of sparger orifices producing bubbles: 5

Label this length of strip chart output: N2 *

Final Dissolved oxygen ppm*: 00.0 Liquid Temp.: 25 °C

COMMENT: Liquid comp: 5 wt% sucrose

Date: 7/7

GAS FLOW NOT EQUAL TO ZERO*

Gas Flow: Gauge Reading: 2.5 PSIG
Flow Rate: 6.4 mls/sec

Gas Composition: Air

Dissolved Oxygen: Beginning ppm: 00.0

Exposure label (take three data points): 7/7G 7/7H 7/7I

Bubble size: Strobe light RPM (take three data points): 1360 1340 1360

MAKE SURE THE FLASH-BUBBLE RATIO IS ONE-TO-ONE

Number of sparger orifices producing bubbles: 5

Label this length of strip chart output: A2 *

Final Dissolved oxygen ppm*: 7.7 Liquid Temp.: 24.5 °C

GAS FLOW NOT EQUAL TO ZERO*

Gas Flow: Gauge Reading: 2.5 PSIG
Flow Rate: 6.4 mls/sec

Gas Composition: N_2

Dissolved Oxygen: Beginning ppm: 7.7

Exposure label(take three data points): 7/7J 7/7K OUT OF FILM (END OF ROLL)

Bubble size: Strobe light RPM (take three data points): 1590 1590 1580

MAKE SURE THE FLASH-BUBBLE RATIO IS ONE-TO-ONE

Number of sparger orifices producing bubbles: 5

Label this length of strip chart output: N2 *

Final Dissolved oxygen ppm*: 00.0 Liquid Temp.: 25 °C

COMMENT: Liquid comp: 5 wt% sucrose

EXPERIMENTAL AIRLIFT OPERATION

Data to be used to calculate overall mass-transfer coefficient ($k_l a$), interfacial area, (a) and liquid-phase mass-transfer coefficient (k_l).

Date: 7/5

Orifice plate: Number of orifices: 9

NO GAS FLOW

Liquid Composition: 5 wt% sucrose
Liquid Temperature: 23 °C
Liquid Height (from outside bottom of reactor): 20.1 cm
Liquid Volume : 2700 mls

Draft tube: Distance from outside bottom of reactor to bottom of draft tube: 2.5 cm
Distance from top of draft tube to top of liquid: 2.5 cm

Reactor Lid: Distance from top of liquid to bottom of lid: 2.5 cm

CAMERA

FILM: ☒ B & W ☐ Color TYPE: ☒ TMAX TMY 135 - 36
SHUTTER SPEED: 250 ☐ OTHER:_____

LIGHTING: ☒ 2 Flood lamps @ ~ 6 cm from opposites of reactor wall
☐ OTHER:_____
APERTURE SETTING: 16

GAS FLOW NOT EQUAL TO ZERO*

IF STRIPPING WITH NITROGEN THEN ESTABLISH A STEADY BASELINE (ABOUT 20 MINUTES)

Gas Flow: Gauge Reading: 30 PSIG
Flow Rate: ~ mls/sec

Gas Composition: N_2

Dissolved Oxygen: Beginning ppm: 8.0

Exposure label (take three data points): ___ ___ ___

Bubble size: Strobe light RPM (take three data points): ___ ___ ___

MAKE SURE THE FLASH-BUBBLE RATIO IS ONE-TO-ONE

Number of sparger orifices producing bubbles: 9

Label this length of strip chart output: N1 * Liquid Temp.: 24.5

Final Dissolved oxygen ppm*: 00.0

* Mark this on the strip chart output, also

Date: 7/5

GAS FLOW NOT EQUAL TO ZERO*

Gas Flow: Gauge Reading: 7.2 PSIG
Flow Rate: 11.4 mls/sec

Gas Composition: AIR

Dissolved Oxygen: Beginning ppm: 00.0

Exposure label (take three data points): 7/5 A 7/5 B 7/5 C

Bubble size: Strobe light RPM (take three data points): 1400 1390 1400

MAKE SURE THE FLASH-BUBBLE RATIO IS ONE-TO-ONE

Number of sparger orifices producing bubbles: 9

Label this length of strip chart output: A1 *

Final Dissolved oxygen ppm*: 7.5 Liquid Temp.: 25°C

GAS FLOW NOT EQUAL TO ZERO*

Gas Flow: Gauge Reading: 7.2 PSIG
Flow Rate: 11.4 mls/sec

Gas Composition: N_2

Dissolved Oxygen: Beginning ppm: 7.5

Exposure label(take three data points): 7/5 D 7/5 E 7/5 F

Bubble size: Strobe light RPM (take three data points): 1350 1390 1360

MAKE SURE THE FLASH-BUBBLE RATIO IS ONE-TO-ONE

Number of sparger orifices producing bubbles: 9

Label this length of strip chart output: N2 *

Final Dissolved oxygen ppm*: 00.0 Liquid Temp.: 25°C

COMMENT: Liquid comp: 5 wt% sucrose

Date: 7/5

GAS FLOW NOT EQUAL TO ZERO*

Gas Flow: Gauge Reading: 7.2 PSIG
Flow Rate: 11.4 mls/sec

Gas Composition: AIR

Dissolved Oxygen: Beginning ppm: 00.0

Exposure label (take three data points): 7/5 G 7/5 H 7/5 I

Bubble size: Strobe light RPM (take three data points): 1370 1370 1370

MAKE SURE THE FLASH-BUBBLE RATIO IS ONE-TO-ONE

Number of sparger orifices producing bubbles: 9

Label this length of strip chart output: A2 *

Final Dissolved oxygen ppm*: 7.5

Liquid Temp.: 24 °C

GAS FLOW NOT EQUAL TO ZERO*

Gas Flow: Gauge Reading: 7.2 PSIG
Flow Rate: 11.4 mls/sec

Gas Composition: N_2

Dissolved Oxygen: Beginning ppm: 7.6

Exposure label(take three data points): 7/5 J 7/5 K 7/5 L

Bubble size: Strobe light RPM (take three data points): 1300 1320 1320

MAKE SURE THE FLASH-BUBBLE RATIO IS ONE-TO-ONE

Number of sparger orifices producing bubbles: 9

Label this length of strip chart output: N3 *

Final Dissolved oxygen ppm*: 00.0

Liquid Temp.: 24.5 °C

COMMENT: Liquid comp: 5 wt% sucrose

EXPERIMENTAL AIRLIFT OPERATION

Data to be used to calculate overall mass-transfer coefficient (k_la), interfacial area, (a) and liquid-phase mass-transfer coefficient (k_l).

Date: 7/4

Orifice plate: Number of orifices: 19

NO GAS FLOW

Liquid Composition: 5 wt% sucrose
Liquid Temperature: 25.5 °C
Liquid Height (from outside bottom of reactor): 20.2 cm
Liquid Volume ~~(including that in manometer)~~: 2300 ml's

Draft tube: Distance from outside bottom of reactor to bottom of draft tube: 2.5 cm
Distance from top of draft tube to top of liquid: 2.5 cm

Reactor Lid: Distance from top of liquid to bottom of lid: 2.5 cm

CAMERA

FILM: ☒ B & W ☐ Color TYPE: ☒ TMAX TMY 135-36
SHUTTER SPEED: 250 ☐ OTHER:_____

LIGHTING: ☒ 2 Flood lamps @ ~ 6 cm from opposites of reactor wall
☐ OTHER:_____
APERTURE SETTING: 16

GAS FLOW NOT EQUAL TO ZERO*

IF STRIPPING WITH NITROGEN THEN ESTABLISH A STEADY BASELINE (ABOUT 20 MINUTES)

Gas Flow: Gauge Reading: 30 PSIG
Flow Rate: ? mls/sec

Gas Composition: N_2

Dissolved Oxygen: Beginning ppm: ?

Exposure label (take three data points): ____ ____ ____

Bubble size: Strobe light RPM (take three data points): ____ ____ ____

MAKE SURE THE FLASH-BUBBLE RATIO IS ONE-TO-ONE

Number of sparger orifices producing bubbles: 19

Label this length of strip chart output: N1 . Liquid Temp.: 25.5 C

Final Dissolved oxygen ppm*: 00.0

* Mark this on the strip chart output, also

Date: 7/4

GAS FLOW NOT EQUAL TO ZERO*

Gas Flow: Gauge Reading: 22 PSIG
Flow Rate: 22.6 mls/sec

Gas Composition: AIR

Dissolved Oxygen: Beginning ppm: 00.0

Exposure label (take three data points): 7/4 A 7/4 B 7/4 C

Bubble size: Strobe light RPM (take three data points): 1620 1610 1610

MAKE SURE THE FLASH-BUBBLE RATIO IS ONE-TO-ONE

Number of sparger orifices producing bubbles: 19

Label this length of strip chart output: A1 *

Final Dissolved oxygen ppm*: 7.7 Liquid Temp.: 25 °C

GAS FLOW NOT EQUAL TO ZERO*

Gas Flow: Gauge Reading: 22 PSIG
Flow Rate: 22.6 mls/sec

Gas Composition: N_2

Dissolved Oxygen: Beginning ppm: 7.7

Exposure label(take three data points): 7/4 D 7/4 E 7/4 F

Bubble size: Strobe light RPM (take three data points): 1610 1620 1620

MAKE SURE THE FLASH-BUBBLE RATIO IS ONE-TO-ONE

Number of sparger orifices producing bubbles: 19

Label this length of strip chart output: N2 *

Final Dissolved oxygen ppm*: 00.0 Liquid Temp.: 25 °C

COMMENT: Liquid comp: 5 wt% sucrose

Date: 7/4

GAS FLOW NOT EQUAL TO ZERO*

Gas Flow: Gauge Reading: 22 PSIG
Flow Rate: 22.6 mls/sec

Gas Composition: Air

Dissolved Oxygen: Beginning ppm: 00.0

Exposure label (take three data points): 7/4G 7/4H 7/4I

Bubble size: Strobe light RPM (take three data points): 1610 1600 1600

MAKE SURE THE FLASH-BUBBLE RATIO IS ONE-TO-ONE

Number of sparger orifices producing bubbles: 19

Label this length of strip chart output: A2 *

Final Dissolved oxygen ppm*: 7.7 Liquid Temp.: 25°C

GAS FLOW NOT EQUAL TO ZERO*

Gas Flow: Gauge Reading: 22 PSIG
Flow Rate: 22.6 mls/sec

Gas Composition: N_2

Dissolved Oxygen: Beginning ppm: 7.7

Exposure label(take three data points): 7/4J 7/4K 7/4L

Bubble size: Strobe light RPM (take three data points): 1620 1610 1610

MAKE SURE THE FLASH-BUBBLE RATIO IS ONE-TO-ONE

Number of sparger orifices producing bubbles: 19

Label this length of strip chart output: N3 *

Final Dissolved oxygen ppm*: 00.0 Liquid Temp.: 25°C

COMMENT: Liquid comp: 5 wt% sucrose

EXPERIMENTAL AIRLIFT OPERATION

Data to be used to calculate overall mass-transfer coefficient ($k_l a$), interfacial area, (a) and liquid-phase mass-transfer coefficient (k_l).

Date: 6/10

Orifice plate: Number of orifices: 5

NO GAS FLOW

Liquid Composition: WCM-4 (pH 4.5)
Liquid Temperature: 25°C
Liquid Height (from outside bottom of reactor): 20.1 cm
Liquid Volume (including that in manometer): 2300 mls

Draft tube: Distance from outside bottom of reactor to bottom of draft tube: 2.5 cm
Distance from top of draft tube to top of liquid: 2.5 cm

Reactor Lid: Distance from top of liquid to bottom of lid: 2.5 cm

CAMERA

FILM: ☒ B & W ☐ Color TYPE: ☒ TMAX TMY-BS-36
SHUTTER SPEED: 250 ☐ OTHER:_____

LIGHTING: ☒ 2 Flood lamps @ ~ 6 cm from opposites of reactor wall
☐ OTHER:_____
APERTURE SETTING: 10

GAS FLOW NOT EQUAL TO ZERO*

IF STRIPPING WITH NITROGEN THEN ESTABLISH A STEADY BASELINE (ABOUT 20 MINUTES)

Gas Flow: Gauge Reading: 2.3 PSIG
Flow Rate: 6.7 mls/sec

Gas Composition: N_2

Dissolved Oxygen: Beginning ppm: ?

Exposure label (take three data points): _____ _____ _____

Bubble size: Strobe light RPM (take three data points): _____ _____ _____

MAKE SURE THE FLASH-BUBBLE RATIO IS ONE-TO-ONE

Number of sparger orifices producing bubbles: 5

Label this length of strip chart output: N1 Liquid Temp.: 25°C

Final Dissolved oxygen ppm*: 00.0

* Mark this on the strip chart output, also

(2)

Date: 6/10

GAS FLOW NOT EQUAL TO ZERO*

Gas Flow: Gauge Reading: 2.3 PSIG
Flow Rate: 6.7 mls/sec

NEW ROLL OF FILM TMY 135-3

Gas Composition: AIR

Dissolved Oxygen: Beginning ppm: 00.0

Exposure label (take three data points): 6/10Y | 6/10Y 6/10Z 6/10A1

Bubble size: Strobe light RPM (take three data points): 1100 1090 1090

MAKE SURE THE FLASH-BUBBLE RATIO IS ONE-TO-ONE

Number of sparger orifices producing bubbles: 5

Label this length of strip chart output: A1 *

Final Dissolved oxygen ppm*: 7.0

Liquid Temp.: 24°C

GAS FLOW NOT EQUAL TO ZERO*

Gas Flow: Gauge Reading: 2.3 PSIG
Flow Rate: 6.7 mls/sec

Gas Composition: N_2

Dissolved Oxygen: Beginning ppm: 7.0

Exposure label(take three data points): 6/10AR 6/10AC 6/10AD

Bubble size: Strobe light RPM (take three data points): 1090 1100 1090

MAKE SURE THE FLASH-BUBBLE RATIO IS ONE-TO-ONE

Number of sparger orifices producing bubbles: 5

Label this length of strip chart output: N2 *

Final Dissolved oxygen ppm*: 00.0

Liquid Temp.: 25°C

COMMENT: Liquid comp: WCM-4

(3)

Date: 6/10

GAS FLOW NOT EQUAL TO ZERO*

Gas Flow: Gauge Reading: 2.3 PSIG
Flow Rate: 6.7 mls/sec

Gas Composition: AIR

Dissolved Oxygen: Beginning ppm: 00.0

Exposure label (take three data points): 6/10 AE 6/10 AF 6/10 AG

Bubble size: Strobe light RPM (take three data points): 1090 1090 1103

MAKE SURE THE FLASH-BUBBLE RATIO IS ONE-TO-ONE

Number of sparger orifices producing bubbles: 5

Label this length of strip chart output: A2 *

Final Dissolved oxygen ppm*: 6.3 but assume 2* is still 7.0

Liquid Temp.: 24.5 °C

GAS FLOW NOT EQUAL TO ZERO*

Gas Flow: Gauge Reading: 2.3 PSIG
Flow Rate: 6.7 mls/sec

Gas Composition: N_2

Dissolved Oxygen: Beginning ppm: 6.3 ← NOT 7.0 but use 7.0 = C*

Exposure label(take three data points): 6/10 AH 6/10 AI 6/10 AJ

Bubble size: Strobe light RPM (take three data points): 1090 1090 1090

MAKE SURE THE FLASH-BUBBLE RATIO IS ONE-TO-ONE

Number of sparger orifices producing bubbles: 5

Label this length of strip chart output: N3 *

Final Dissolved oxygen ppm*: 00.0

Liquid Temp.: 24.5°C

COMMENT: Liquid comp: WCM-4

EXPERIMENTAL AIRLIFT OPERATION

Data to be used to calculate overall mass-transfer coefficient ($k_l a$), interfacial area, (a) and liquid-phase mass-transfer coefficient (k_l).

Date: 6/10

Orifice plate: Number of orifices: 9

NO GAS FLOW

Liquid Composition: WCM-4 (pH 4.5)
Liquid Temperature: 25 °C
Liquid Height (from outside bottom of reactor): 20.1 cm
Liquid Volume (including that in manometer): 2300 ml

Draft tube: Distance from outside bottom of reactor to bottom of draft tube: 2.5 cm
Distance from top of draft tube to top of liquid: 2.5 cm

Reactor Lid: Distance from top of liquid to bottom of lid: 2.5 cm

CAMERA

FILM: ☒ B & W ☐ Color TYPE: ☒ TMAX TMY 135-36
SHUTTER SPEED: 250 ☐ OTHER:_____

LIGHTING: ☒ 2 Flood lamps @ ~ 6 cm from opposites of reactor wall
☐ OTHER:_____
APERTURE SETTING: 16

GAS FLOW NOT EQUAL TO ZERO*

IF STRIPPING WITH NITROGEN THEN ESTABLISH A STEADY BASELINE (ABOUT 20 MINUTES)

Gas Flow: Gauge Reading: 6.7 PSIG
Flow Rate: 12.1 mls/sec

Gas Composition: N_2

Dissolved Oxygen: Beginning ppm: ?

Exposure label (take three data points): _____ _____ _____

Bubble size: Strobe light RPM (take three data points): _____ _____ _____

MAKE SURE THE FLASH-BUBBLE RATIO IS ONE-TO-ONE

Number of sparger orifices producing bubbles:

Label this length of strip chart output: 00.0 * Liquid Temp.: 24.5°C

Final Dissolved oxygen ppm*: 00.0

* Mark this on the strip chart output, also

Date: 6/10

GAS FLOW NOT EQUAL TO ZERO*

Gas Flow: Gauge Reading: 6.7 PSIG
Flow Rate: 12.1 mls/sec

Gas Composition: AIR

Dissolved Oxygen: Beginning ppm: 00.0

Exposure label (take three data points): 6/10M 6/10N 6/10O

Bubble size: Strobe light RPM (take three data points): 1330 1320 1320

MAKE SURE THE FLASH-BUBBLE RATIO IS ONE-TO-ONE

Number of sparger orifices producing bubbles: 9

Label this length of strip chart output: A1 *

Final Dissolved oxygen ppm*: 7.1 Liquid Temp.: 25 °C

GAS FLOW NOT EQUAL TO ZERO*

change chart speed from 0.2 to 0.1"/min

Gas Flow: Gauge Reading: 6.7 PSIG
Flow Rate: 12.1 mls/sec

Gas Composition: N_2

Dissolved Oxygen: Beginning ppm: 7.1

Exposure label(take three data points): 6/10P 6/10Q 6/10R

Bubble size: Strobe light RPM (take three data points): 1330 1330 1330

MAKE SURE THE FLASH-BUBBLE RATIO IS ONE-TO-ONE

Number of sparger orifices producing bubbles: 9

Label this length of strip chart output: N2 *

Final Dissolved oxygen ppm*: 00.0 Liquid Temp.: 25 °C

COMMENT: Liquid comp: WCM-4

(3)

Date: 6/10

GAS FLOW NOT EQUAL TO ZERO*

Gas Flow: Gauge Reading: 67 PSIG
Flow Rate: 12.1 mls/sec

Gas Composition: AIR

Dissolved Oxygen: Beginning ppm: 00.0

Exposure label (take three data points): 6/10 S 6/10 T 6/10 U

Bubble size: Strobe light RPM (take three data points): 1330 1330 1330

MAKE SURE THE FLASH-BUBBLE RATIO IS ONE-TO-ONE

Number of sparger orifices producing bubbles: 9

Label this length of strip chart output: A2 *

Final Dissolved oxygen ppm*: 7.0 Liquid Temp.: 25°C

GAS FLOW NOT EQUAL TO ZERO*

Gas Flow: Gauge Reading: 67 PSIG
Flow Rate: 12.1 mls/sec

Gas Composition: N_2

Dissolved Oxygen: Beginning ppm: 7.0

Exposure label(take three data points): 6/10 V 6/10 W 6/10 X

Bubble size: Strobe light RPM (take three data points): 1330 1330 1330

MAKE SURE THE FLASH-BUBBLE RATIO IS ONE-TO-ONE

Number of sparger orifices producing bubbles: 9

Label this length of strip chart output: N3 *

Final Dissolved oxygen ppm*: 00.0 Liquid Temp.: 25°C

COMMENT: Liquid comp: WCM-4

EXPERIMENTAL AIRLIFT OPERATION

Data to be used to calculate overall mass-transfer coefficient ($k_l a$), interfacial area, (a) and liquid-phase mass-transfer coefficient (k_l).

Date: 6/10

Orifice plate: Number of orifices: 19

NO GAS FLOW

Liquid Composition: WCM -4 (pH 4.5)
Liquid Temperature: 26°C
Liquid Height (from outside bottom of reactor): 20.4 cm
Liquid Volume (~~including that in manometer~~): 2300 mls

Draft tube: Distance from outside bottom of reactor to bottom of draft tube: 2.5 cm
Distance from top of draft tube to top of liquid: 2.5 cm

Reactor Lid: Distance from top of liquid to bottom of lid: 2.5 cm

CAMERA

FILM: ☒ B & W ☐ Color TYPE: ☒ TMAX TMY 135-36
SHUTTER SPEED: 250 ☐ OTHER:_____

LIGHTING: ☒ 2 Flood lamps @ ~ 6 cm from opposites of reactor wall
☐ OTHER:_____
APERTURE SETTING: 16

GAS FLOW NOT EQUAL TO ZERO*

IF STRIPPING WITH NITROGEN THEN ESTABLISH A STEADY BASELINE (ABOUT 20 MINUTES)

Gas Flow: Gauge Reading: 24.1 PSIG
Flow Rate: 25.5 mls/sec

Gas Composition: N_2

Dissolved Oxygen: Beginning ppm: ?

Exposure label (take three data points): ____ ____ ____

Bubble size: Strobe light RPM (take three data points): ____ ____ ____

MAKE SURE THE FLASH-BUBBLE RATIO IS ONE-TO-ONE

Number of sparger orifices producing bubbles: 19

Label this length of strip chart output: N1 * Liquid Temp.: 26°C

Final Dissolved oxygen ppm*: 00.0

* Mark this on the strip chart output, also

Date: 6/10

GAS FLOW NOT EQUAL TO ZERO*

Gas Flow: Gauge Reading: 24.1 PSIG
Flow Rate: 25.5 mls/sec

Gas Composition: AIR

Dissolved Oxygen: Beginning ppm: 00.0

Exposure label (take three data points): 6/10 A 6/10 B 6/10 C

Bubble size: Strobe light RPM (take three data points): 1600 1620 1620

MAKE SURE THE FLASH-BUBBLE RATIO IS ONE-TO-ONE

Number of sparger orifices producing bubbles: 19

Label this length of strip chart output: A1 *

Final Dissolved oxygen ppm*: 7.0 Liquid Temp.: 26°C

GAS FLOW NOT EQUAL TO ZERO*

Gas Flow: Gauge Reading: 24.1 PSIG
Flow Rate: 25.5 mls/sec

Gas Composition: N_2

Dissolved Oxygen: Beginning ppm: 7.0

Exposure label(take three data points): 6/10 D 6/10 E 6/10 F

Bubble size: Strobe light RPM (take three data points): 1620 1620 1620

MAKE SURE THE FLASH-BUBBLE RATIO IS ONE-TO-ONE

Number of sparger orifices producing bubbles: 19

Label this length of strip chart output: N2 *

Final Dissolved oxygen ppm*: 00.0 Liquid Temp.: 26°C

COMMENT: Liquid comp: WCM-4

* Mark this on the strip chart output also

Date: 6/10

GAS FLOW NOT EQUAL TO ZERO*

Gas Flow: Gauge Reading: 24.1 PSIG
Flow Rate: 25.5 mls/sec

Gas Composition: AIR

Dissolved Oxygen: Beginning ppm: 00.0

Exposure label (take three data points): 6/10 G 6/10 H 6/10 I

Bubble size: Strobe light RPM (take three data points): 1620 1610 1610

MAKE SURE THE FLASH-BUBBLE RATIO IS ONE-TO-ONE

Number of sparger orifices producing bubbles: 19

Label this length of strip chart output: A2 *

Final Dissolved oxygen ppm*: 7.0 Liquid Temp.: 25.5°C

GAS FLOW NOT EQUAL TO ZERO*

Gas Flow: Gauge Reading: 24.1 PSIG
Flow Rate: 25.5 mls/sec

Gas Composition: N_2

Dissolved Oxygen: Beginning ppm: 7.0

Exposure label(take three data points): 6/10 J 6/10 K 6/10 L

Bubble size: Strobe light RPM (take three data points): 1600 1600 1610

MAKE SURE THE FLASH-BUBBLE RATIO IS ONE-TO-ONE

Number of sparger orifices producing bubbles: 19

Label this length of strip chart output: N3 *

Final Dissolved oxygen ppm*: 00.0 Liquid Temp.: 25.5°C

COMMENT: Liquid comp: WM-4

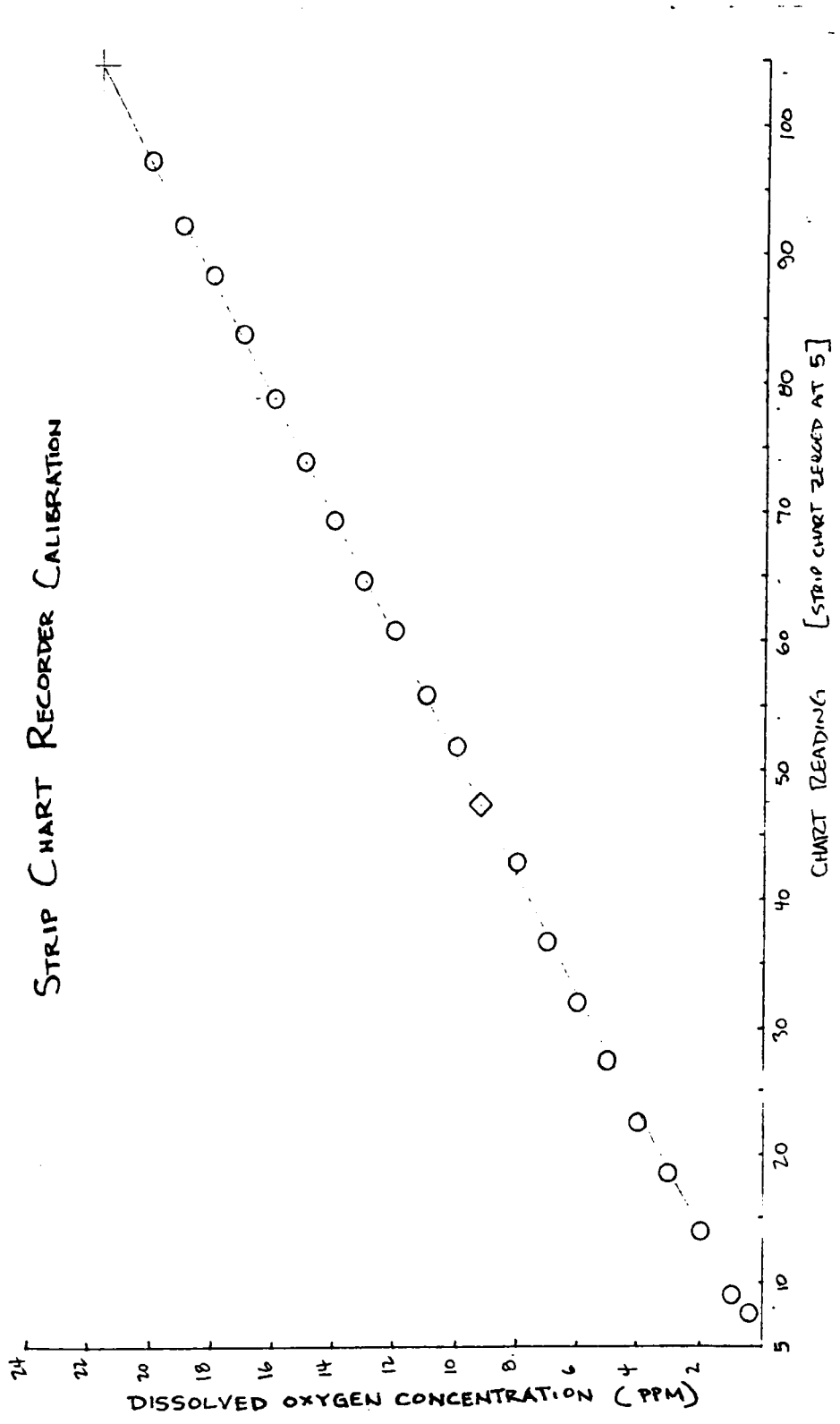
STRIP CHART RECORDER CALIBRATION
DISSOLVED OXYGEN CONCENTRATION (PPM)
24
22
20
18
16
14
12
10
8
6
4
2
5
10
20
30
40
50
60
70
80
90
100
CHART READING [STRIP CHART ZEROED AT 5]

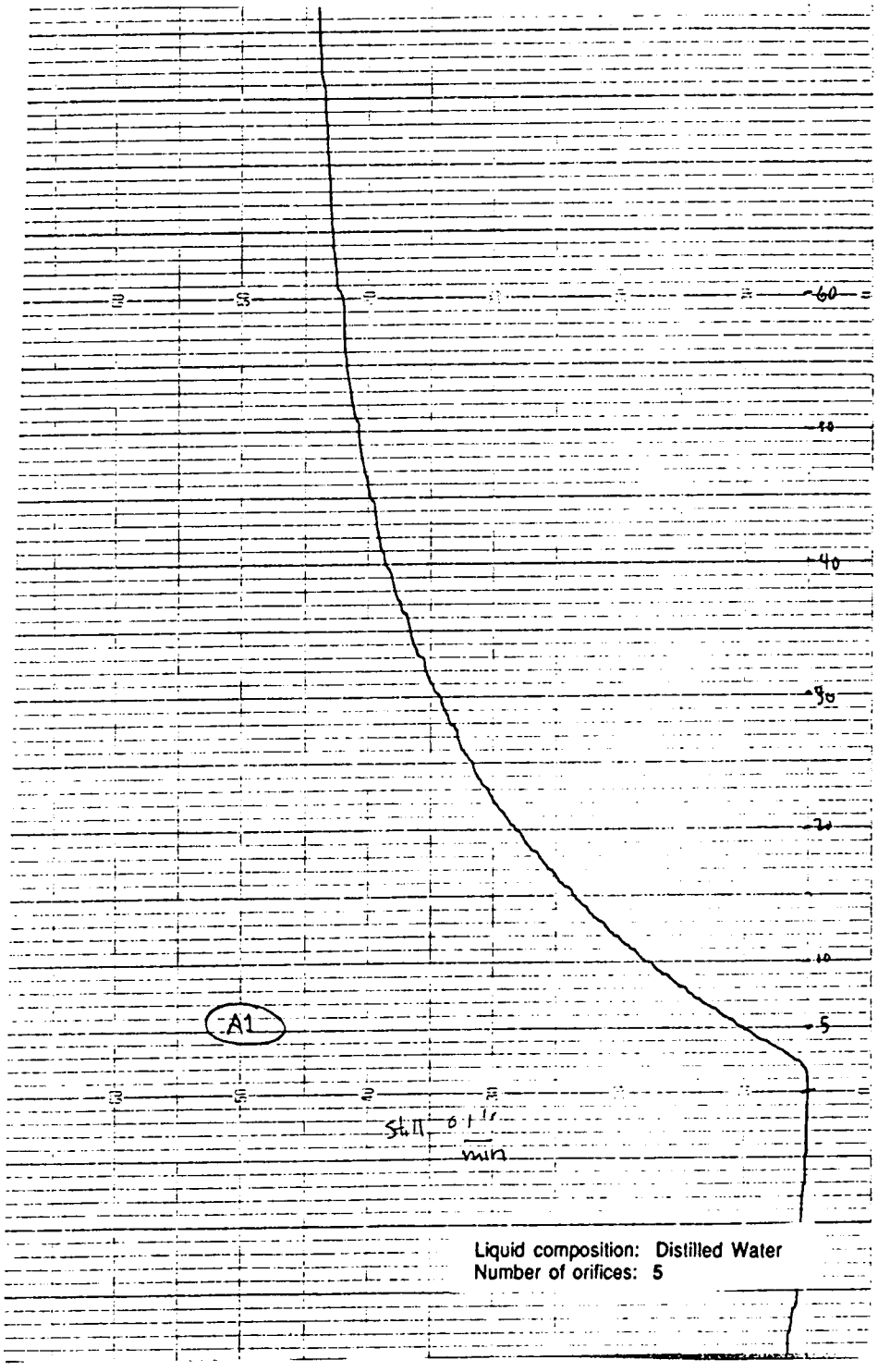
A1
Liquid composition: Distilled Water
Number of orifices: 5

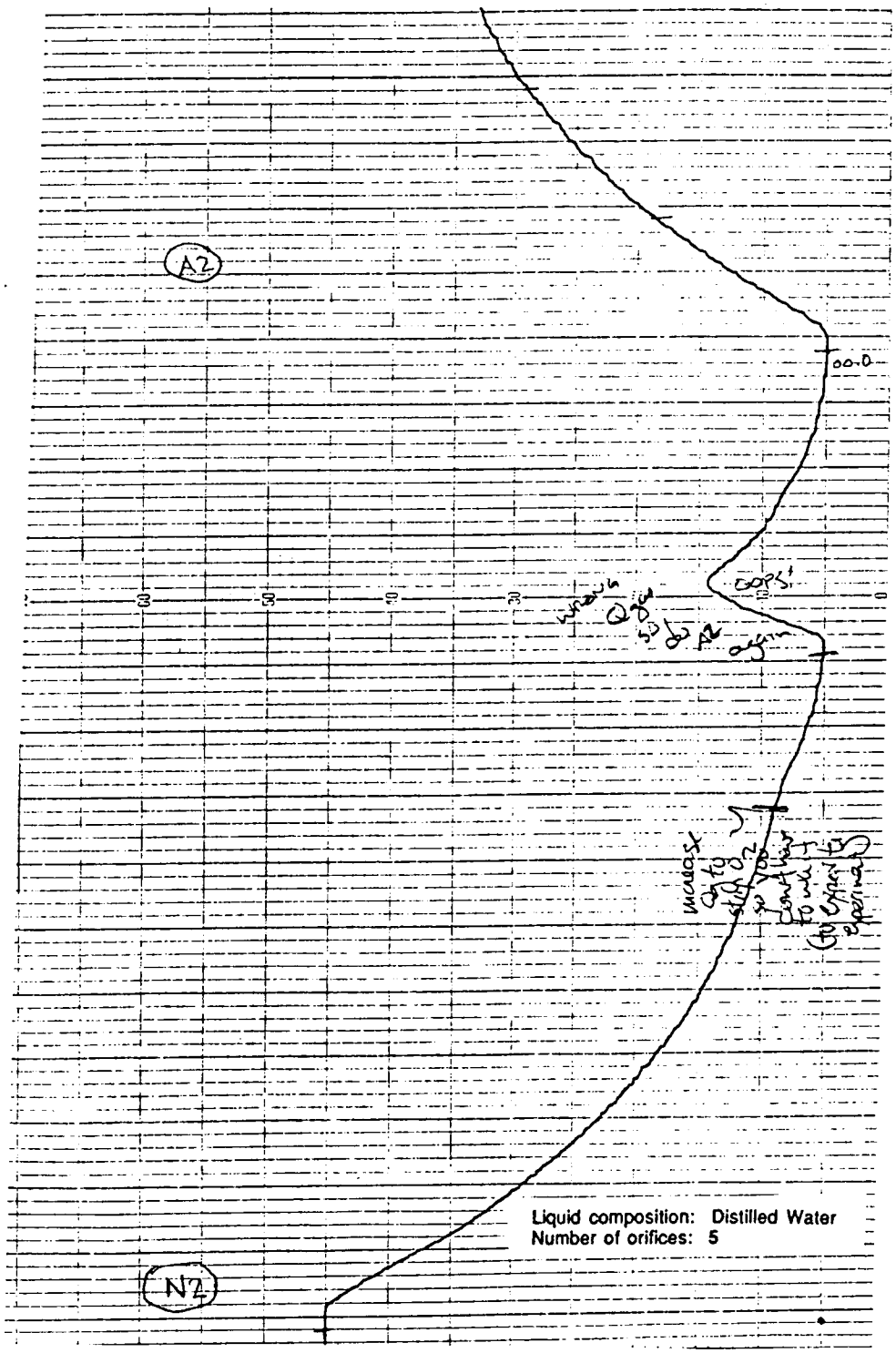
A2
N2
Liquid composition: Distilled Water
Number of orifices: 5

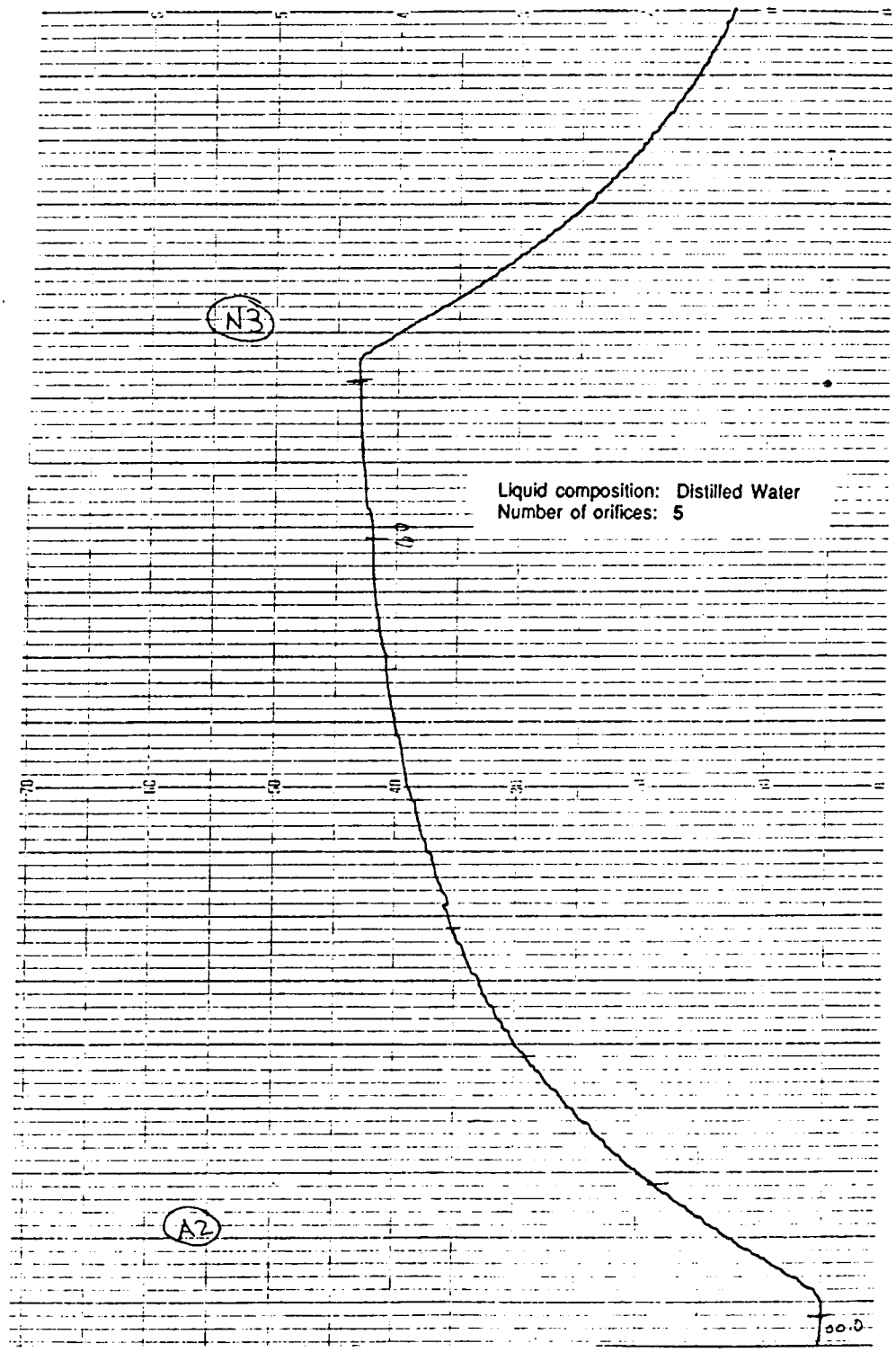
N3
Liquid composition: Distilled Water
Number of orifices: 5
A2

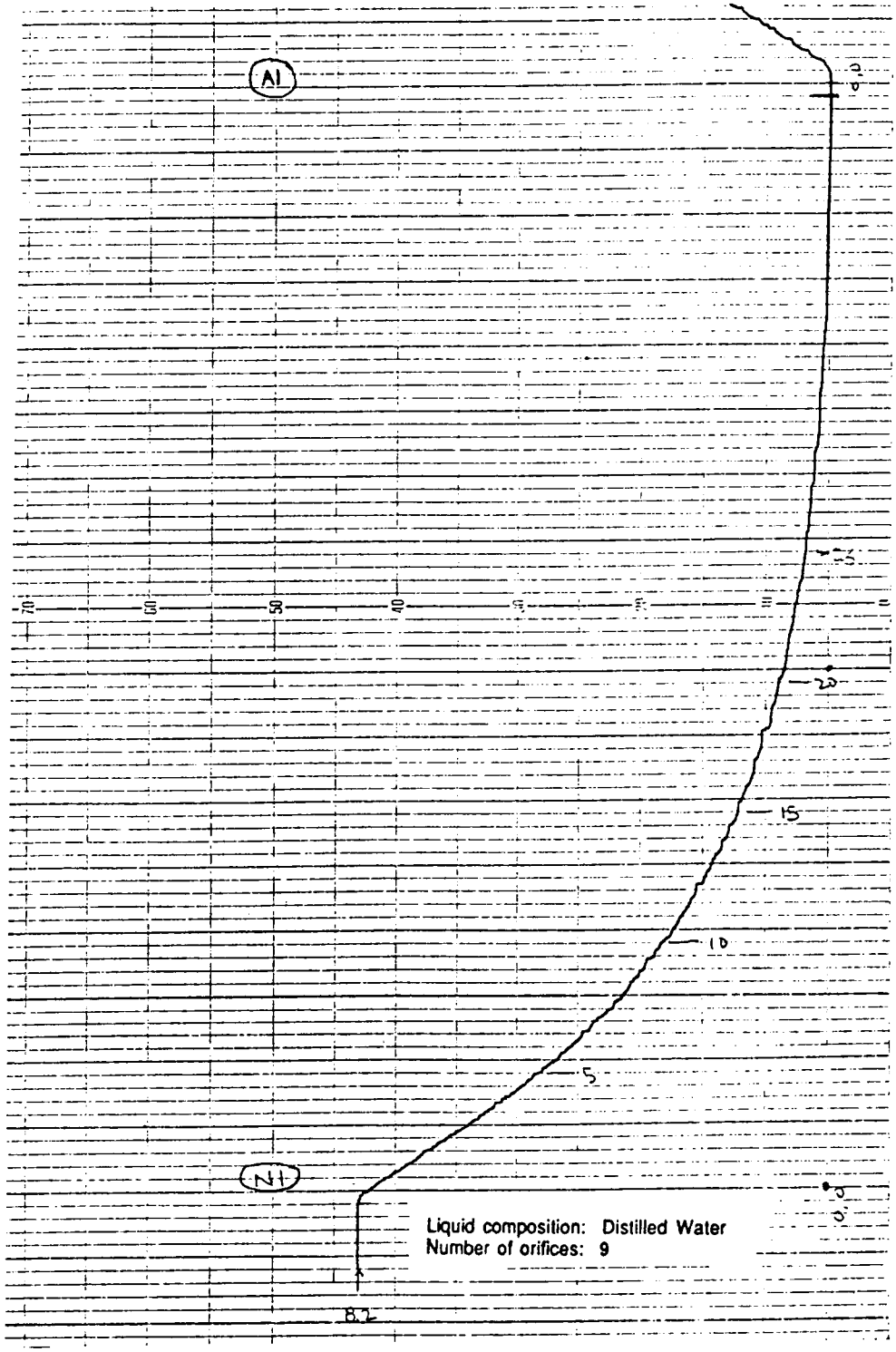
A1
N1
Liquid composition: Distilled Water
Number of orifices: 9

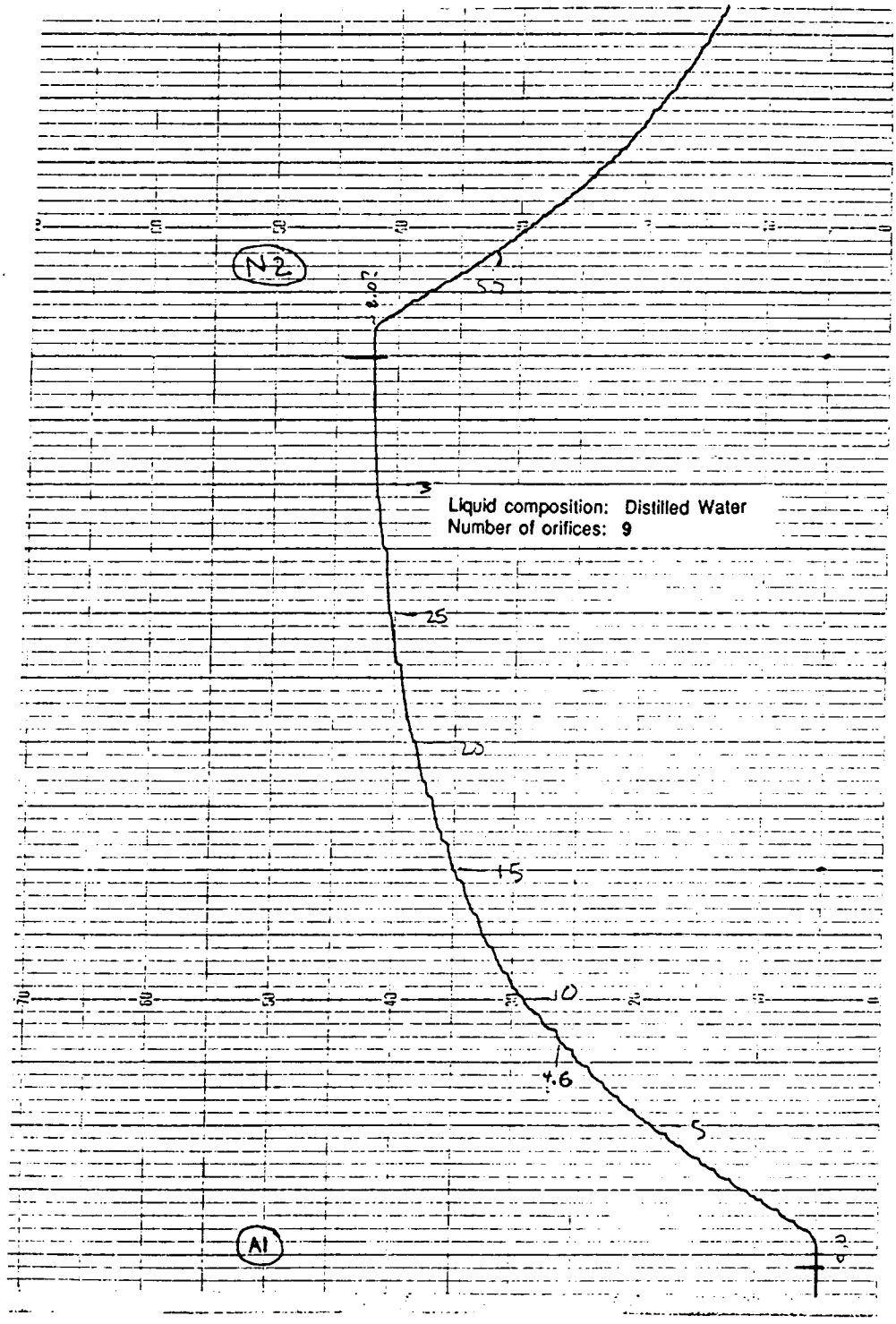
N2
Liquid composition: Distilled Water
Number of orifices: 9
25
20
15
10
4.6
5
Al

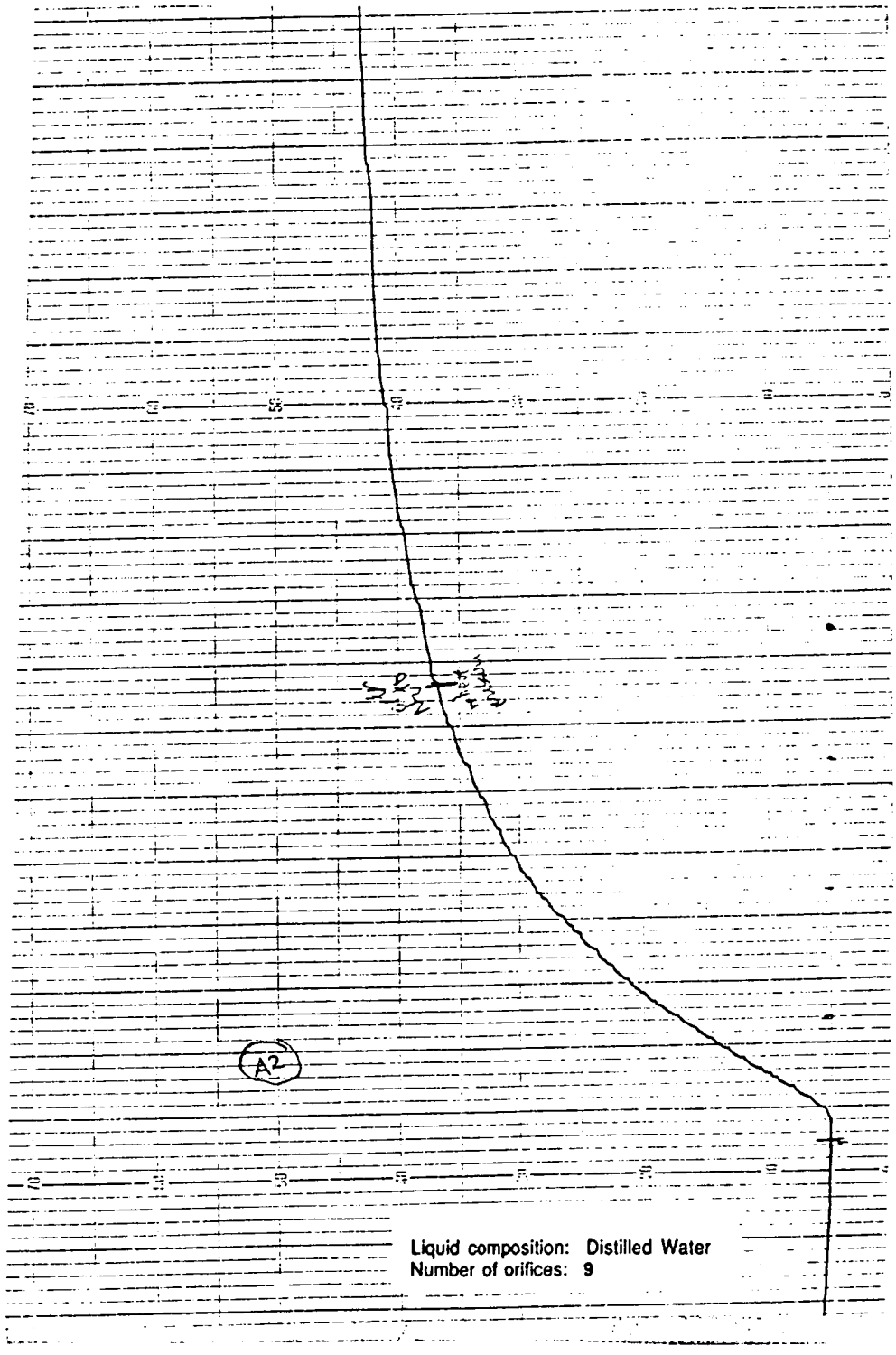
A2
Liquid composition: Distilled Water
Number of orifices: 9

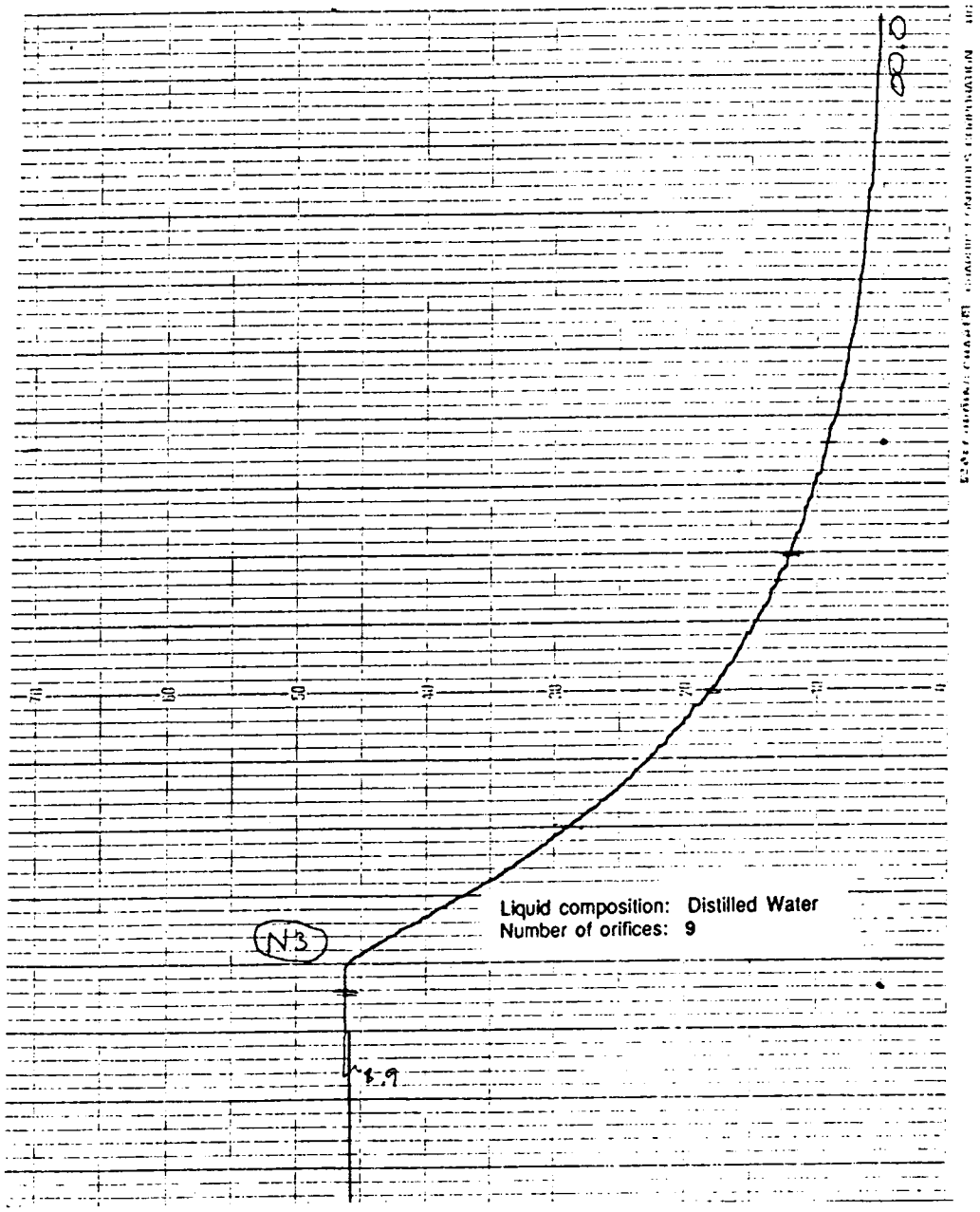
Liquid composition: Distilled Water
Number of orifices: 9
N3

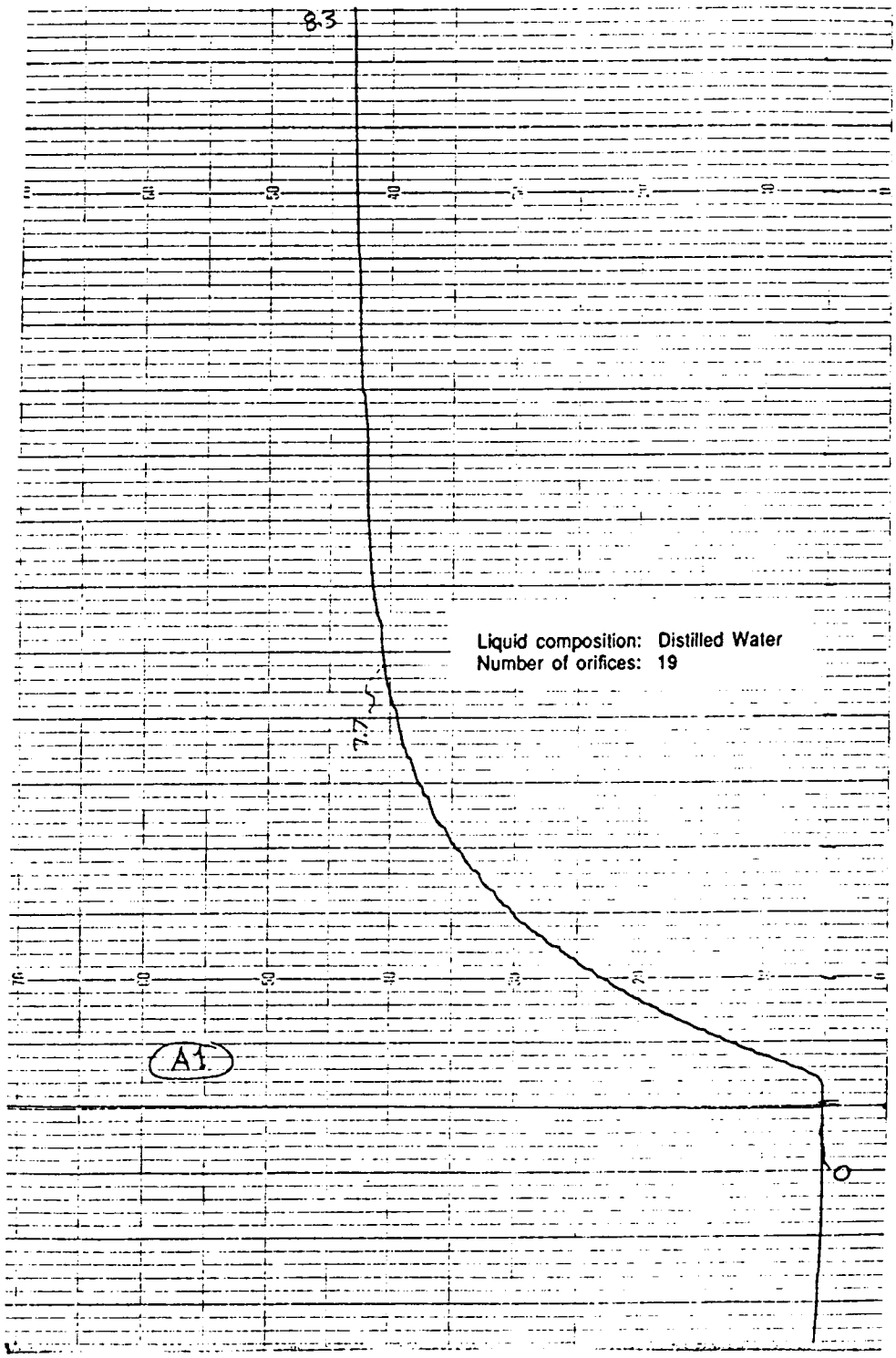
83
Liquid composition: Distilled Water
Number of orifices: 19
A1

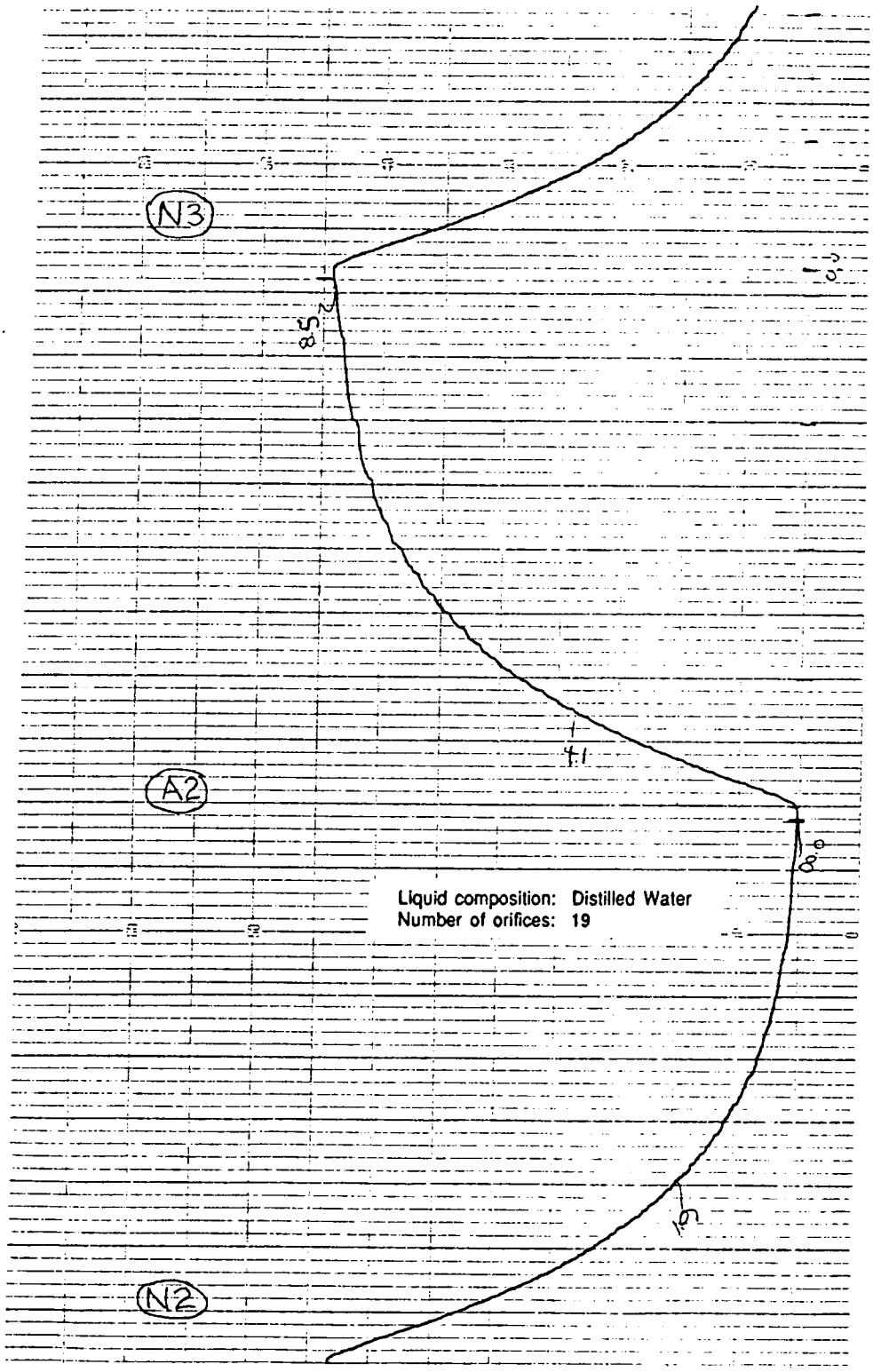
N3
A2
N2
Liquid composition: Distilled Water
Number of orifices: 19

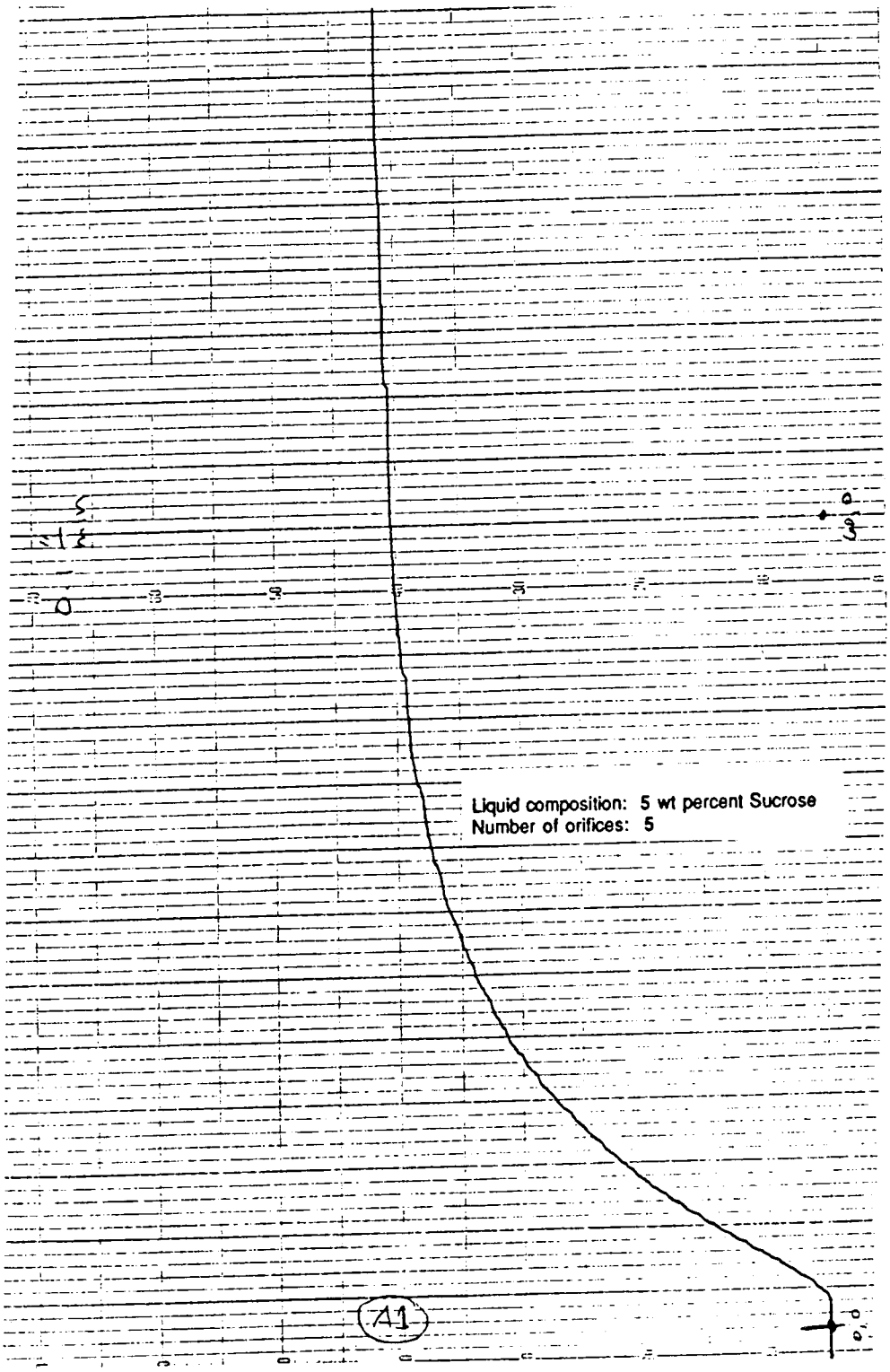
Liquid composition: 5 wt percent Sucrose
Number of orifices: 5
A1

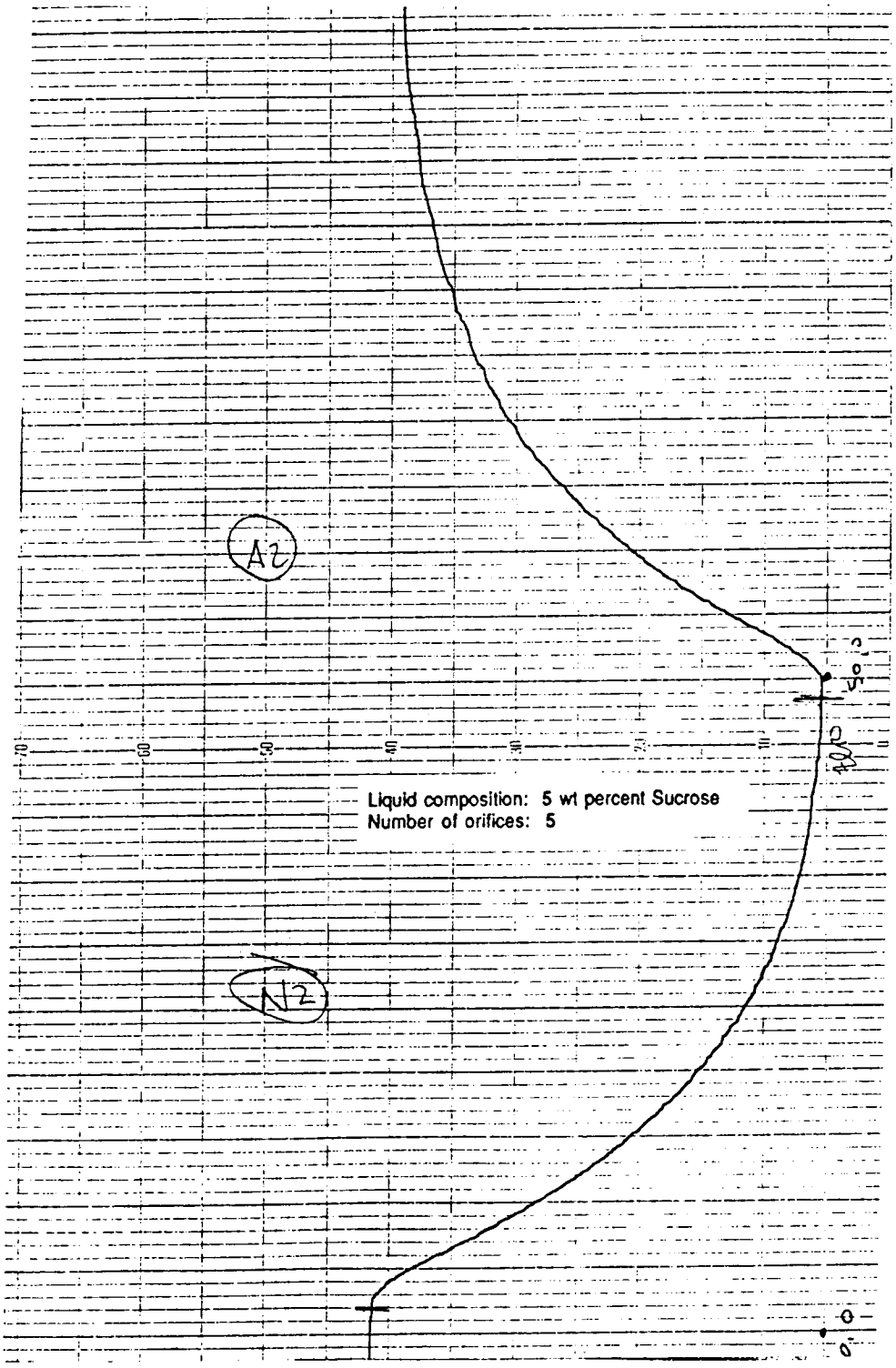
Liquid composition: 5 wt percent Sucrose
Number of orifices: 5

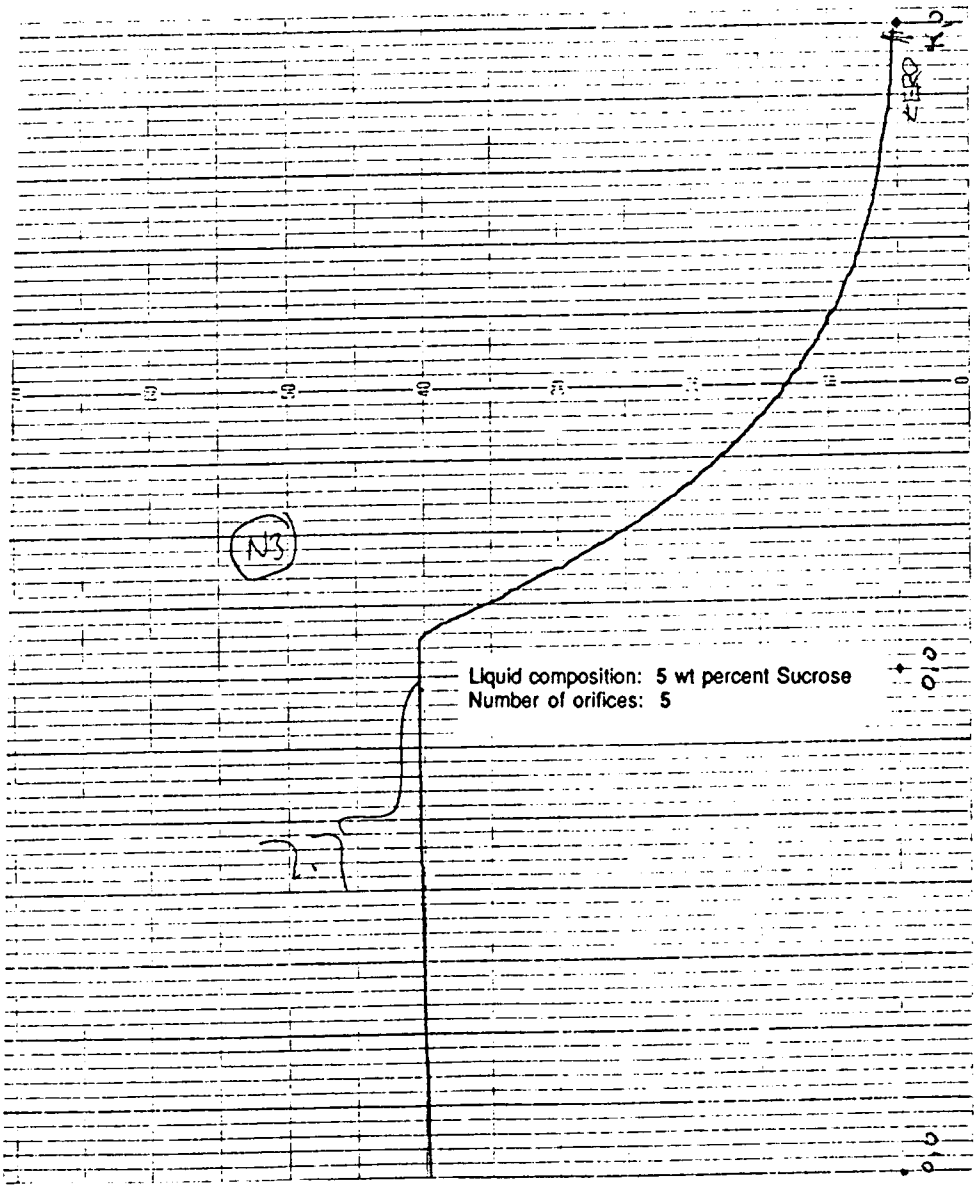
Liquid composition: 5 wt percent Sucrose
Number of orifices: 5

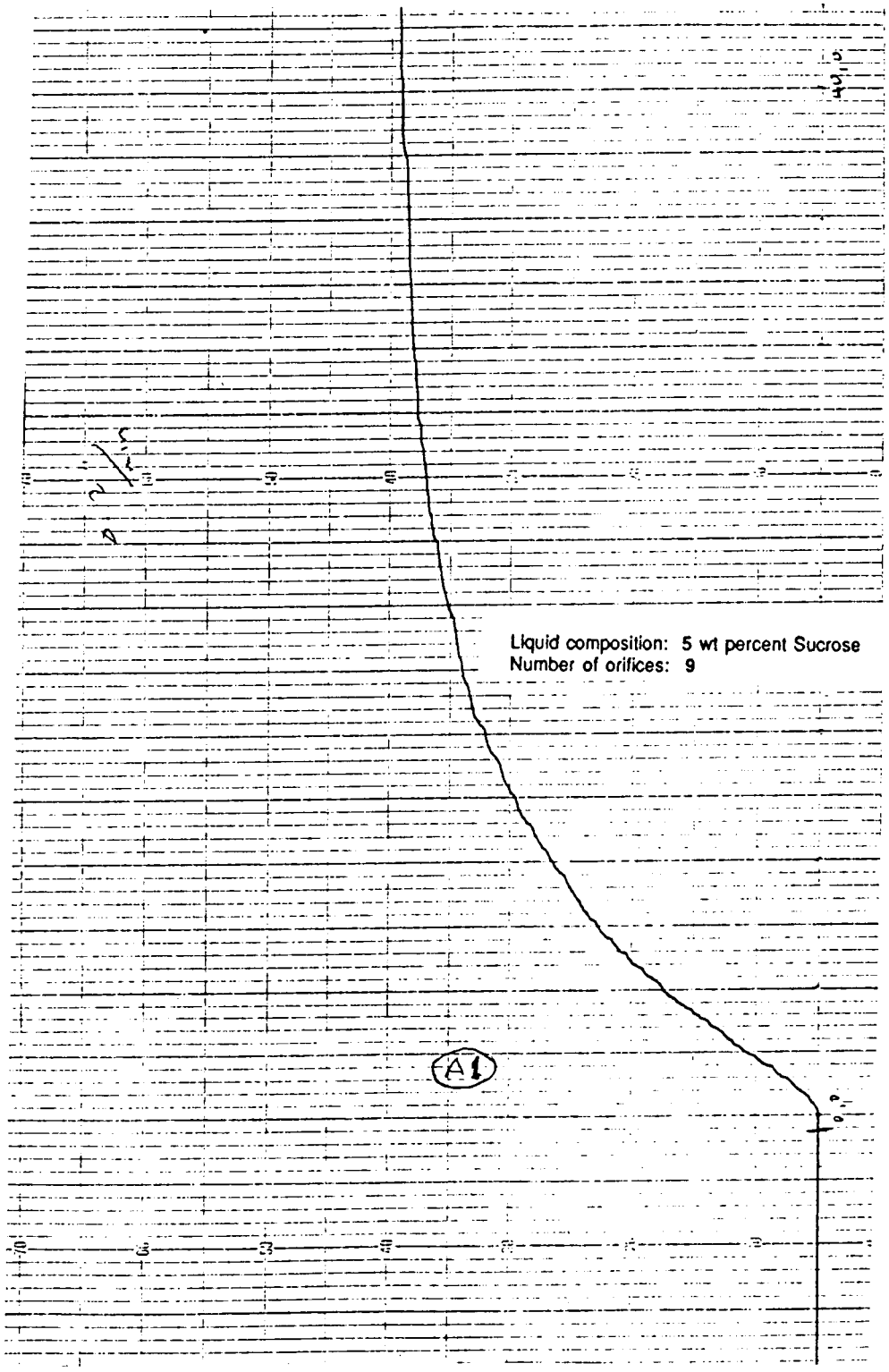
Liquid composition: 5 wt percent Sucrose
Number of orifices: 9
A1

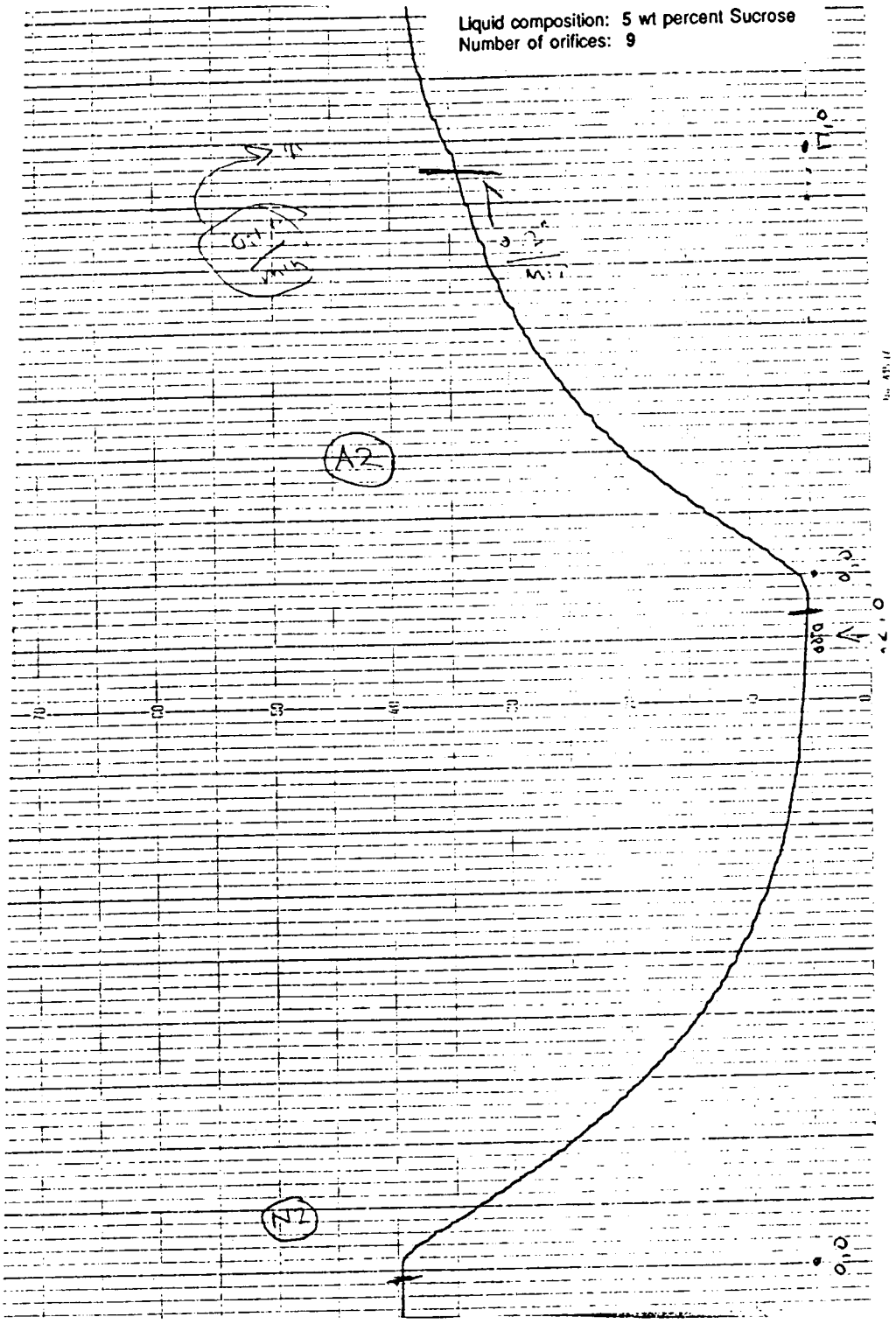
Liquid composition: 5 wt percent Sucrose
Number of orifices: 9
A2
N2

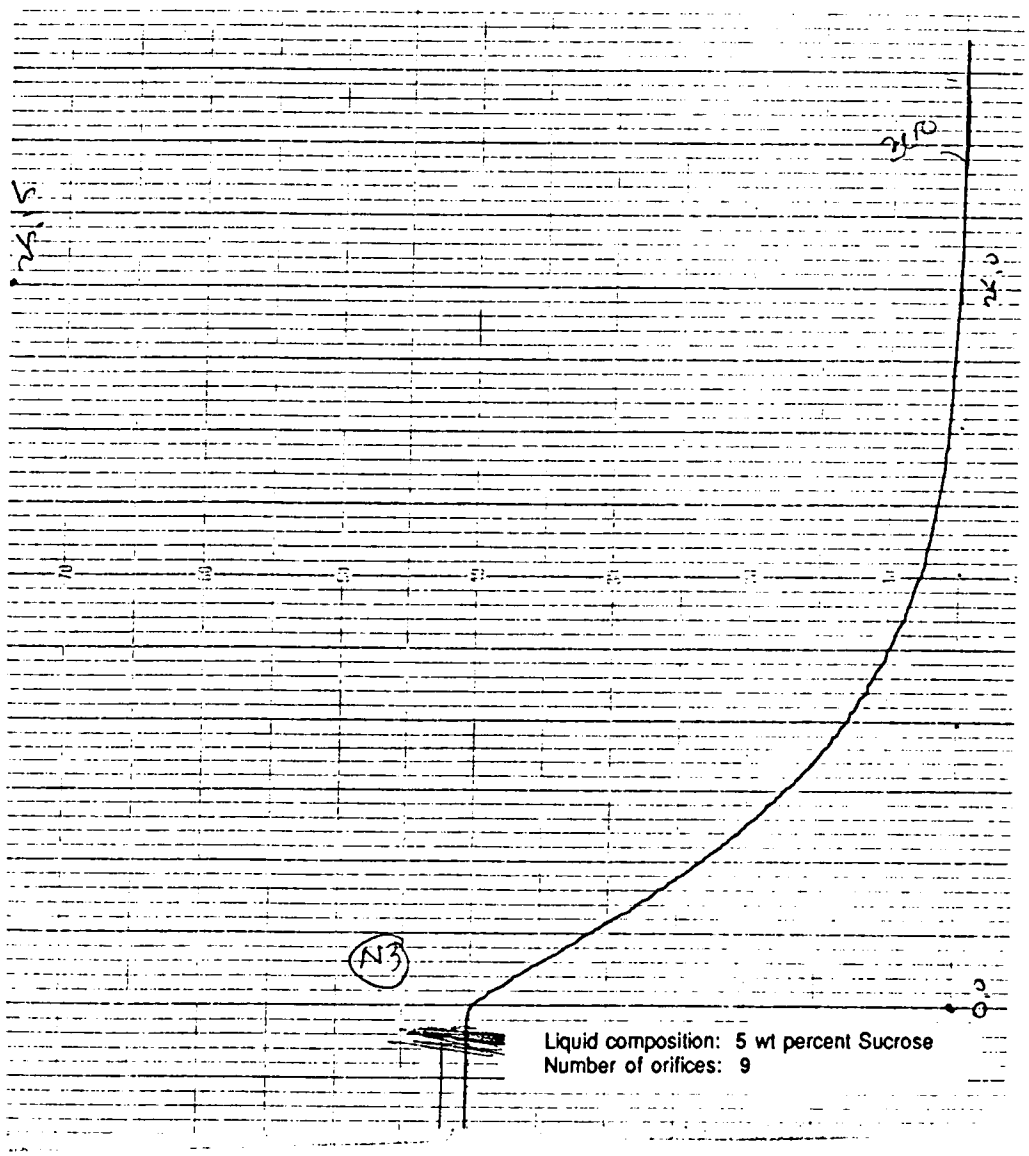
Liquid composition: 5 wt percent Sucrose
Number of orifices: 9

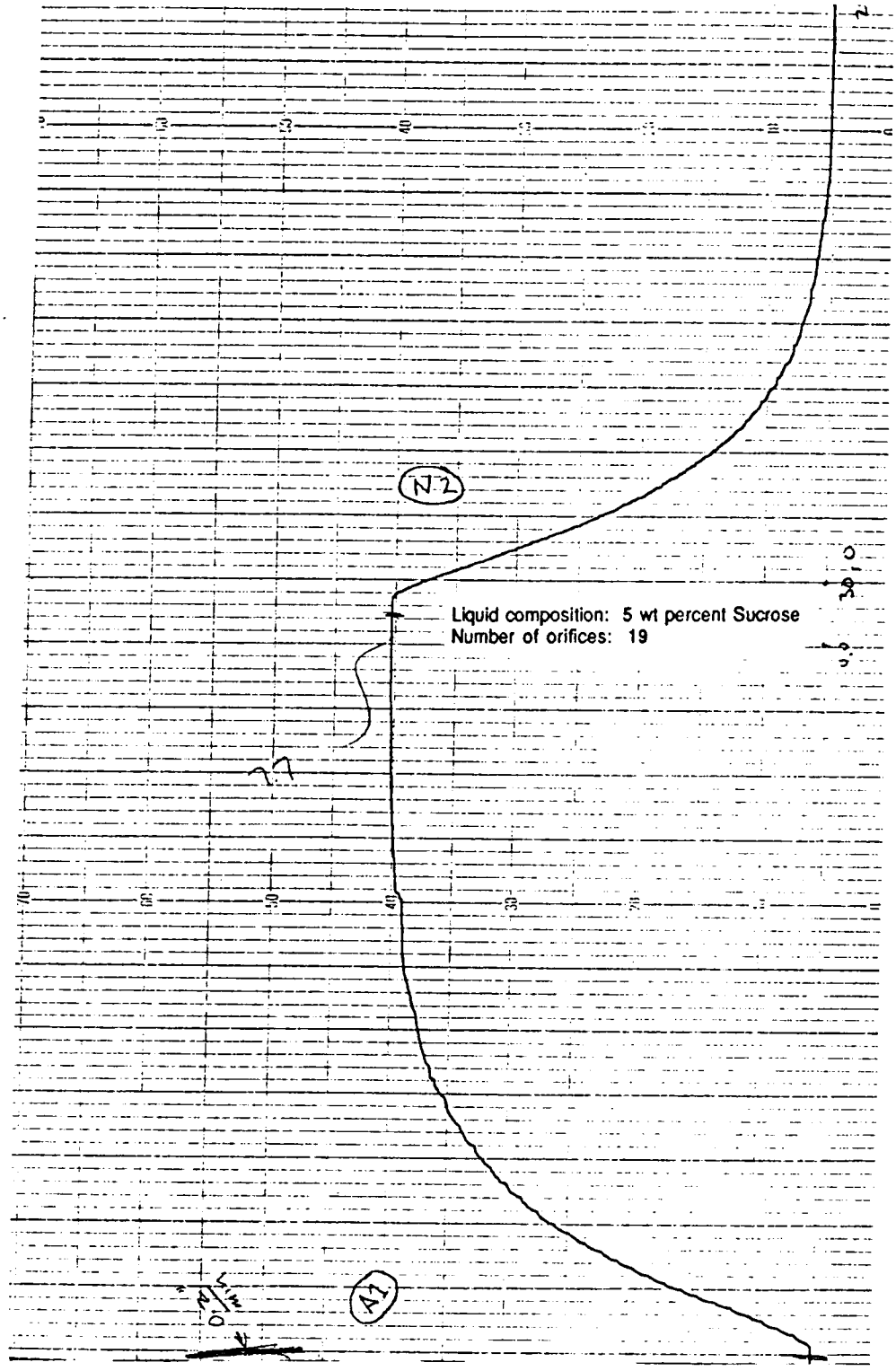
Liquid composition: 5 wt percent Sucrose
Number of orifices: 19

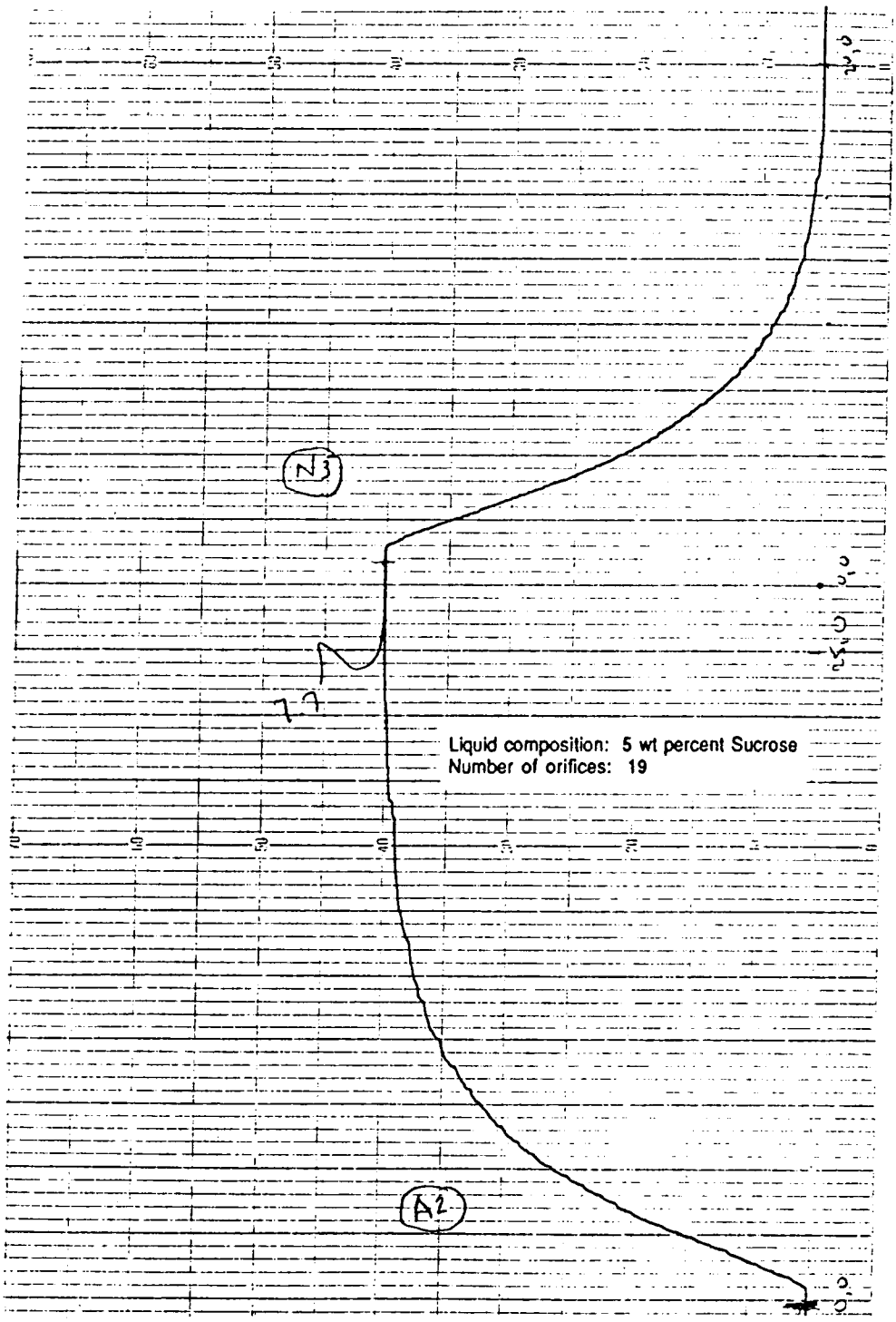
Liquid composition: 5 wt percent Sucrose
Number of orifices: 19

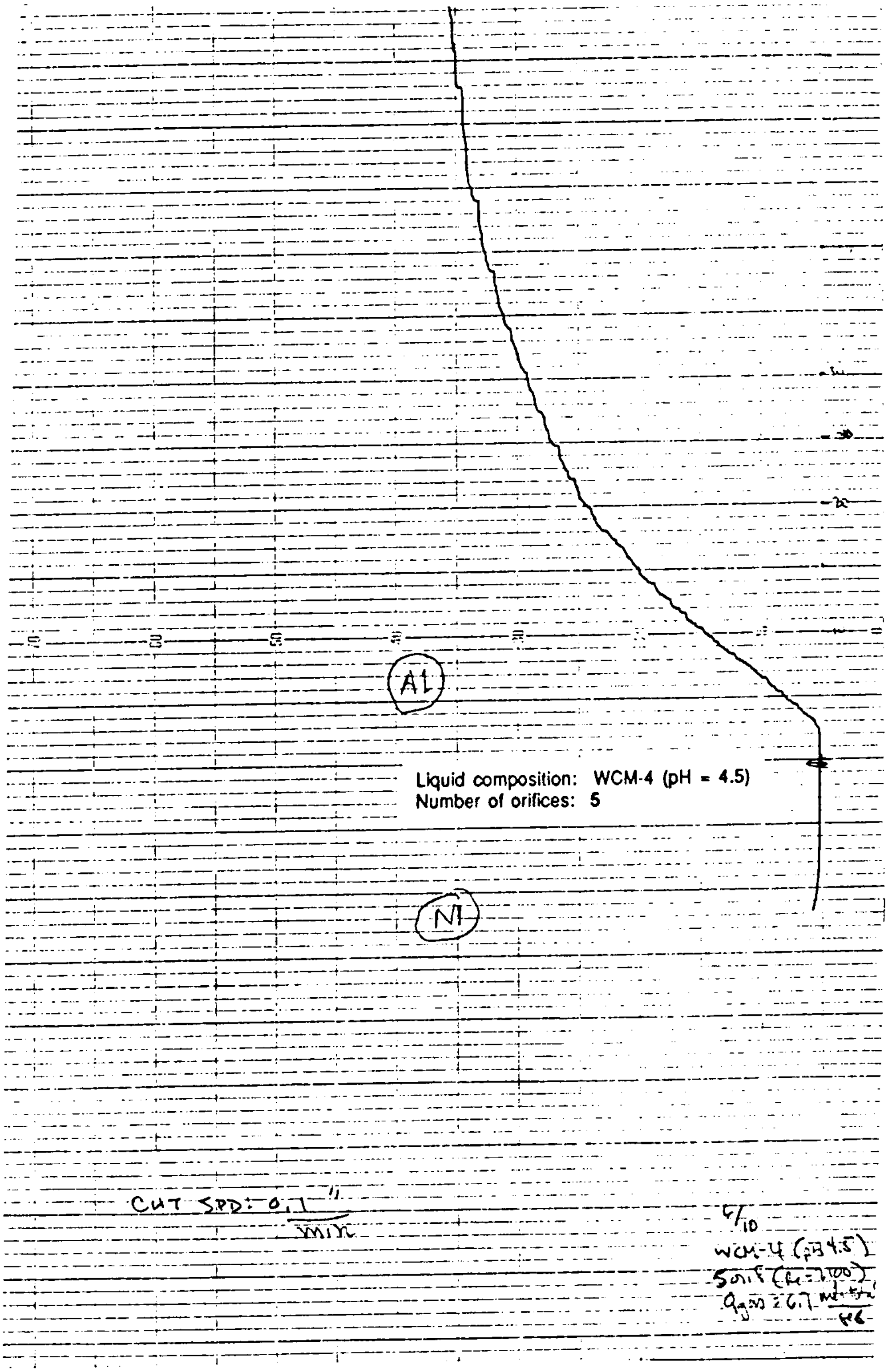
A1
Liquid composition: WCM-4 (pH = 4.5)
Number of orifices: 5
N1
CUT SPD: 0.1 "/min
WCM-4

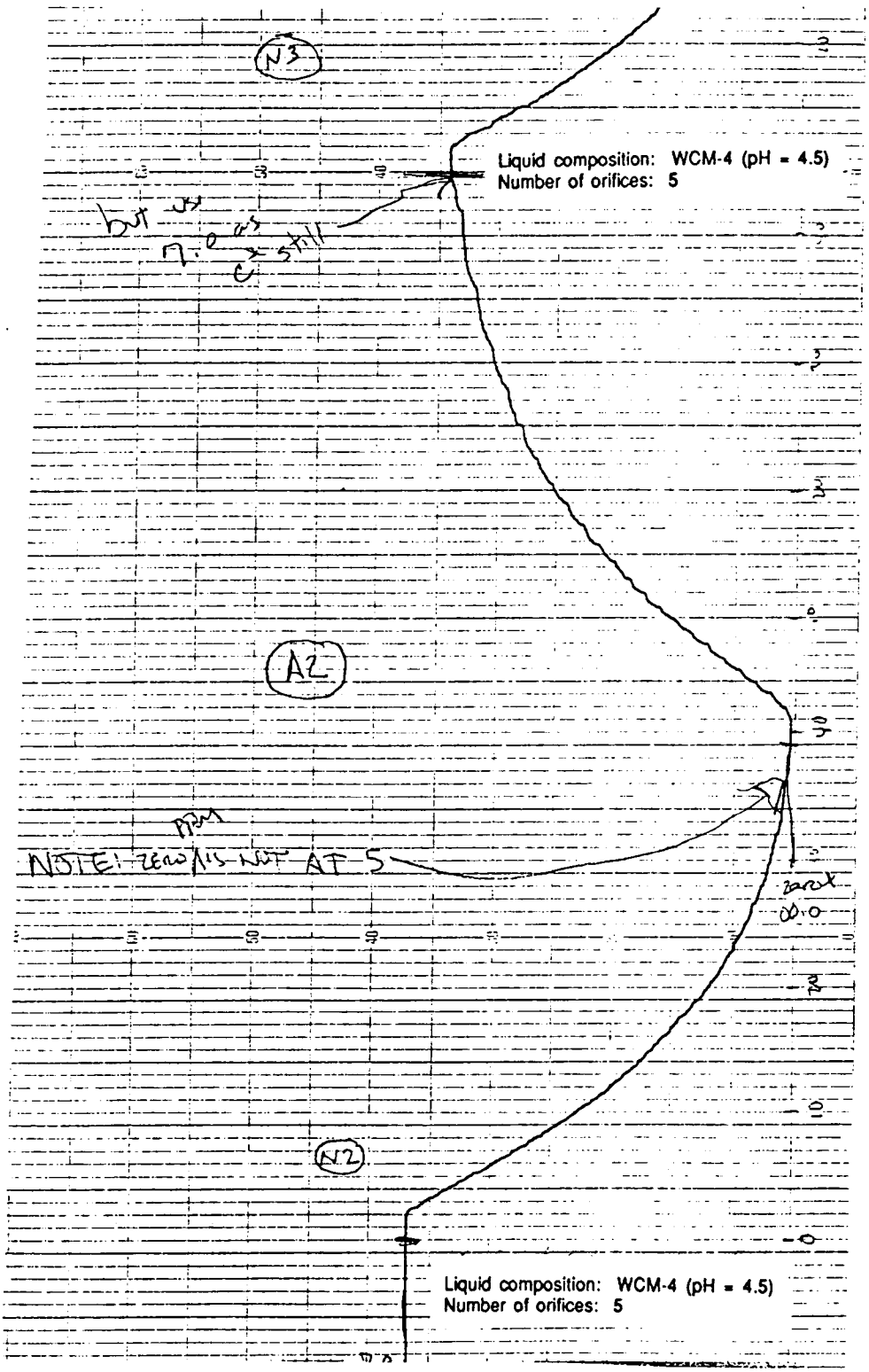
N3
Liquid composition: WCM-4 (pH = 4.5)
Number of orifices: 5
A2
NOTE: ZERO IS NOT AT 5
N2
Liquid composition: WCM-4 (pH = 4.5)
Number of orifices: 5

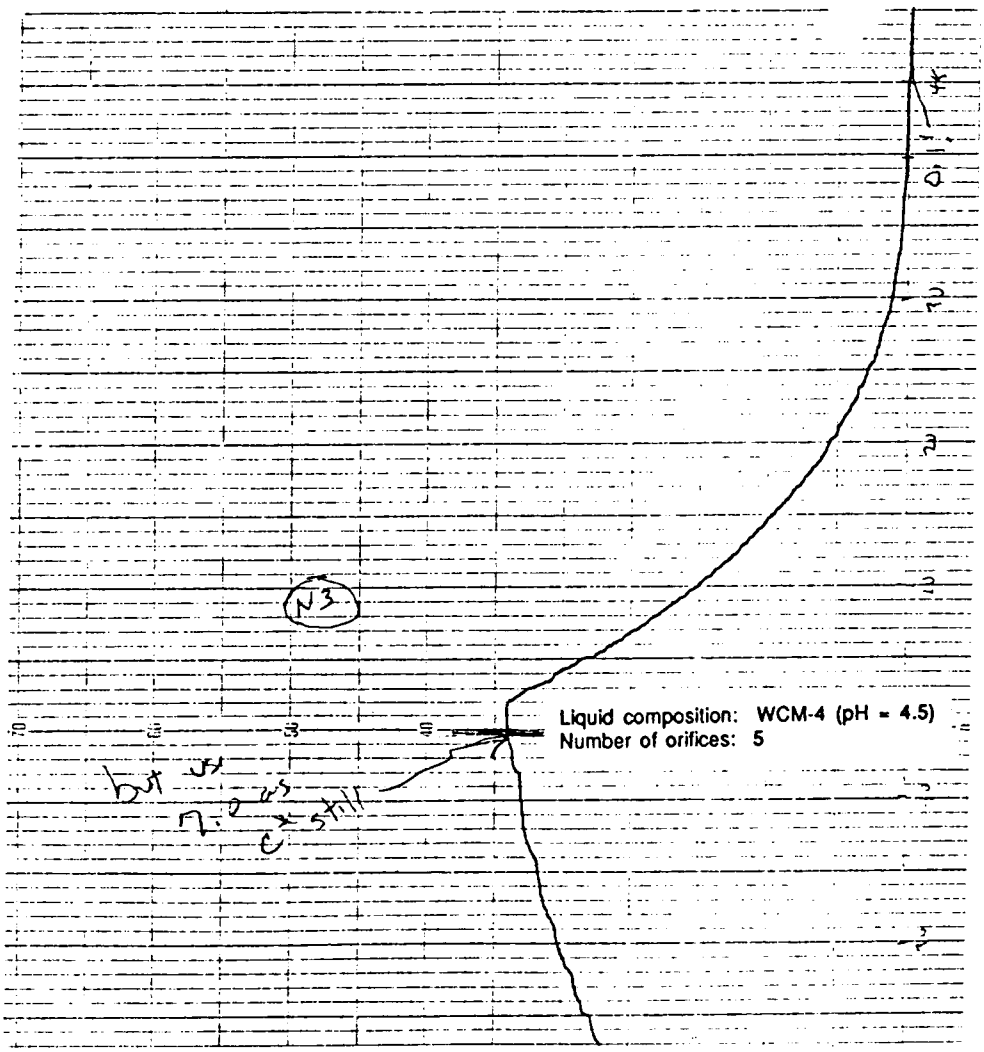
Liquid composition: WCM-4 (pH = 4.5)
Number of orifices: 5

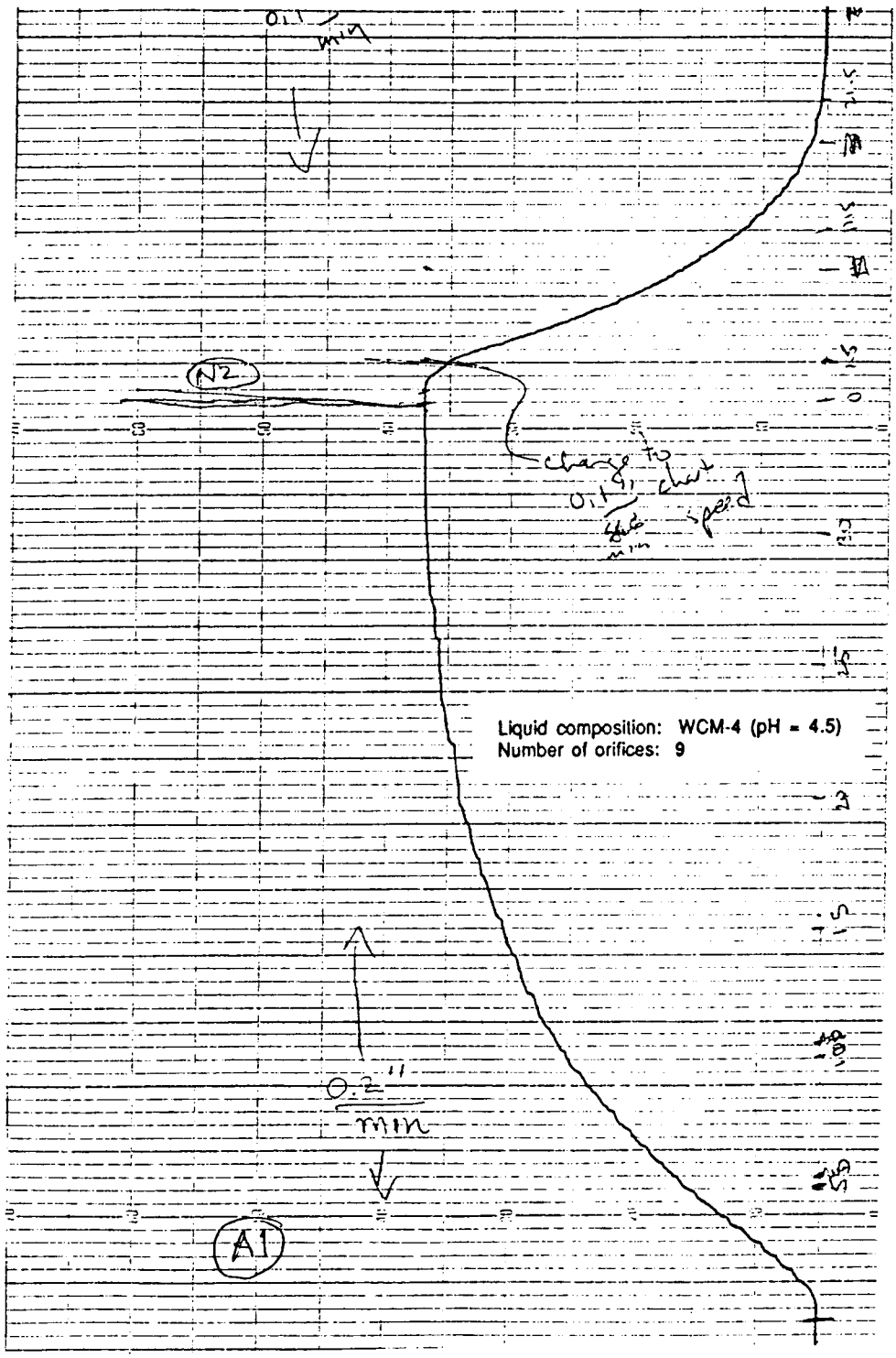
0.1 mm
N2
change to 0.1 chart speed
Liquid composition: WCM-4 (pH = 4.5)
Number of orifices: 9
0.2 mm
A1

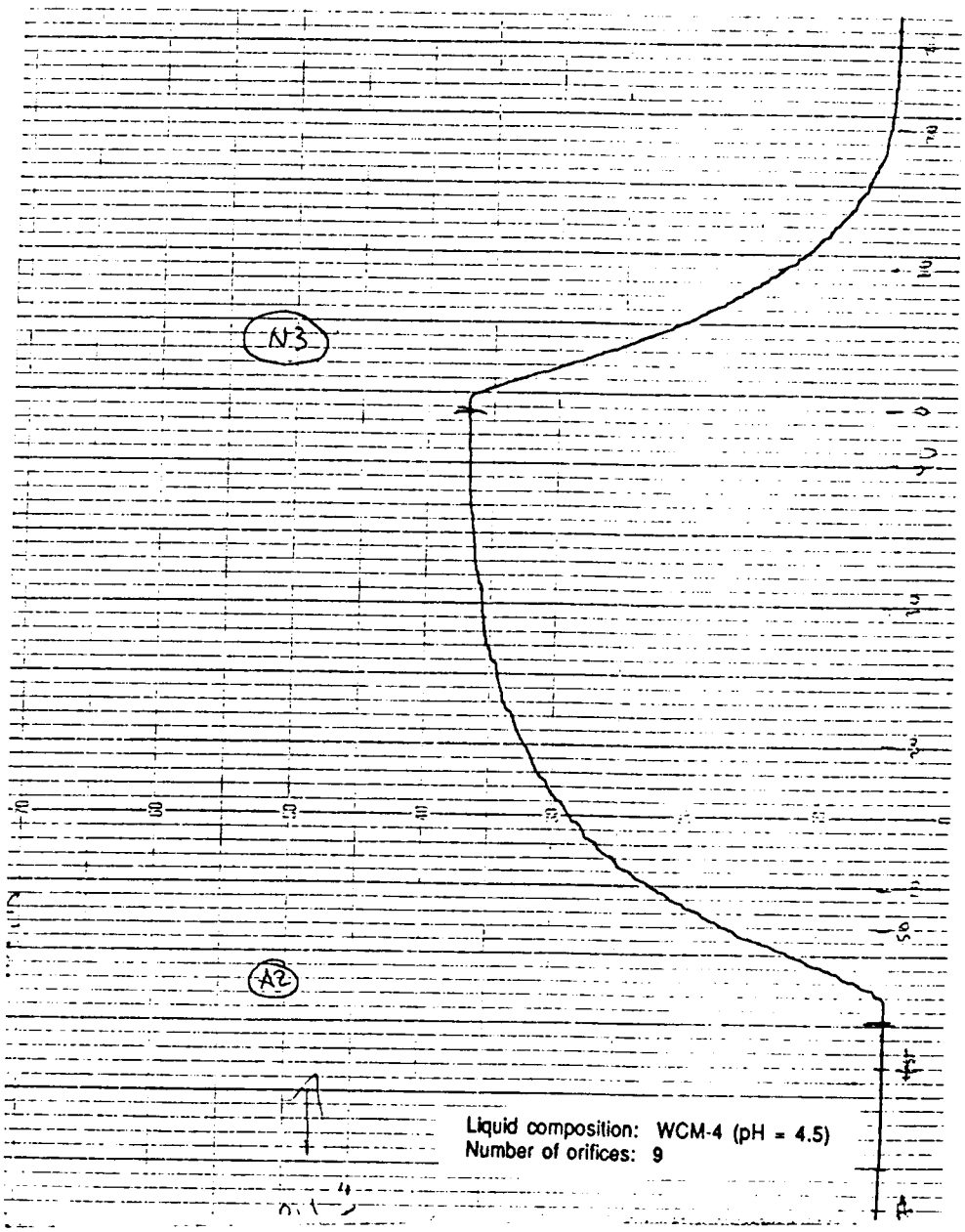
N3
A2
Liquid composition: WCM-4 (pH = 4.5)
Number of orifices: 9

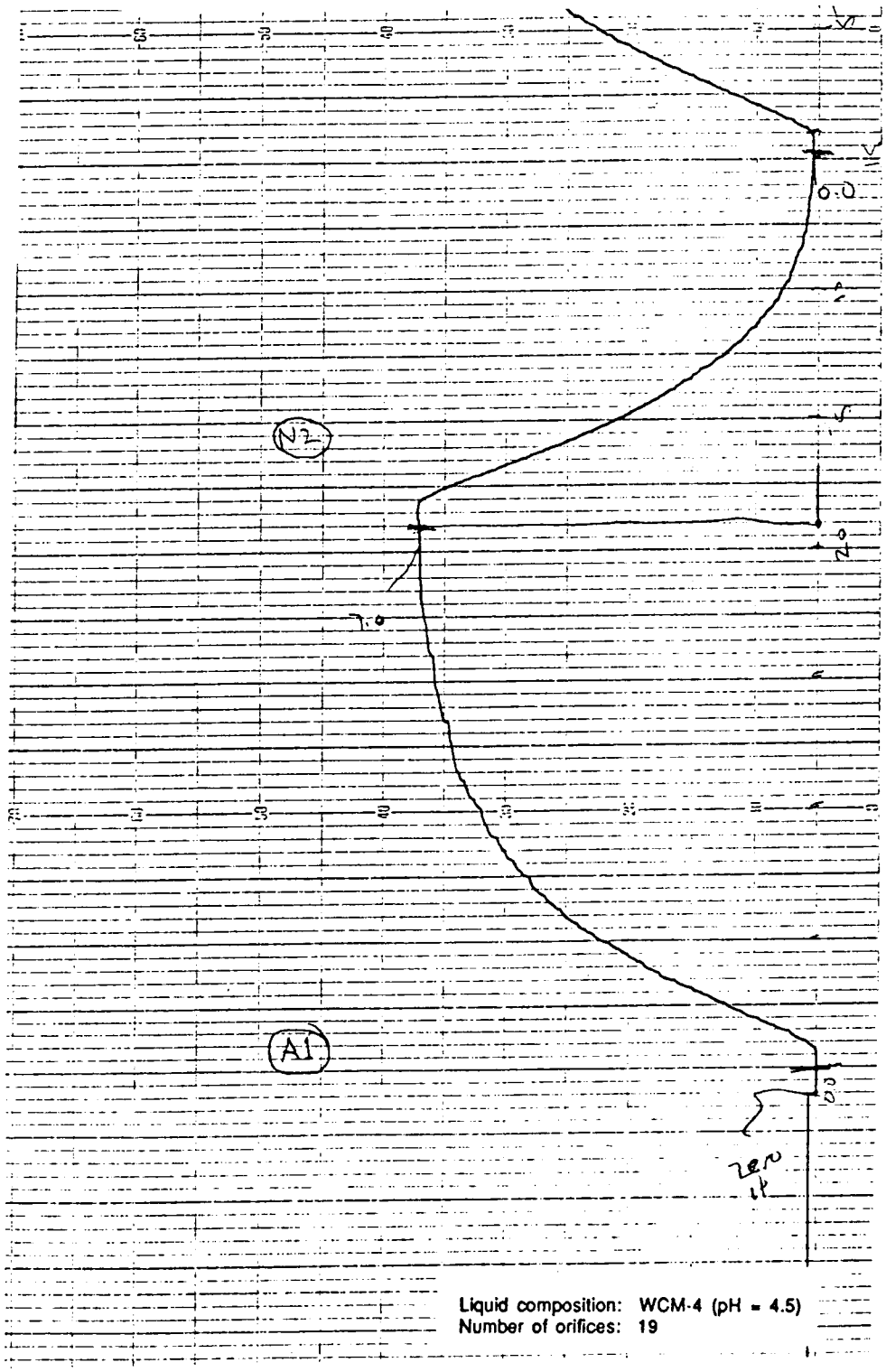
N2
A1
Liquid composition: WCM-4 (pH = 4.5)
Number of orifices: 19

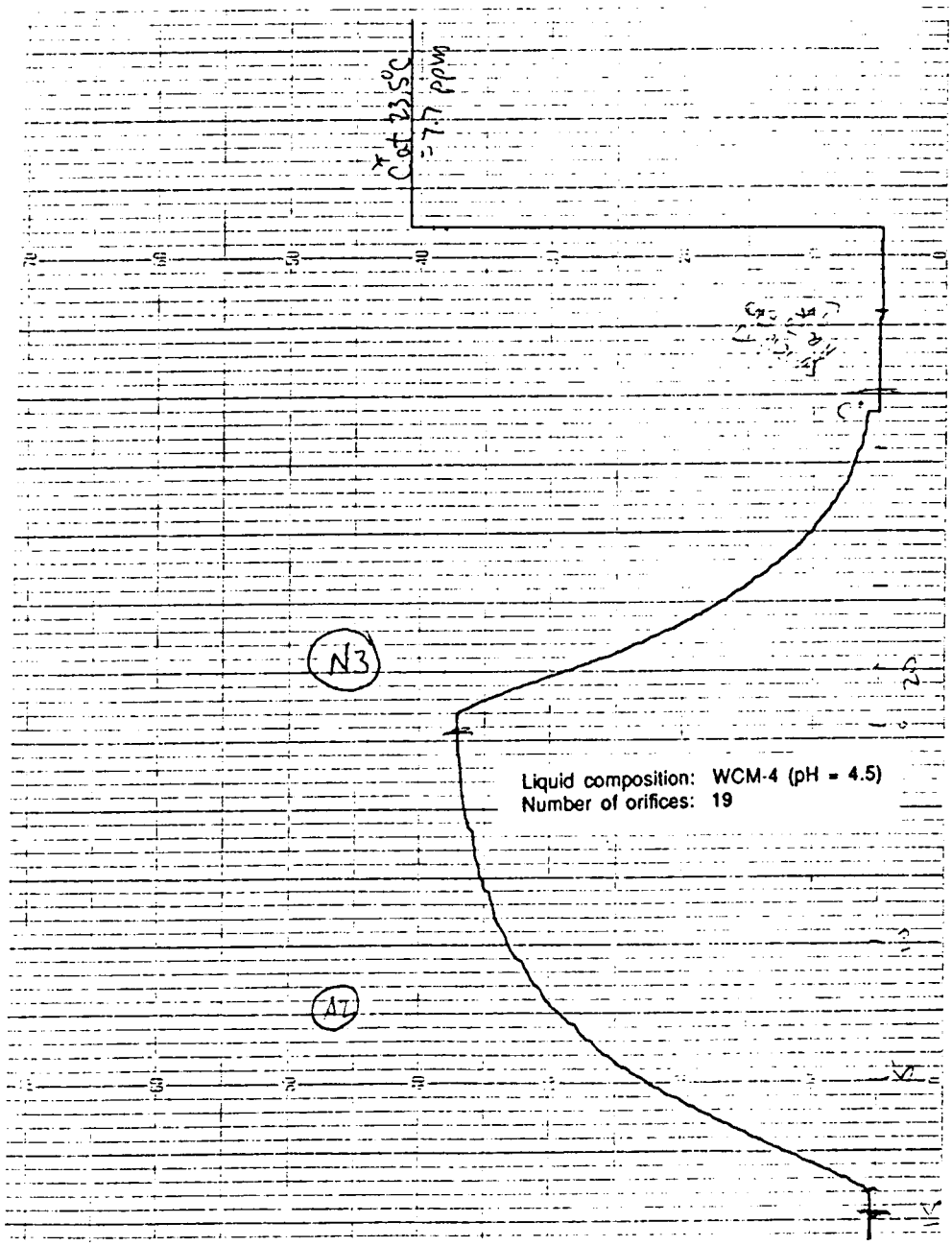
Liquid composition: WCM-4 (pH = 4.5)
Number of orifices: 19

Airlift Reactor Experiment

Liquid Composition: Distilled Water Date:

Exposure Label	Number of Bubbles	No. of orifices	Exposure Label	Number of Bubbles	No. of orifices
6/3A	126	9	6/2A	147	19
6/3B	117		6/2B	144	
6/3C	117		6/2C	210	
6/3D	111		6/2D	194	
~~C~~~~D~~	114		6/2E	190	
6/3E	112		6/2F	201	
6/3F	114		6/2G	170	
6/3G	118		6/2H	176	
6/3H	109		6/2I	210	
6/3I	118		6/2J	188	
6/3J	115		6/2K	200	
6/3K	120		6/2L	190	
6/3L	134		6/2M	209	
6/3M	60				
6/3N	63	5			
6/3O	54				
6/3P	57				
6/3Q	61				
6/3R	56				
6/3S	57				
6/3T	72				
6/3U	57				
6/3V	56				
6/3W	53				
6/3X	54				
6/3Y	59				
6/3Z	57				

Airlift Reactor Experiment

Liquid Composition: 5 wt percent sucrose Date: 7/12

Exposure Label	Number of Bubbles	No. of orifices	Exposure Label	Number of Bubbles	No. of orifices
7/4A	259	19	7/7A	87	5
7/4B	231		7/7B	88	
7/4C	246		7/7C	88	
7/4D	256		7/7D	95	
7/4E	247		7/7E	91	
7/4F	246		7/7F	88	
7/4G	266		7/7G	93	
7/4H	242		7/7H	101	
7/4I	224		7/7I	102	
7/4J	243		7/7J	106	
7/4K	243		7/7K	104	
7/4L	242				
7/5A	145	9			
7/5B	137				
7/5C	143				
7/5D	135				
7/5E	147				
7/5F	158				
7/5G	143				
7/5H	156				
7/5I	155				
7/5J	138				
7/5K	129				
7/5L	14				

Airlift Reactor Experiment

Liquid Composition: WCM-4 Date: 7/4

Exposure Label	Number of Bubbles	No. of orifices	Exposure Label	Number of Bubbles	No. of orifices
6/10A	181	19	6/10AA	?	
6/10B	181		6/10AB	?	
6/10C	162		6/10AC	49	5
6/10D	189		6/10AD	49	
6/10E	181		6/10AE	57	
6/10F	187		6/10AF	51	
6/10G	179		6/10AG	70	
6/10H	182		6/10AH	76	
6/10I	190		6/10AI	69	
6/10J	184		6/10AJ	69	
6/10K	181				
6/10L	185				
6/10M	113	9			
6/10N	116				
6/10O	121				
6/10P	104				
6/10Q	118				
6/10R	104				
6/10S	111				
6/10T	121				
6/10U	99				
6/10V	110				
6/10W	106				
6/10X	110				
6/10Y	56				

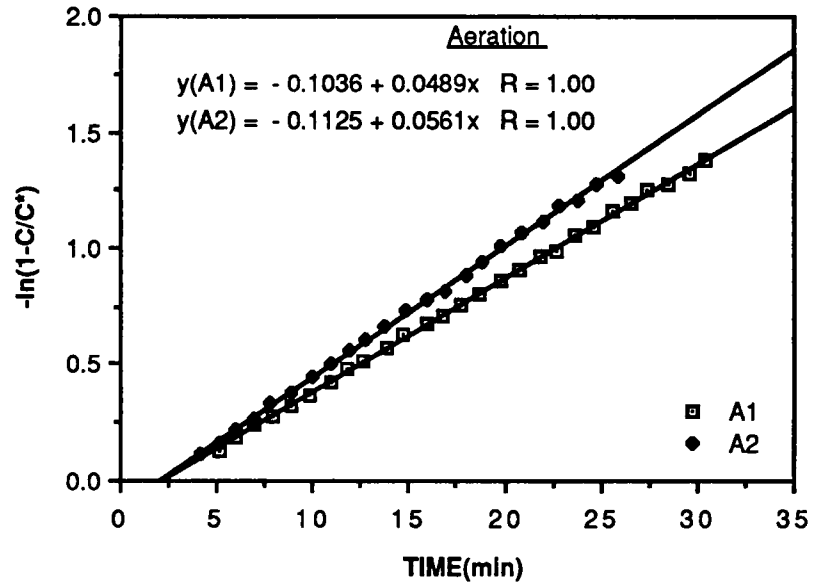

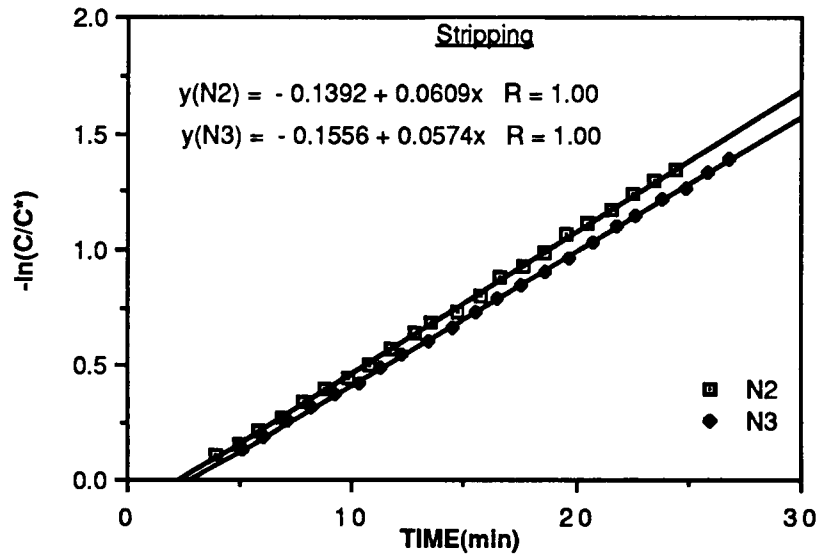

: -ln(dimensionless concentration) as a function of time.
Liquid composition: Distilled Water Number of orifices: 5
Date: 6/3/88 Maximum C = 75% C*
Updated: 6/30/88

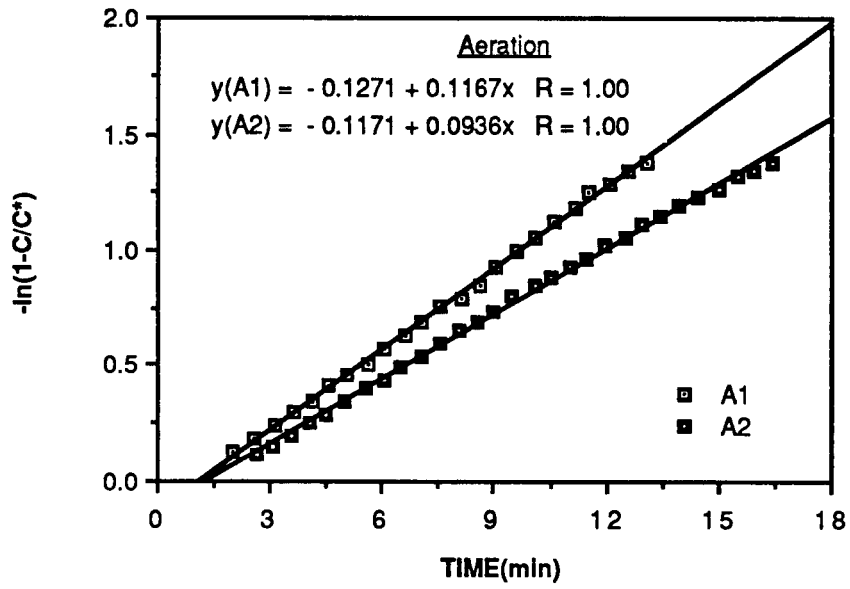

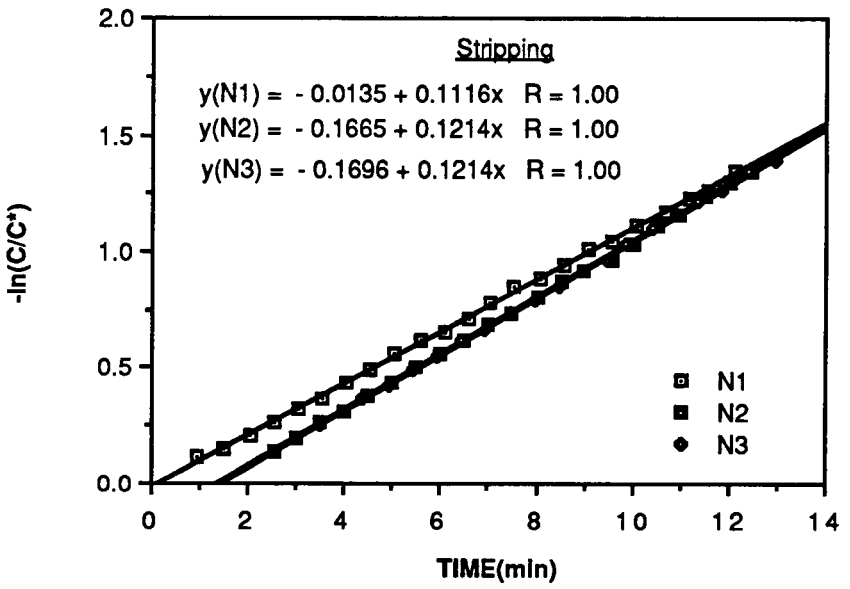

: -ln(dimensionless concentration) as a function of time.
Liquid composition: Distilled Water Number of orifices: 9
Date: 6/3/88 Maximum C = 75% C*
Updated: 6/30/88

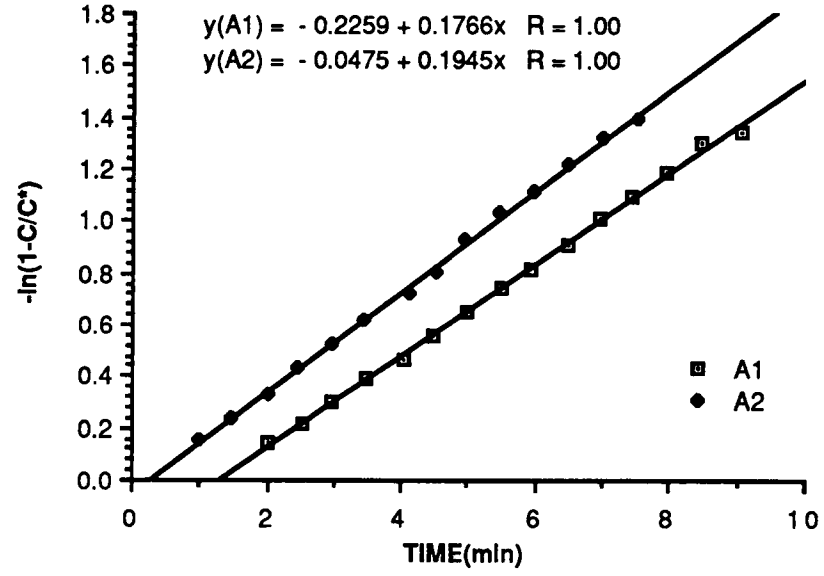

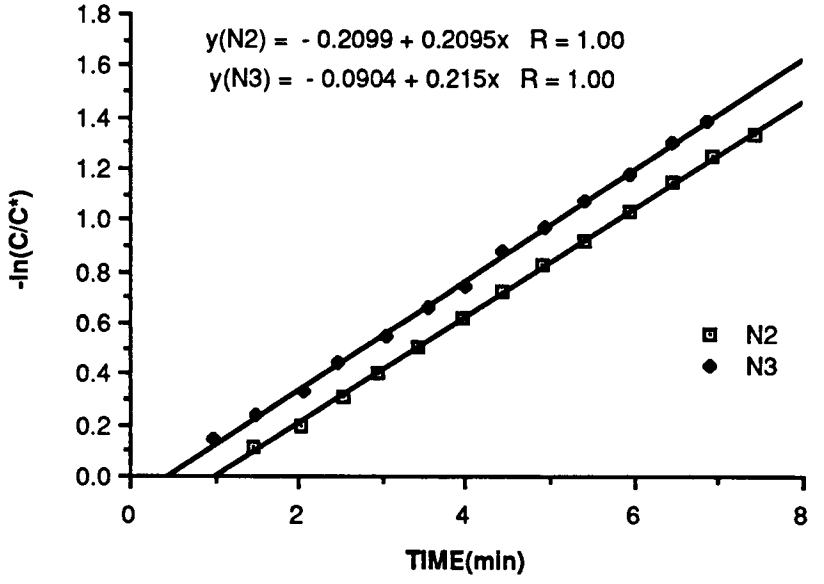

: Dimensionless concentration as a function of time.

Liquid composition: Distilled Water Number of orifices: 19

Date: 6/2/88 Re = 2100

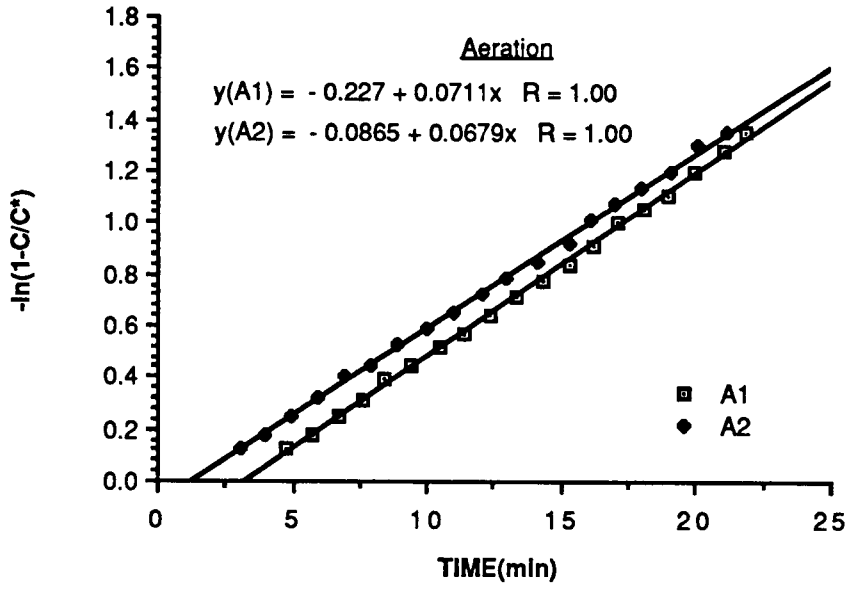

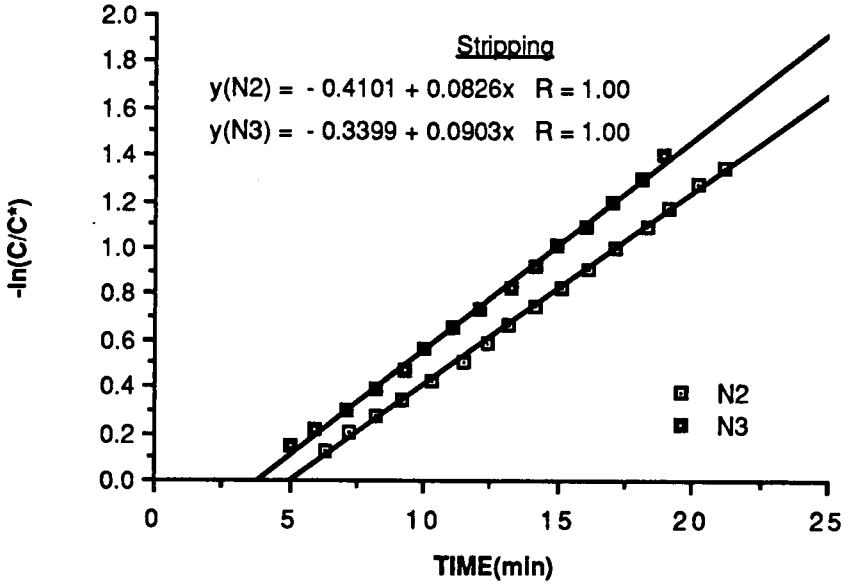

: -ln(dimensionless conc'n) as a function of time.
Liquid composition: 5 wt % sucrose Orifice no.: 5
Date: 7/7/88 Maximum C = 75% C*

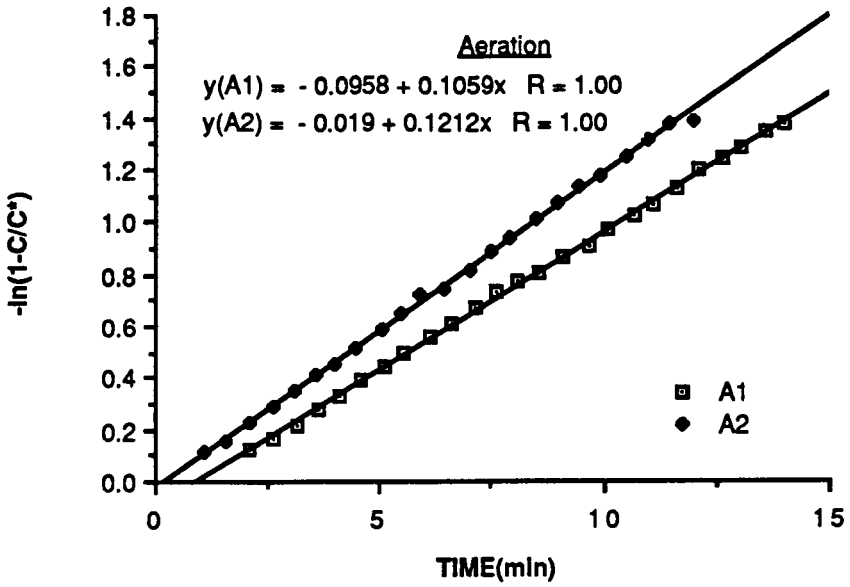

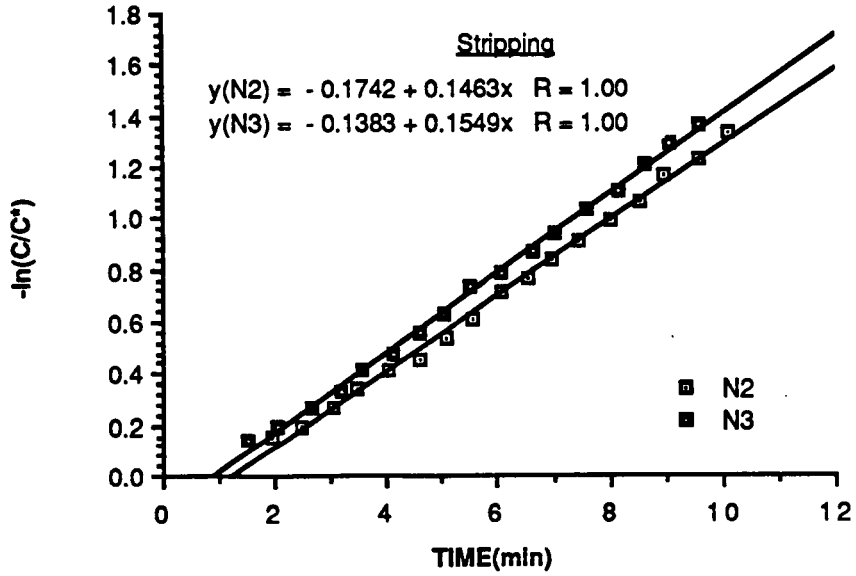

: -ln(dimensionless conc'n) as a function of time.
Liquid composition: 5 wt % sucrose Orifice no.: 9
Date: 7/5/88 Maximum C = 75% C*

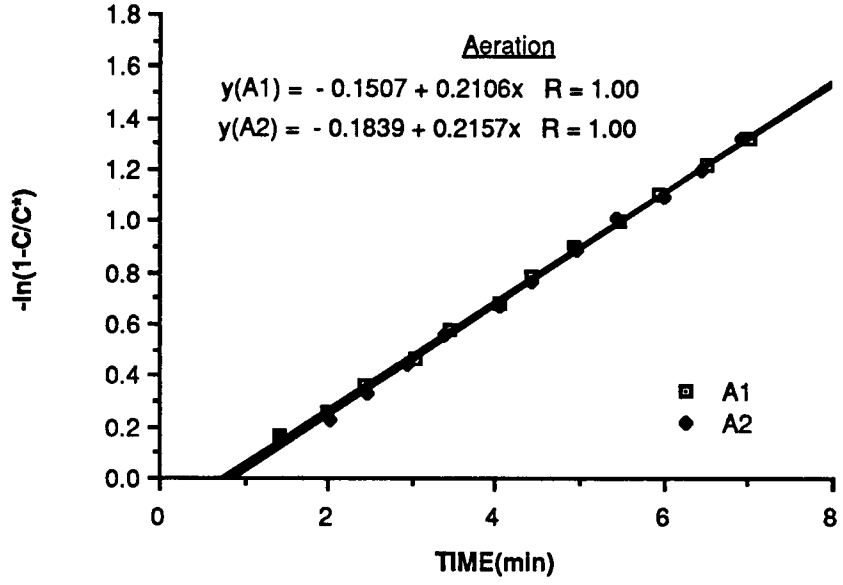

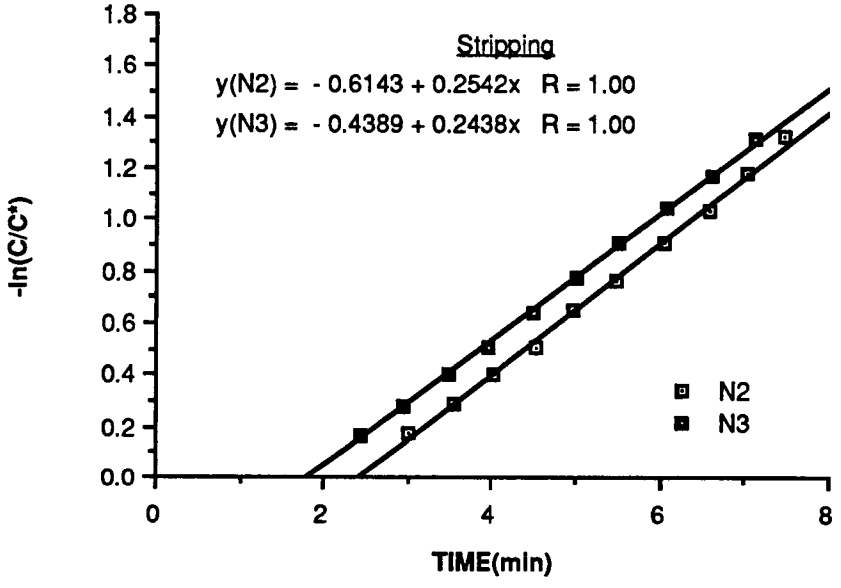

: -ln(dimensionless conc'n) as a function of time.
Liquid composition: 5 wt % sucrose Orifice no.: 19
Date: 7/4/88 Maximum C = 75% C*

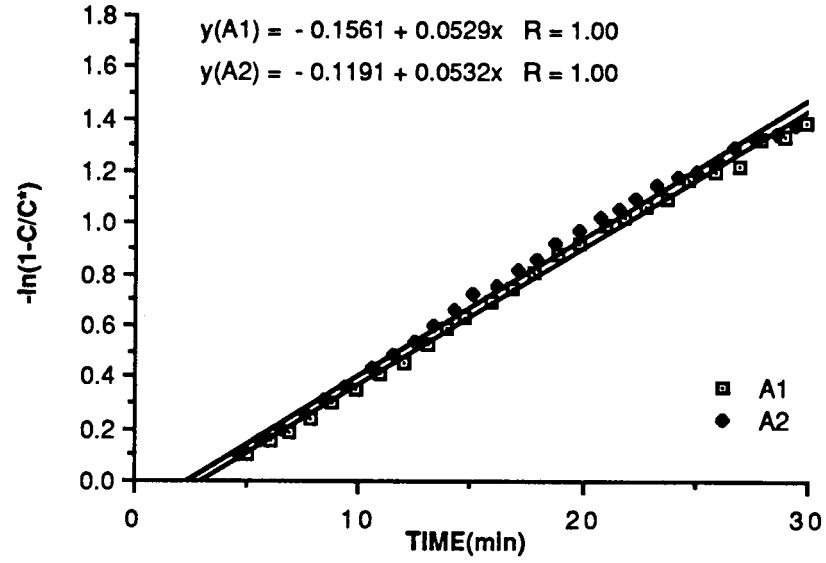

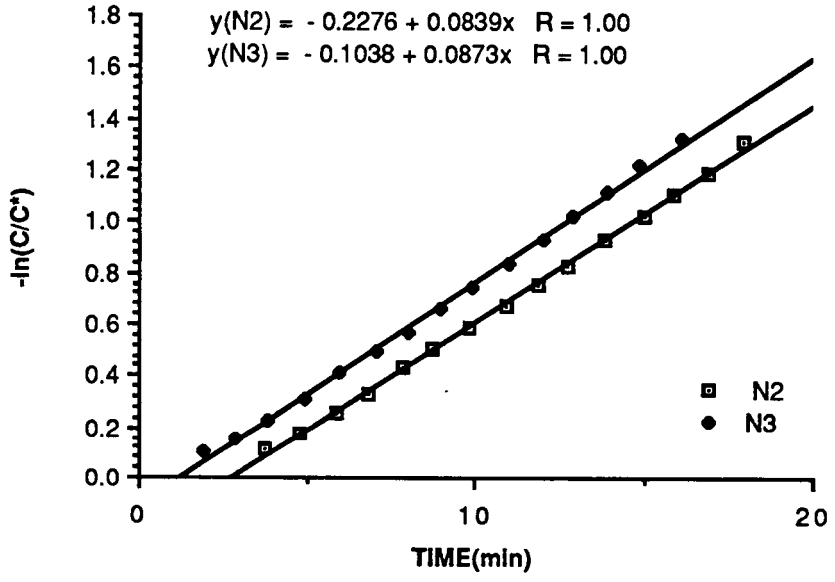

: Dimensionless concentration as a function of time.

Liquid composition: WCM-4 (pH = 4.5) Number of orifices: 5

Date: 6/10/88 Re = 2100

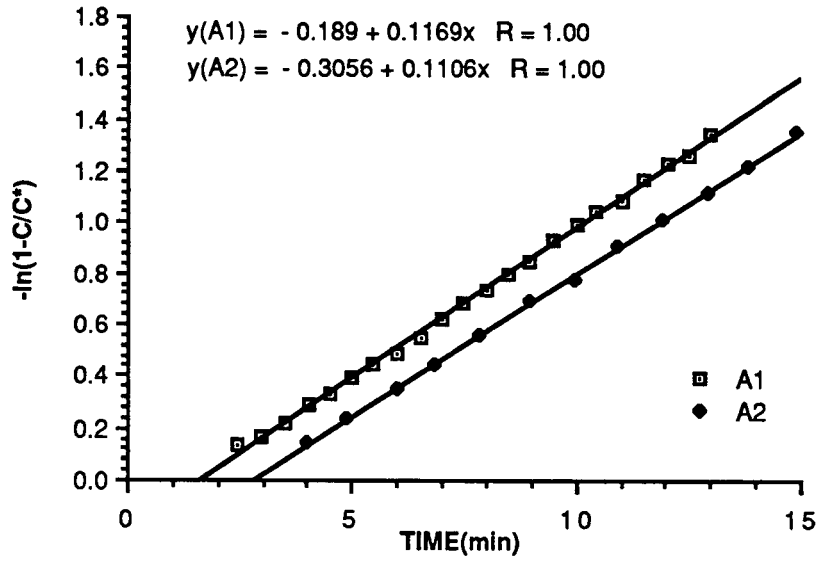

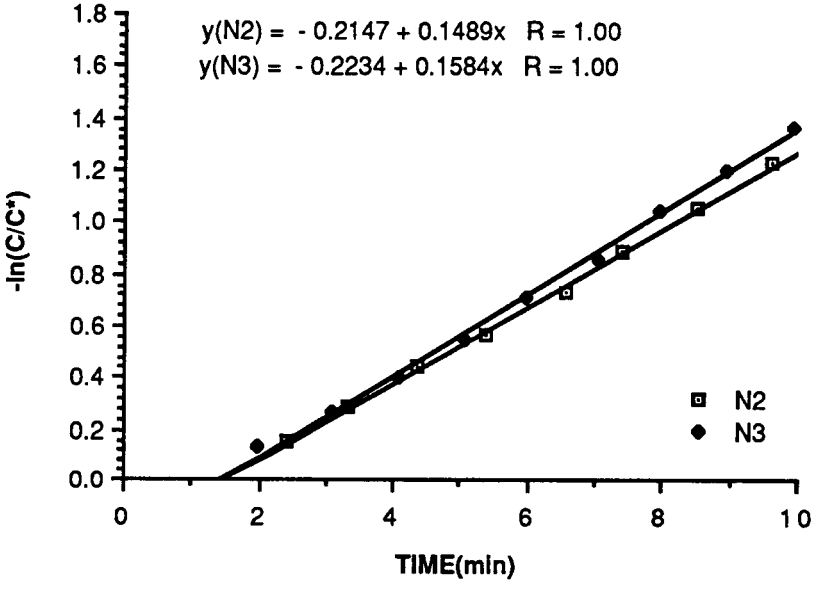

: Dimensionless concentration as a function of time.

Liquid composition: WCM-4 (pH = 4.5) Number of orifices: 9

Date: 6/10/88 Re = 2100 $C_{jet} = 75\% C^*$

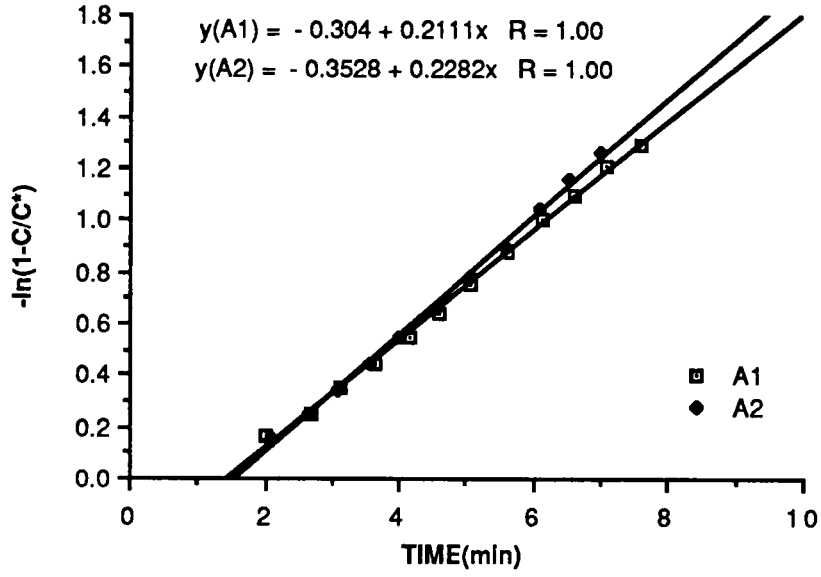

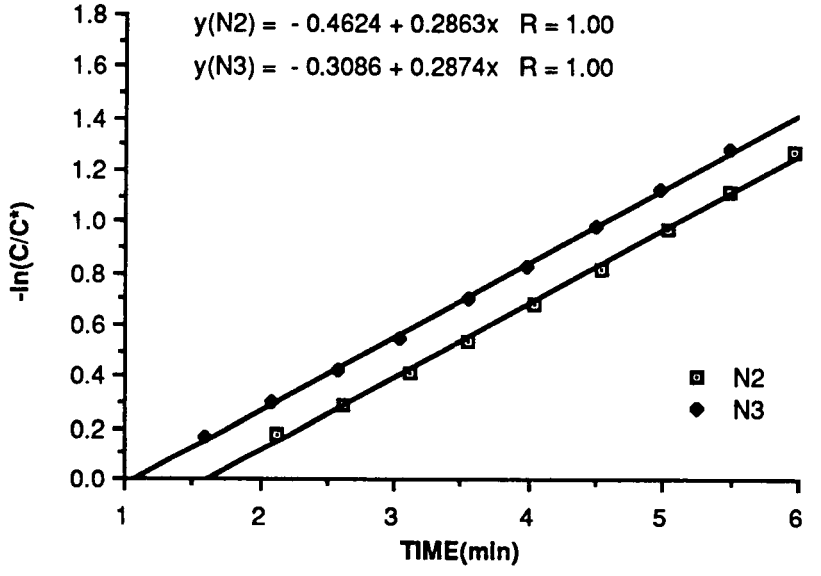

: Dimensionless concentration as a function of time.

Liquid composition: WCM-4 (pH = 4.5) Number of orifices: 19

Date: 6/10/88 Re = 2100

Date of experiment: 6/3
Liquid Composition: Distilled water

Chart label: a1

Number of orifices: 5
Total gas flow rate: 4.9 mls/sec Gas flow rate per orifice .98
Strobe flash rate: 776.6667 RPM
Average number of bubbles: 58
Liquid volume: 2300 mls

Gas holdup (dimensionless): 0.00191
Spherical bubble diameter: 0.525 cm
Interfacial area per unit dispersion: 0.02178 1/cm

Date of experiment: 6/3
Liquid Composition: Distilled water

Chart label: n2

Number of orifices: 5
Total gas flow rate: 4.9 mls/sec Gas flow rate per orifice .98
Strobe flash rate: 770 RPM
Average number of bubbles: 58
Liquid volume: 2300 mls

Gas holdup (dimensionless): 0.00192
Spherical bubble diameter: 0.526 cm
Interfacial area per unit dispersion: 0.02191 1/cm

Date of experiment: 6/3
Liquid Composition: Distilled water

Chart label: a2

Number of orifices: 5
Total gas flow rate: 4.9 mls/sec Gas flow rate per orifice .98
Strobe flash rate: 773.3333 RPM
Average number of bubbles: 55.33333
Liquid volume: 2300 mls

Gas holdup (dimensionless): 0.00183
Spherical bubble diameter: 0.526 cm
Interfacial area per unit dispersion: 0.02084 1/cm

Date of experiment: 6/3
Liquid Composition: Distilled water

Chart label: n3

Number of orifices: 5
Total gas flow rate: 4.9 mls/sec Gas flow rate per orifice .98
Strobe flash rate: 780 RPM
Average number of bubbles: 56.66667
Liquid volume: 2300 mls

Gas holdup (dimensionless): 0.00185
Spherical bubble diameter: 0.524 cm
Interfacial area per unit dispersion: 0.02122 1/cm

Date of experiment: 6/3
Liquid Composition: Distilled water

Chart label: a1

Number of orifices: 9
Total gas flow rate: 8.8 mls/sec Gas flow rate per orifice .97
Strobe flash rate: 1170 RPM
Average number of bubbles: 115
Liquid volume: 2300 mls

Gas holdup (dimensionless): 0.00250
Spherical bubble diameter: 0.458 cm
Interfacial area per unit dispersion: 0.03280 1/cm

Date of experiment: 6/3
Liquid Composition: Distilled water

Chart label: n2

Number of orifices: 9
Total gas flow rate: 8.8 mls/sec Gas flow rate per orifice .97 mls/sec
Strobe flash rate: 1170 RPM
Average number of bubbles: 113.3333
Liquid volume: 2300 mls

Gas holdup (dimensionless): 0.00246
Spherical bubble diameter: 0.458 cm
Interfacial area per unit dispersion: 0.03232 1/cm

Date of experiment: 6/3
Liquid Composition: Distilled water

Chart label: a2

Number of orifices: 9
Total gas flow rate: 8.8 mls/sec Gas flow rate per orifice .97 mls/sec
Strobe flash rate: 1160 RPM
Average number of bubbles: 115
Liquid volume: 2300 mls

Gas holdup (dimensionless): 0.00252
Spherical bubble diameter: 0.459 cm
Interfacial area per unit dispersion: 0.03298 1/cm

Date of experiment: 6/3
Liquid Composition: Distilled water

Chart label: n3

Number of orifices: 9
Total gas flow rate: 8.8 mls/sec Gas flow rate per orifice .97 mls/sec
Strobe flash rate: 1170 RPM
Average number of bubbles: 123
Liquid volume: 2300 mls

Gas holdup (dimensionless): 0.00267
Spherical bubble diameter: 0.458 cm
Interfacial area per unit dispersion: 0.03507 1/cm

Date of experiment: 6/2
Liquid Composition: Distilled water

Chart label: a1

Number of orifices: 19
Total gas flow rate: 18.6 mls/sec Gas flow rate per orifice .97 mls/sec
Strobe flash rate: 1460 RPM
Average number of bubbles: 196.6667
Liquid volume: 2300 mls

Gas holdup (dimensionless): 0.00343
Spherical bubble diameter: 0.425 cm
Interfacial area per unit dispersion: 0.04838 1/cm

Date of experiment: 6/2
Liquid Composition: Distilled water

Chart label: n2

Number of orifices: 19
Total gas flow rate: 18.6 mls/sec Gas flow rate per orifice .97 mls/sec
Strobe flash rate: 1470 RPM
Average number of bubbles: 187
Liquid volume: 2300 mls

Gas holdup (dimensionless): 0.00324
Spherical bubble diameter: 0.424 cm
Interfacial area per unit dispersion: 0.04581 1/cm

Date of experiment: 6/2
Liquid Composition: Distilled water

Chart label: a2

Number of orifices: 19
Total gas flow rate: 18.6 mls/sec Gas flow rate per orifice .97 mls/sec
Strobe flash rate: 1460 RPM
Average number of bubbles: 191.3333
Liquid volume: 2300 mls

Gas holdup (dimensionless): 0.00334
Spherical bubble diameter: 0.425 cm
Interfacial area per unit dispersion: 0.04708 1/cm

Date of experiment: 6/2
Liquid Composition: Distilled water

Chart label: n3

Number of orifices: 19
Total gas flow rate: 18.6 mls/sec Gas flow rate per orifice .97 mls/sec
Strobe flash rate: 1461.667 RPM
Average number of bubbles: 199.6667
Liquid volume: 2300 mls

Gas holdup (dimensionless): 0.00348
Spherical bubble diameter: 0.425 cm
Interfacial area per unit dispersion: 0.04908 1/cm

Date of experiment: 6/10
Liquid Composition: WCM-4 (pH=4.5)

Chart label: a1

Number of orifices: 5
Total gas flow rate: 6.7 mls/sec Gas flow rate per orifice 1.34 mls/sec
Strobe flash rate: 1093.333 RPM
Average number of bubbles: 56
Liquid volume: 2300 mls

Gas holdup (dimensionless): 0.00179
Spherical bubble diameter: 0.520 cm
Interfacial area per unit dispersion: 0.02063 1/cm

Date of experiment: 6/10
Liquid Composition: WCM-4 (pH=4.5)

Chart label: n2

Number of orifices: 5
Total gas flow rate: 6.7 mls/sec Gas flow rate per orifice 1.34 mls/sec
Strobe flash rate: 1093.333 RPM
Average number of bubbles: 49
Liquid volume: 2300 mls

Gas holdup (dimensionless): 0.00156
Spherical bubble diameter: 0.520 cm
Interfacial area per unit dispersion: 0.01806 1/cm

Date of experiment: 6/10
Liquid Composition: WCM-4 (pH=4.5)

Chart label: a2

Number of orifices: 5
Total gas flow rate: 6.7 mls/sec
Strobe flash rate: 1093.333 RPM
Average number of bubbles: 59.33333
Liquid volume: 2300 mls

Gas flow rate per orifice 1.34 mls/sec

Gas holdup (dimensionless): 0.00189
Spherical bubble diameter: 0.520 cm
Interfacial area per unit dispersion: 0.02186 1/cm

Date of experiment: 6/10
Liquid Composition: WCM-4 (pH=4.5)

Chart label: n3

Number of orifices: 5
Total gas flow rate: 6.7 mls/sec
Strobe flash rate: 1086.667 RPM
Average number of bubbles: 71.33334
Liquid volume: 2300 mls

Gas flow rate per orifice 1.34 mls/sec

Gas holdup (dimensionless): 0.00229
Spherical bubble diameter: 0.521 cm
Interfacial area per unit dispersion: 0.02637 1/cm

Date of experiment: 6/10
Liquid Composition: WCM-4 (pH=4.5)

Chart label: a1

Number of orifices: 9
Total gas flow rate: 12.1 mls/sec
Strobe flash rate: 1326.667 RPM
Average number of bubbles: 116.6667
Liquid volume: 2300 mls

Gas flow rate per orifice 1.34 mls/sec

Gas holdup (dimensionless): 0.00307
Spherical bubble diameter: 0.488 cm
Interfacial area per unit dispersion: 0.03781 1/cm

Date of experiment: 6/10
Liquid Composition: WCM-4 (pH=4.5)

Chart label: n2

Number of orifices: 9
Total gas flow rate: 12.1 mls/sec Gas flow rate per orifice 1.34 mls/sec
Strobe flash rate: 1330 RPM
Average number of bubbles: 108.6667
Liquid volume: 2300 mls

Gas holdup (dimensionless): 0.00286
Spherical bubble diameter: 0.487 cm
Interfacial area per unit dispersion: 0.03517 1/cm

Date of experiment: 6/10
Liquid Composition: WCM-4 (pH=4.5)

Chart label: a2

Number of orifices: 9
Total gas flow rate: 12.1 mls/sec Gas flow rate per orifice 1.34 mls/sec
Strobe flash rate: 1330 RPM
Average number of bubbles: 110.3333
Liquid volume: 2300 mls

Gas holdup (dimensionless): 0.00290
Spherical bubble diameter: 0.487 cm
Interfacial area per unit dispersion: 0.03571 1/cm

Date of experiment: 6/10
Liquid Composition: WCM-4 (pH=4.5)

Chart label: n3

Number of orifices: 9
Total gas flow rate: 12.1 mls/sec Gas flow rate per orifice 1.34 mls/sec
Strobe flash rate: 1330 RPM
Average number of bubbles: 108.6667
Liquid volume: 2300 mls

Gas holdup (dimensionless): 0.00286
Spherical bubble diameter: 0.487 cm
Interfacial area per unit dispersion: 0.03517 1/cm

Date of experiment: 6/10
Chart label: a1 Liquid Composition: WCM-4 (pH=4.5)

Number of orifices: 19
Total gas flow rate: 25.5 mls/sec Gas flow rate per orifice 1.34 mls/sec
Strobe flash rate: 1613.333 RPM
Average number of bubbles: 174.6667
Liquid volume: 2300 mls

Gas holdup (dimensionless): 0.00378
Spherical bubble diameter: 0.457 cm
Interfacial area per unit dispersion: 0.04960 1/cm

Date of experiment: 6/10
Chart label: n2 Liquid Composition: WCM-4 (pH=4.5)

Number of orifices: 19
Total gas flow rate: 25.5 mls/sec Gas flow rate per orifice 1.34 mls/sec
Strobe flash rate: 1620 RPM
Average number of bubbles: 185.6667
Liquid volume: 2300 mls

Gas holdup (dimensionless): 0.00400
Spherical bubble diameter: 0.456 cm
Interfacial area per unit dispersion: 0.05257 1/cm

Date of experiment: 6/10
Chart label: a2 Liquid Composition: WCM-4 (pH=4.5)

Number of orifices: 19
Total gas flow rate: 25.5 mls/sec Gas flow rate per orifice 1.34 mls/sec
Strobe flash rate: 1613.333 RPM
Average number of bubbles: 183.6667
Liquid volume: 2300 mls

Gas holdup (dimensionless): 0.00397
Spherical bubble diameter: 0.457 cm
Interfacial area per unit dispersion: 0.05214 1/cm

Data of experiment: 6/10
Liquid composition: WCM-4 (pH:4.5)

Number of orifices: 19
Total gas flow rate: 25.5 mls/sec
Strobe flash rate: 1603.333 RPM
Average number of bubbles: 183.3333
Liquid volume: 2300 mls

Gas flow rate per orifice 1.34 mls/sec

Gas holdup (dimensionless): 0.00399
Spherical bubble diameter: 0.458 cm
Interfacial area per unit dispersion: 0.05226 1/cm

Date of experiment: 7/7
Liquid Composition: 5 % sucrose

Chart label: A1

Number of orifices: 5
Total gas flow rate: 6.4 mls/sec Gas flow rate per orifice 1.28 mls/sec
Strobe flash rate: 1160 RPM
Average number of bubbles: 87.66666
Liquid volume: 2300 mls

Gas holdup (dimensionless): 0.00252
Spherical bubble diameter: 0.502 cm
Interfacial area per unit dispersion: 0.03009 1/cm

Date of experiment: 7/7
Liquid Composition: 5 % sucrose

Chart label: N2

Number of orifices: 5
Total gas flow rate: 6.4 mls/sec Gas flow rate per orifice 1.28 mls/sec
Strobe flash rate: 1346.667 RPM
Average number of bubbles: 91.33334
Liquid volume: 2300 mls

Gas holdup (dimensionless): 0.00226
Spherical bubble diameter: 0.478 cm
Interfacial area per unit dispersion: 0.02839 1/cm

Date of experiment: 7/7
Liquid Composition: 5 % sucrose

Chart label: A2

Number of orifices: 5
Total gas flow rate: 6.4 mls/sec Gas flow rate per orifice 1.28 mls/sec
Strobe flash rate: 1353.333 RPM
Average number of bubbles: 98.66666
Liquid volume: 2300 mls

Gas holdup (dimensionless): 0.00243
Spherical bubble diameter: 0.477 cm
Interfacial area per unit dispersion: 0.03056 1/cm

Date of experiment: 7/7
Liquid Composition: 5 % sucrose

Chart label: N3

Number of orifices: 5
Total gas flow rate: 6.4 mls/sec Gas flow rate per orifice 1.28 mls/sec
Strobe flash rate: 1586.667 RPM
Average number of bubbles: 105
Liquid volume: 2300 mls

Gas holdup (dimensionless): 0.00220
Spherical bubble diameter: 0.452 cm
Interfacial area per unit dispersion: 0.02926 1/cm

Date of experiment: 7/5
Liquid Composition: 5 % sucrose

Chart label: A1

Number of orifices: 9
Total gas flow rate: 11.4 mls/sec Gas flow rate per orifice 1.26 mls/sec
Strobe flash rate: 1396.667 RPM
Average number of bubbles: 141.6667
Liquid volume: 2300 mls

Gas holdup (dimensionless): 0.00334
Spherical bubble diameter: 0.470 cm
Interfacial area per unit dispersion: 0.04263 1/cm

Date of experiment: 7/5
Liquid Composition: 5 % sucrose

Chart label: N2

Number of orifices: 9
Total gas flow rate: 11.4 mls/sec Gas flow rate per orifice 1.26 mls/sec
Strobe flash rate: 1366.667 RPM
Average number of bubbles: 146.6667
Liquid volume: 2300 mls

Gas holdup (dimensionless): 0.00353
Spherical bubble diameter: 0.474 cm
Interfacial area per unit dispersion: 0.04477 1/cm

Date of experiment: 7/5
Liquid Composition: 5 % sucrose

Chart label: A2

Number of orifices: 9
Total gas flow rate: 11.4 mls/sec Gas flow rate per orifice 1.26 mls/sec
Strobe flash rate: 1370 RPM
Average number of bubbles: 151.3333
Liquid volume: 2300 mls

Gas holdup (dimensionless): 0.00364
Spherical bubble diameter: 0.473 cm
Interfacial area per unit dispersion: 0.04611 1/cm

Chart label: N3

Date of Experiment: 7/5
Liquid Composition: 5% sucrose

Number of orifices: 9
Total gas flow rate: 11.4 mls/sec Gas flow rate per orifice 1.26 mls/sec
Strobe flash rate: 1313.333 RPM
Average number of bubbles: 136
Liquid volume: 2300 mls

Gas holdup (dimensionless): 0.00341
Spherical bubble diameter: 0.480 cm
Interfacial area per unit dispersion: 0.04264 1/cm

Date of experiment: 7/4
Liquid Composition: 5 % sucrose

Chart label: A1

Number of orifices: 19
Total gas flow rate: 22.6 mls/sec Gas flow rate per orifice 1.18 mls/sec
Strobe flash rate: 1613.333 RPM
Average number of bubbles: 245.3333
Liquid volume: 2300 mls

Gas holdup (dimensionless): 0.00470
Spherical bubble diameter: 0.439 cm
Interfacial area per unit dispersion: 0.06422 1/cm

Date of experiment: 7/4
Liquid Composition: 5 % sucrose

Chart label: N2

Number of orifices: 19
Total gas flow rate: 22.6 mls/sec Gas flow rate per orifice 1.18 mls/sec
Strobe flash rate: 1616.667 RPM
Average number of bubbles: 249.6667
Liquid volume: 2300 mls

Gas holdup (dimensionless): 0.00477
Spherical bubble diameter: 0.438 cm
Interfacial area per unit dispersion: 0.06526 1/cm

Date of experiment: 7/4
Liquid Composition: 5 % sucrose

Chart label: A2

Number of orifices: 19
Total gas flow rate: 22.6 mls/sec Gas flow rate per orifice 1.18 mls/sec
Strobe flash rate: 1603.333 RPM
Average number of bubbles: 244
Liquid volume: 2300 mls

Gas holdup (dimensionless): 0.00470
Spherical bubble diameter: 0.440 cm
Interfacial area per unit dispersion: 0.06413 1/cm

Date of experiment: 7/4
Liquid Composition: 5 % sucrose

Chart label: N3

Number of orifices: 19
Total gas flow rate: 22.6 mls/sec Gas flow rate per orifice 1.18 mls/sec
Strobe flash rate: 1613.333 RPM
Average number of bubbles: 242.6667
Liquid volume: 2300 mls

Gas holdup (dimensionless): 0.00465
Spherical bubble diameter: 0.439 cm
Interfacial area per unit dispersion: 0.06352 1/cm

Average $k_l a$,Values Based on Experimental Data.

$k_l a$ (1/min)	H2O[a]	SUC	WCM-4
5 orifices:			
A1[b]	0.0489	0.0711	0.0529
A2	0.0561	0.0679	0.0532
N2	0.0609	0.0826	0.0839
N3	0.0574	0.0903	0.0873
Air Average:	0.0525	0.0695	0.0531
Nit. Average:	0.0592	0.0865	0.0856
Average All:	0.0558	0.0780	0.0693
9 orifices:			
A1	0.1167	0.1059	0.1169
A2	0.0936	0.1212	0.1106
N2	0.1214	0.1463	0.1489
N3	0.1214	0.1549	0.1584
Air Average:	0.1052	0.1136	0.1138
Nit. Average:	0.1214	0.1506	0.1537
Average All:	0.1133	0.1321	0.1337
19 orifices:			
A1	0.1766	0.2106	0.2111
A2	0.1945	0.2157	0.2282
N2	0.2095	0.2542	0.2863
N3	0.2150	0.2438	0.2874
Air Average:	0.1856	0.2132	0.2197
Nit. Average:	0.2123	0.2490	0.2869
Average All:	0.1989	0.2311	0.2533

[a]Gas flow rate per orifice: H2O, 0.98 ml/s; SUC, 1.28 ml/s; WCM-4, 1.35 ml/s.

[b]A1 = first oxygen run; A2 = second oxygen run; N2 = first nitrogen run; N3 = second nitrogen run.

Table 6.3: Interfacial Area Based on Airlift Reactor Experimental Bubble Diameter

area (1/cm)	H2O	SUC	WCM-4
5 orifices:			
A1	0.0218	0.0301	0.0206
A2	0.0208	0.0306	0.0219
N2	0.0219	0.0284	0.0181
N3	0.0212	0.0293	0.0264
Air Average:	0.0213	0.0303	0.0212
Nit. Average:	0.0216	0.0288	0.0222
Average All:	0.0214	0.0296	0.0217
9 orifices:			
A1	0.0328	0.0426	0.0378
A2	0.0330	0.0461	0.0357
N2	0.0323	0.0448	0.0352
N3	0.0351	0.0426	0.0352
Air Average:	0.0329	0.0444	0.0368
Nit. Average:	0.0337	0.0437	0.0352
Average All:	0.0333	0.0440	0.0360
19 orifices:			
A1	0.0484	0.0642	0.0496
A2	0.0471	0.0641	0.0521
N2	0.0458	0.0653	0.0526
N3	0.0491	0.0635	0.0523
Air Average:	0.0477	0.0642	0.0509
Nit. Average:	0.0474	0.0644	0.0524
Average All:	0.0476	0.0643	0.0516

[a]Gas flow rate per orifice: H2O, 0.98 ml/s; SUC, 1.28 ml/s; WCM-4, 1.35 ml/s.

[b]A1 = first oxygen run; A2 = second oxygen run; N2 = first nitrogen run; N3 = second nitrogen run.

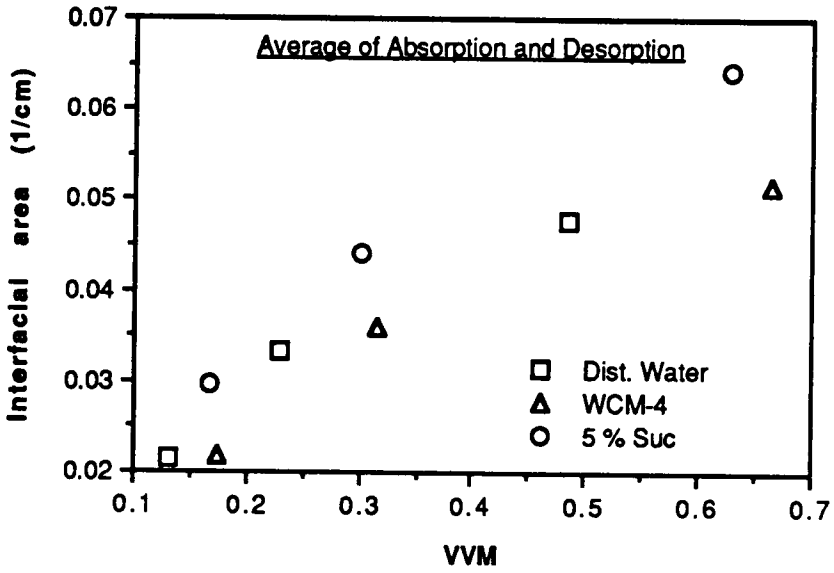

Summary of interfacial area vs. vvm.

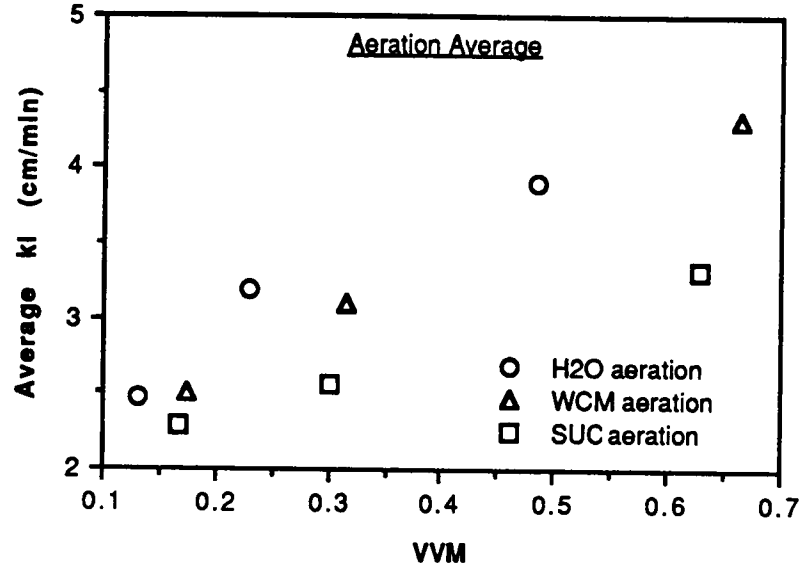

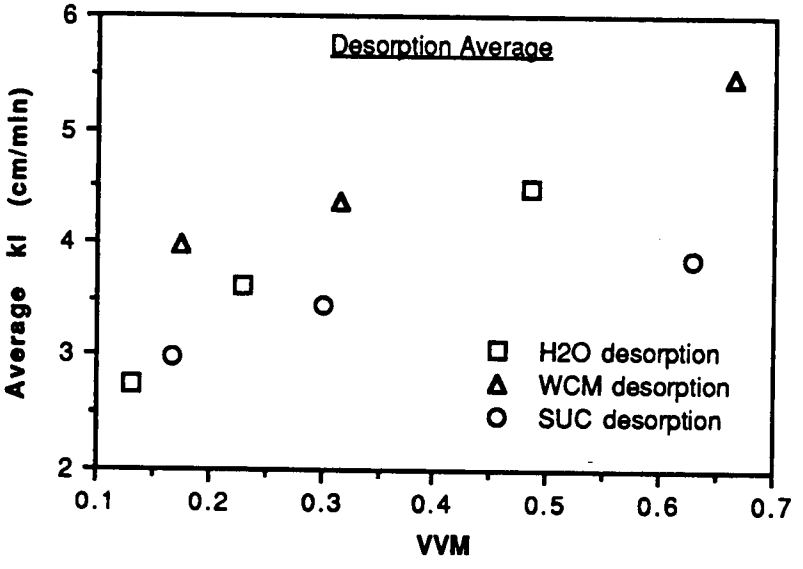

Summary of liquid phase mass transfer coefficients, k_l. vs. vvm for absorption and desorption in H2O, SUC and WCM-4 solutions.

VITA

The youngest of three children, James Thomas Gambill was born to Ed and Sarah Gambill on August 26, 1963 in Oak Ridge, Tennessee. In 1981 he was graduated from Oak Ridge High School. That same year he matriculated at the University of Tennessee in Knoxville. Mr. Gambill was awarded his Bachelor of Science degree in Chemical Engineering in 1985. After a brief hiatus, he entered the graduate program of the same university to earn a Master of Science degree with a major in Chemical Engineering. On August 21, 1988, Mr. Gambill began his engineering career as an employee of Ethyl Corporation in Baton Rouge, Louisiana.